ATHENA X-IFU'S TES/SQUID DETECTION CHAIN

DRTBT 2024

2024/03/28

P. Peille

cnes

Outline

- **Athena and X-IFU instrument overview**
  - Scientific context
  - Athena mission
  - X-IFU instrument
- **TES detectors for X-IFU**
  - TES small signal model and main resolution drivers
  - Influence of count rate
  - Evolution of TES design across project lifetime
- **The X-IFU TDM detection chain**
  - Functioning principle and overview
  - Dimensioning rules
  - Case study: how to optimize the pixel speed wrt. performance targets
  - Current dimensioning point in large signal
- **Going beyond signal to noise ratio optimization**
  - TDM bandwidths constraints
  - Crosstalk
  - Gain drifts and associated correction algorithms
- **What is next for X-IFU?**
  - Long term timeline
  - Short term demonstration activities

ATHENA X-IFU SCIENTIFIC CONTEXT AND INSTRUMENT OVERVIEW

cnes

The Universe seen in X-rays

- **50 % of the ordinary matter is contained in hot plasmas (T ~ 10^6 — 10^7 K)**
- **Key role of supermassive black holes**
- **A part of the Universe that can only be seen from space (Earth atmosphere is opaque)**

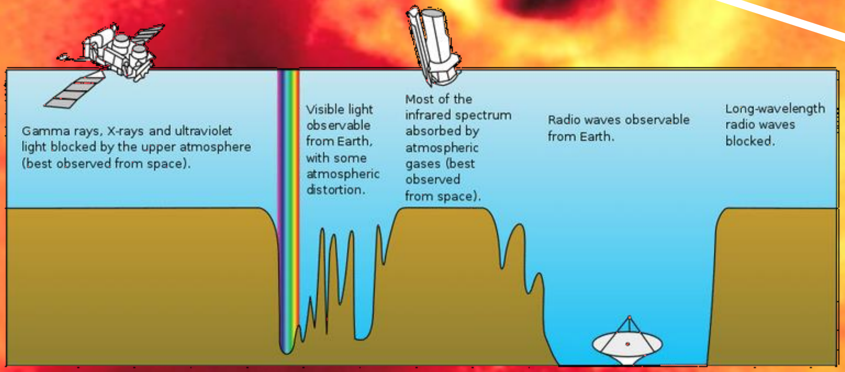

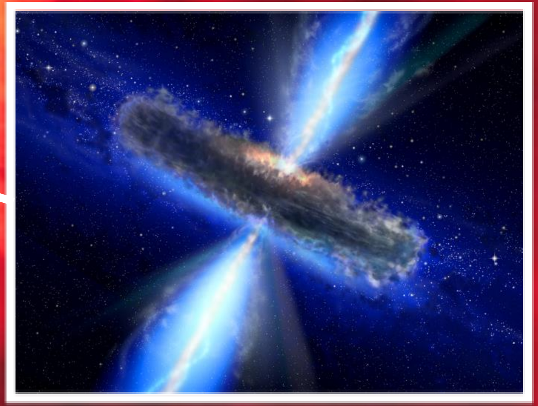

Perseus Cluster: X-ray

The X-ray data in astronomy

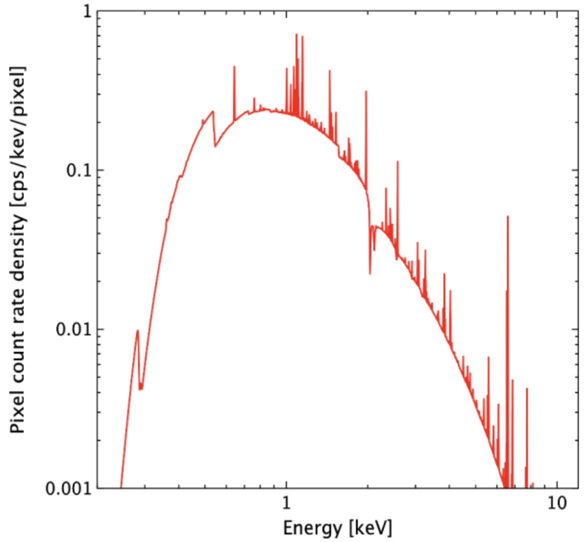

- The final output of most X-ray instruments is an « event list »
- Contrary to longer wavelength experiments where fluxes are measured, each individual X-ray photon is measured. For each one of them, we have:
  - Its arrival time
  - Its energy
  - The impacted pixel (= position)
  - Auxiliary data
- From this we can construct
  - Energy spectra
  - Images
  - Light curves and Fourier spectra
    - Oscillation of the emission of compact objects
    - Pulsars
    - …

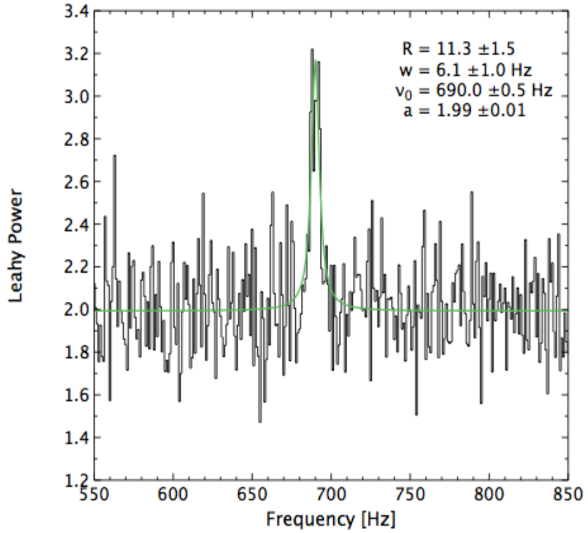

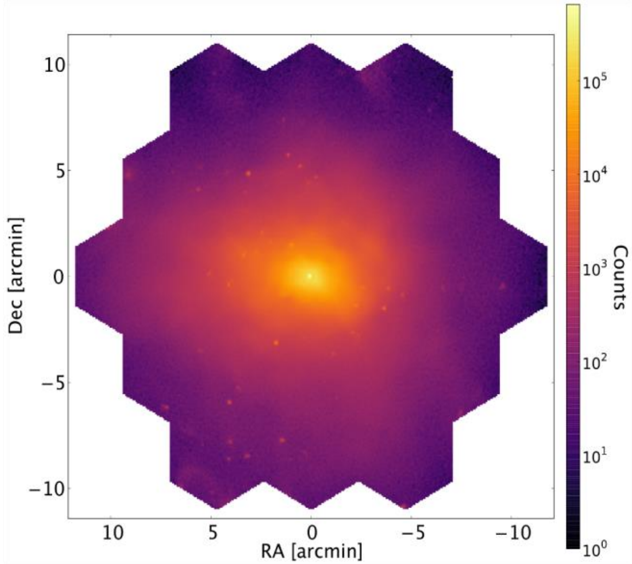

X-ray spectroscopy: composition of an X-ray spectrum

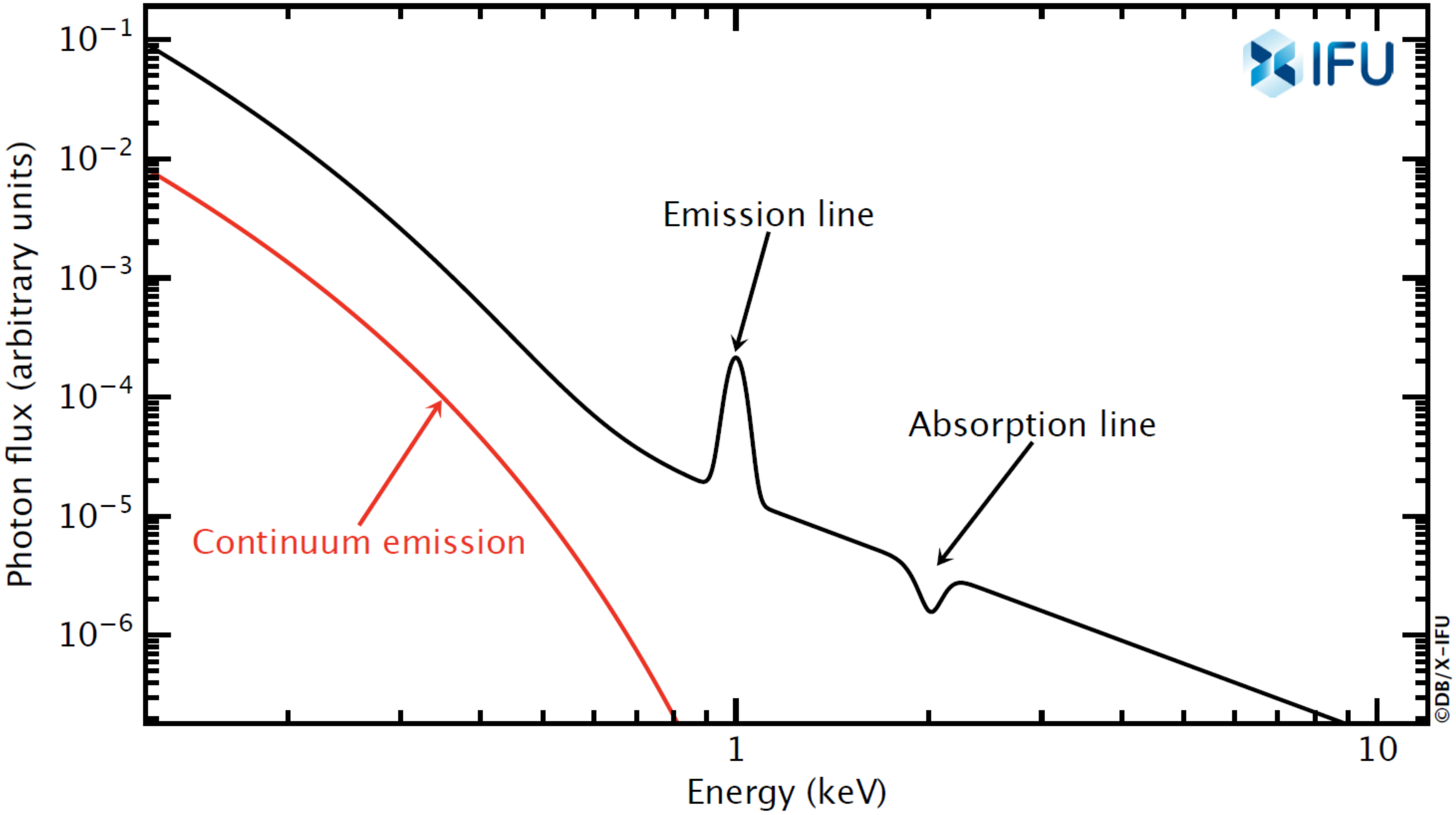

X-ray spectroscopy: what we learn from X-ray lines

- **Rest frame energy: gas composition (atomic element, ionization state)**
  - **The most famous X-ray line in astronomy: neutral iron = 6.4 keV in rest frame**
- **Energy shift: gas velocity from Doppler effect (combined with relativistic redshift from source distance)**
  - **20km/s Doppler shift at 6 keV =** $E \times \frac{\Delta v}{c}$ **= 0.4 eV**
- **Line integral: abundance (relative density of the element in the gas)**
- **Line broadening: state of the gas (temperature, turbulence, …)**

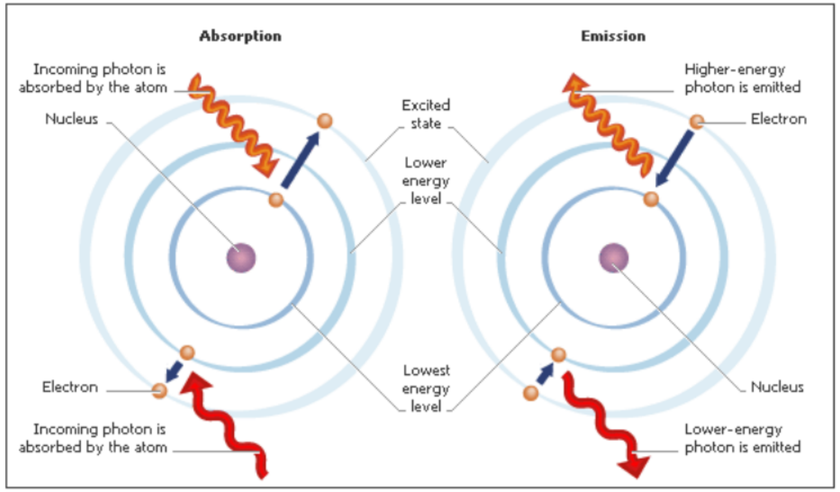

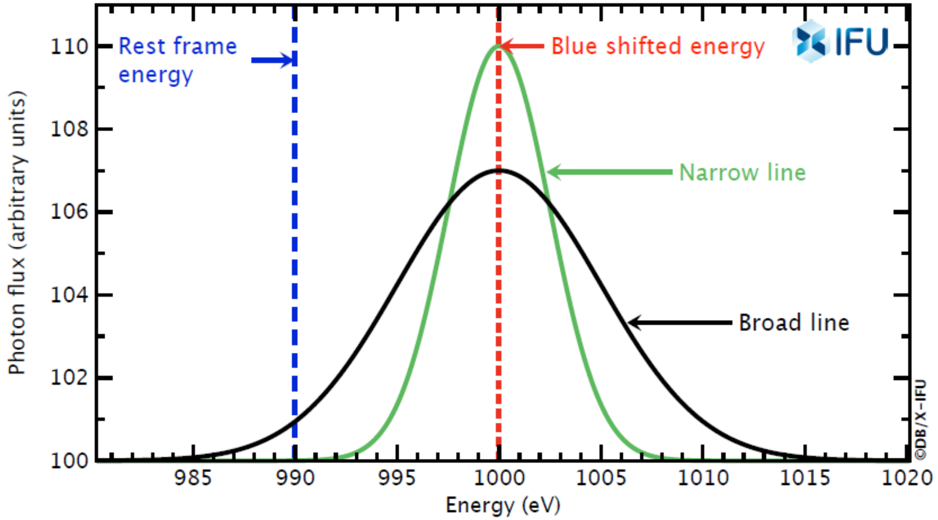

High resolution spectroscopy (microcalorimeters vs. CCDs)

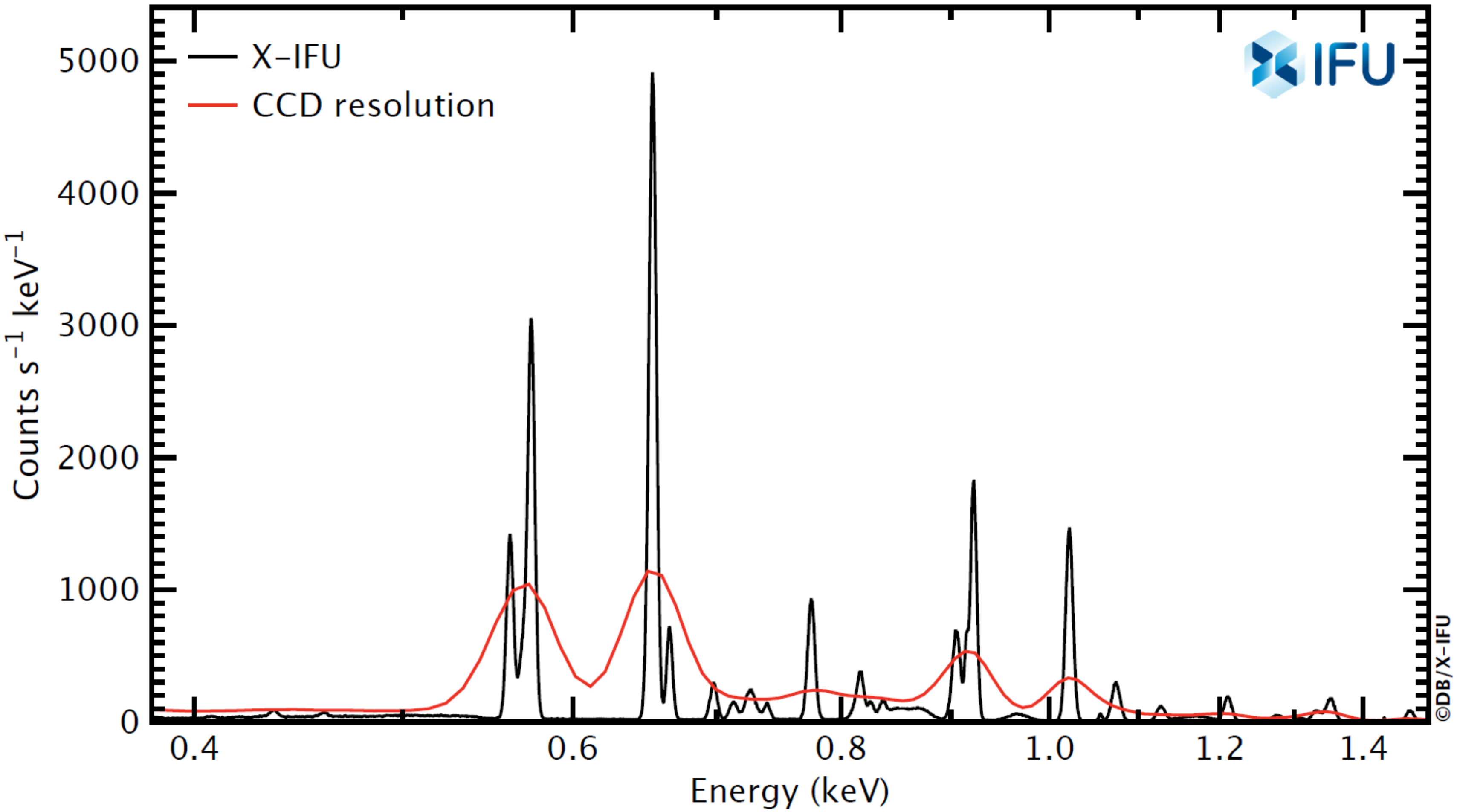

- ❖ **Note: Gratings based CCD spectrometers typically have a better resolution than microcalorimeters at low energy but the spatial information is blurred with the spectral one**

True spatially resolved spectroscopy: from Hitomi to Athena

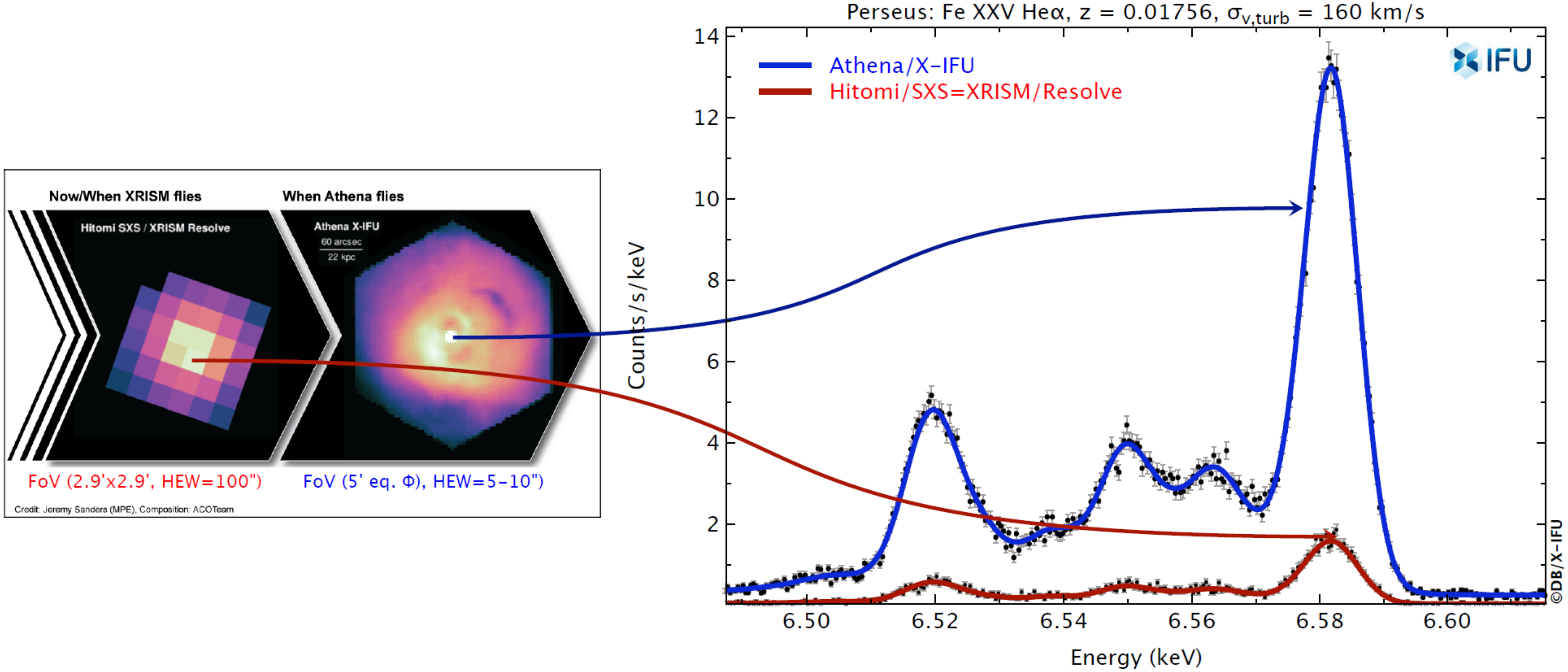

Athena science objectives

- **Athena is the next generation large X-ray observatory**
- **Initially selected to address the hot and energetic Universe science theme**
  - **How did matter assemble to form the large scale structures that we see today?**
    - Formation and evolution of the largest structures of the Universe
    - Detection of the « missing baryons »
    - Mainly through the observation of faint extended sources
  - **How did black holes grow and shape the Universe?**
    - Black hole formation
    - Feedback on galaxy and clusters formation
    - Accretion physics
    - Mainly through the observation of point sources, some among the brightest of the X-ray sky
  - **A large part dedicated to "observatory science" (open observation calls)**

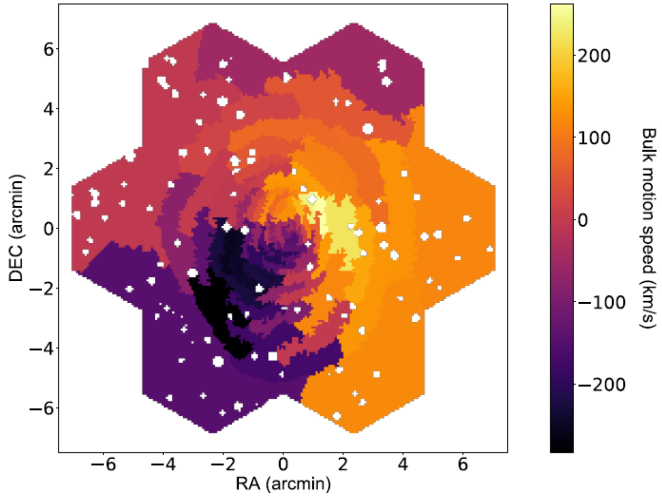

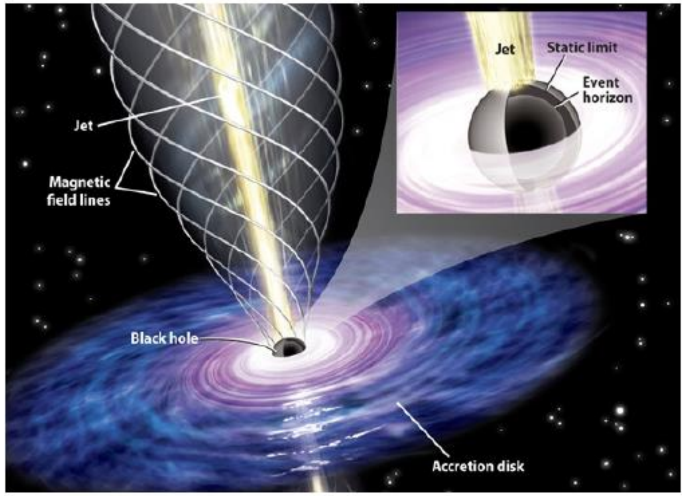

The Athena Observatory

- **ATHENA: Advanced TElescope for High ENergy Astrophysics**
  - **Launch scheduled for 203X on Ariane 6**
  - **Few tons and few kW ~ 14 m long satellite**
  - **Halo orbit around the L1 Lagrange point**
    - Preferred to L2 for stability of soft protons flux (create instrument background)

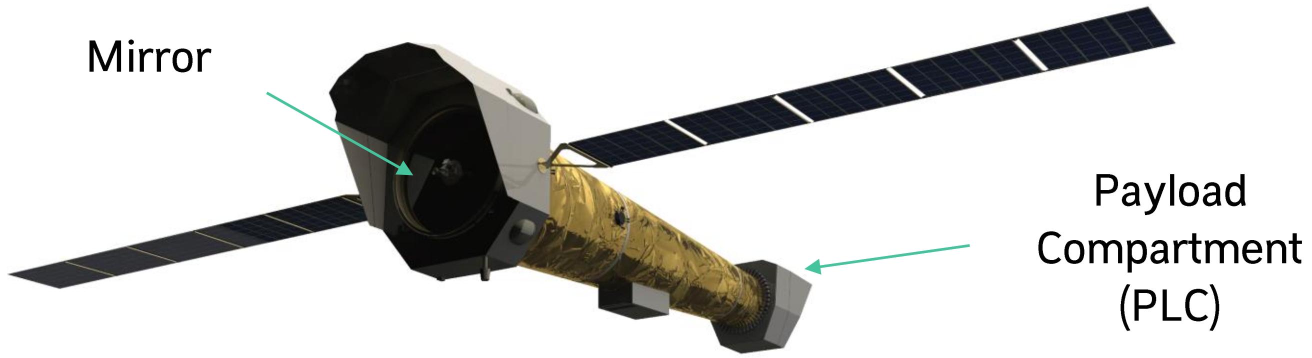

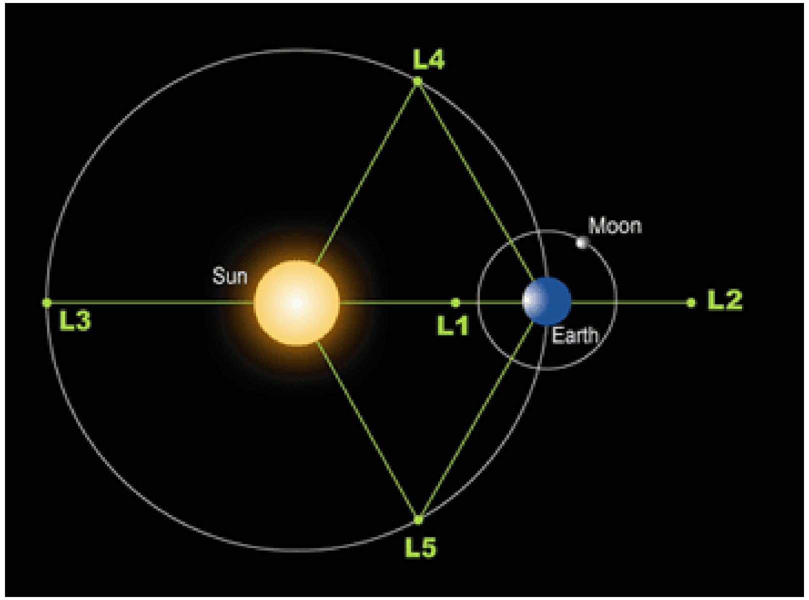

The Athena mirror

- **Silicon pore optics mirror (Wolter I) working in grazing incidence**
  - **Millions of pores stacked into so-called mirror modules**
    - Stacks of Si wafers assembled in a mostly fully automated process
- **Effective area an order of magnitude larger than current X-ray missions**
- **Accommodated on an hexapod platform. Allows:**
  - **Switching between instruments (WFI, X-IFU)**
  - **Defocusing for bright point sources observations**

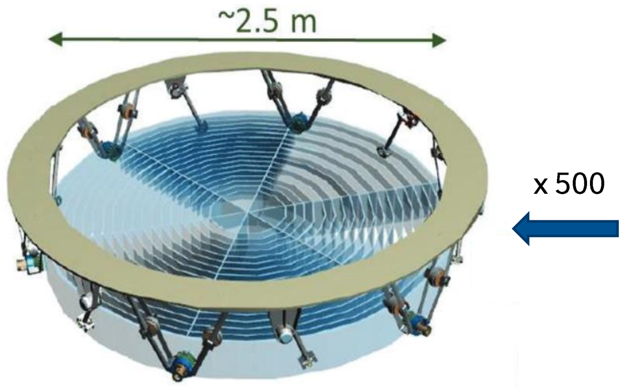

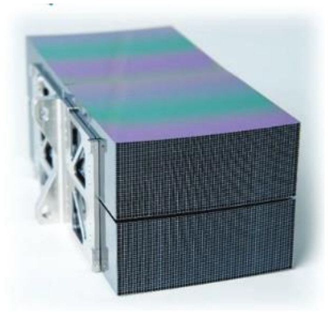

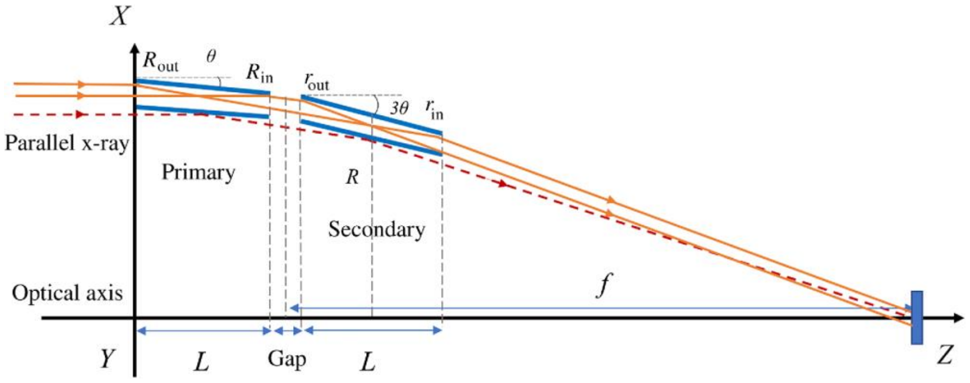

The Athena mirror

- **Silicon pore optics mirror (Wolter I) working in grazing incidence**
  - **Millions of pores stacked into so-called mirror modules**
    - Stacks of Si wafers assembled in a mostly fully automated process
- **Effective area an order of magnitude larger than current X-ray missions**
- **Accommodated on an hexapod platform. Allows:**
  - **Switching between instruments (WFI, X-IFU)**
  - **Defocusing for bright point sources observations**

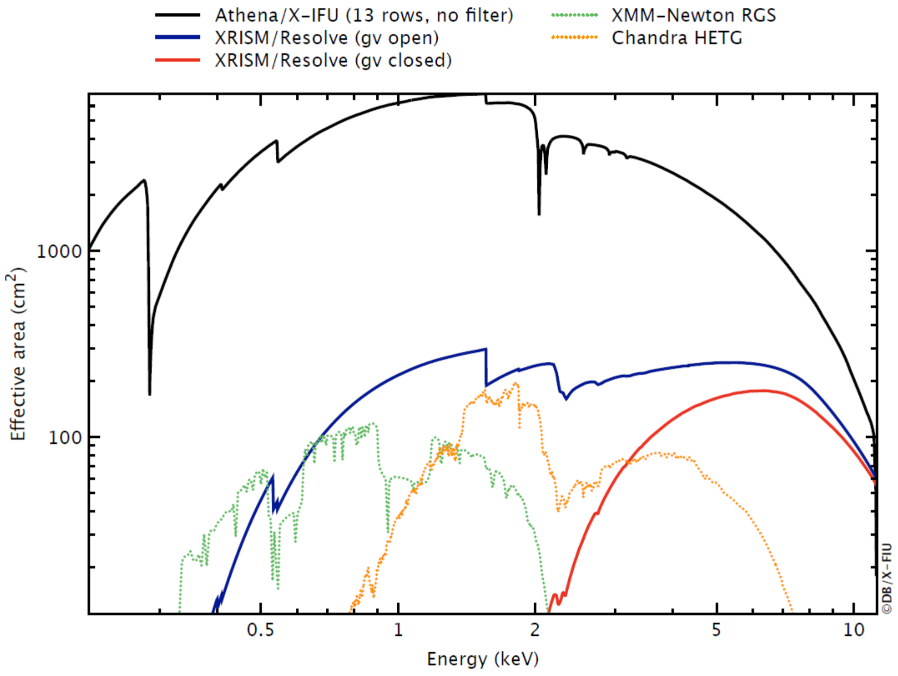

On focus PSF

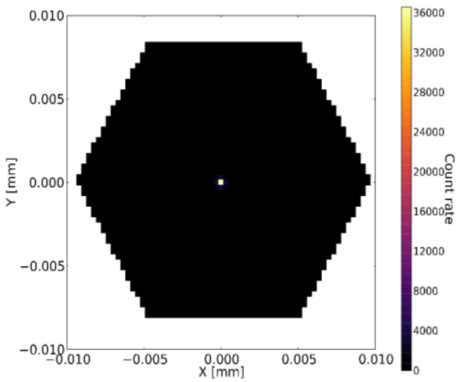

Defocused PSF

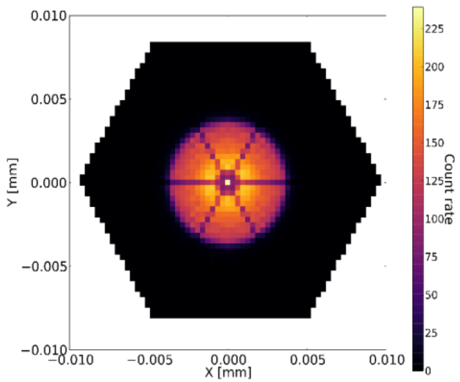

Payload Compartment (PLC) and Wide Field Imager (WFI)

❖ The Payload Compartment (PLC)

- Accommodates both Athena instruments (X-IFU + WFI)
- ~ 2000 kg, few kW
- Major overhaul (aka rescope) of the mission architecture in 2023 following ESA budget constraints
  - Addition of passive cooling down to 50 K for X-IFU thanks to V-groove system
  - Reduction of WFI allocated volume and sky access angle

❖ Wide Field Imager (WFI)

- 40'x40' FoV
- DEPFET detectors (depleted p-channel field-effect transistor)
- Moderate energy resolution (170 eV at 7 keV)
- Small detector mounted out of focus to observe the brightest objects of the X-ray sky

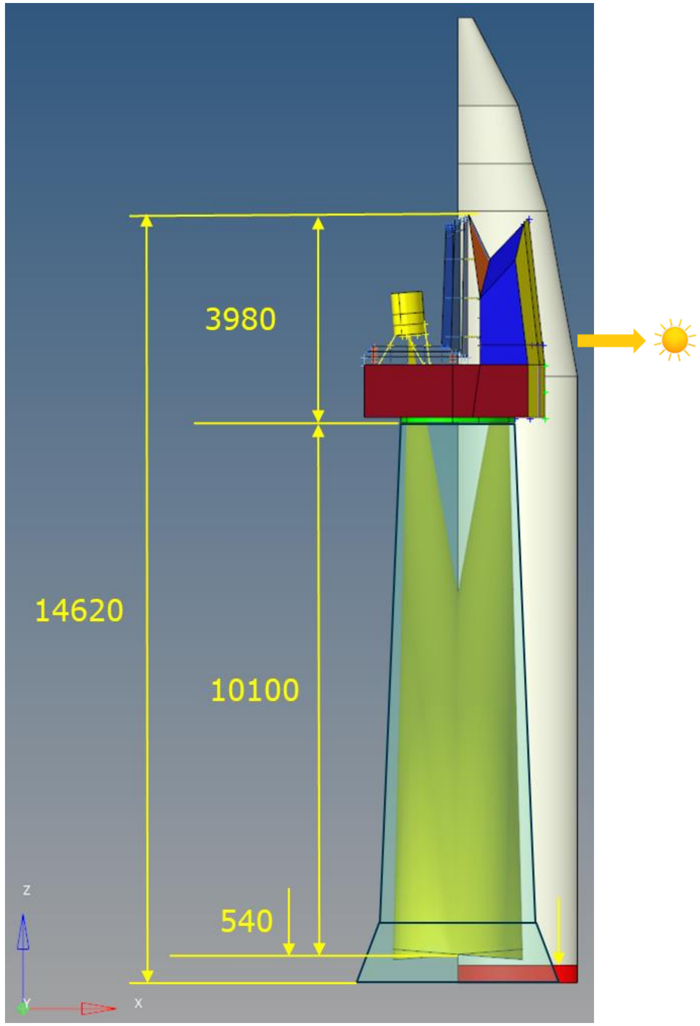

Credit: ESA

Payload Compartment (PLC) and Wide Field Imager (WFI)

❖ The Payload Compartment (PLC)

- Accommodates both Athena instruments (X-IFU + WFI)
- ~ 2000 kg, few kW
- Major overhaul (aka rescope) of the mission architecture in 2023 following ESA budget constraints
  - Addition of passive cooling down to 50 K for X-IFU thanks to V-groove system
  - Reduction of WFI allocated volume and sky access angle

❖ Wide Field Imager (WFI)

- 40‘x40’ FoV
- DEPFET detectors (depleted p-channel field-effect transistor)
- Moderate energy resolution (170 eV at 7 keV)
- Small detector mounted out of focus to observe the brightest objects of the X-ray sky

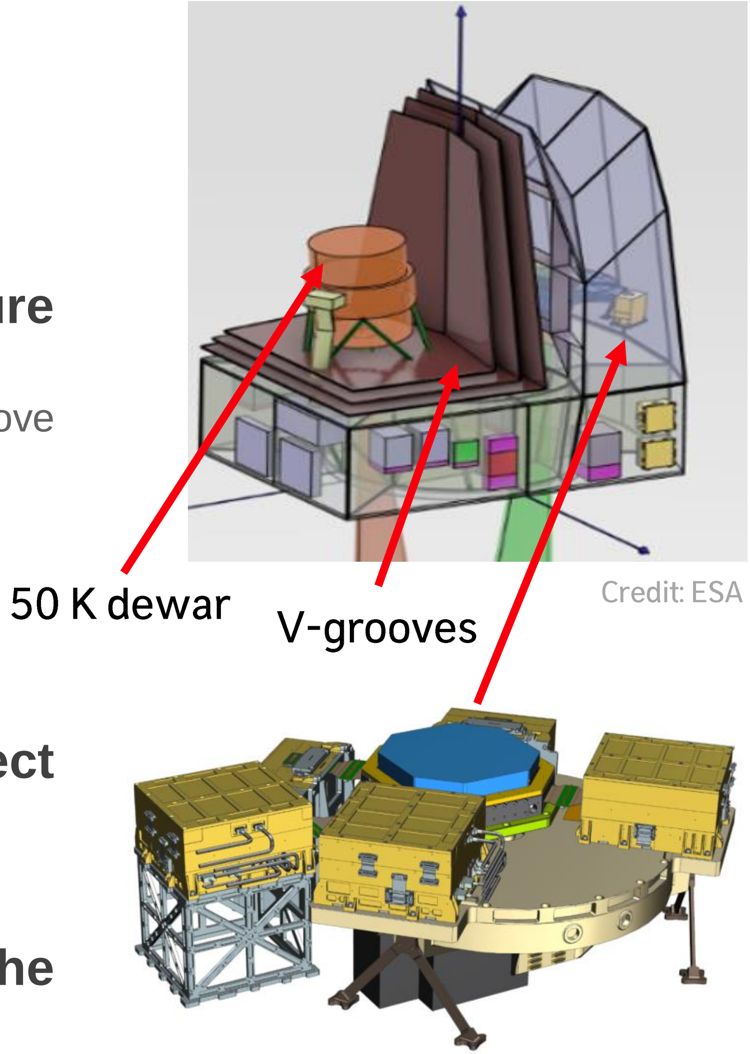

Credit: ESA

Main X-IFU performance requirements

Parameter	Requirement
Energy range	0.2 – 12 keV
Energy resolution	3 eV at 7 keV design target (4 eV requirement)
Field of view	4' equivalent diameter
Pixel size	~ 5" (1504 pixels)
Instrument efficiency	>12%, >56%, >63%, >42% @ 0.35, 1.0, 7.0, 10.0 keV
Count rate capability	80% high res throughput at 1 mCrab (goal at 10 mCrab) 80% high res throughput on Perseus cluster (goal at CasA) 50 % 10 eV throughput at 1 Crab (5-8 keV)

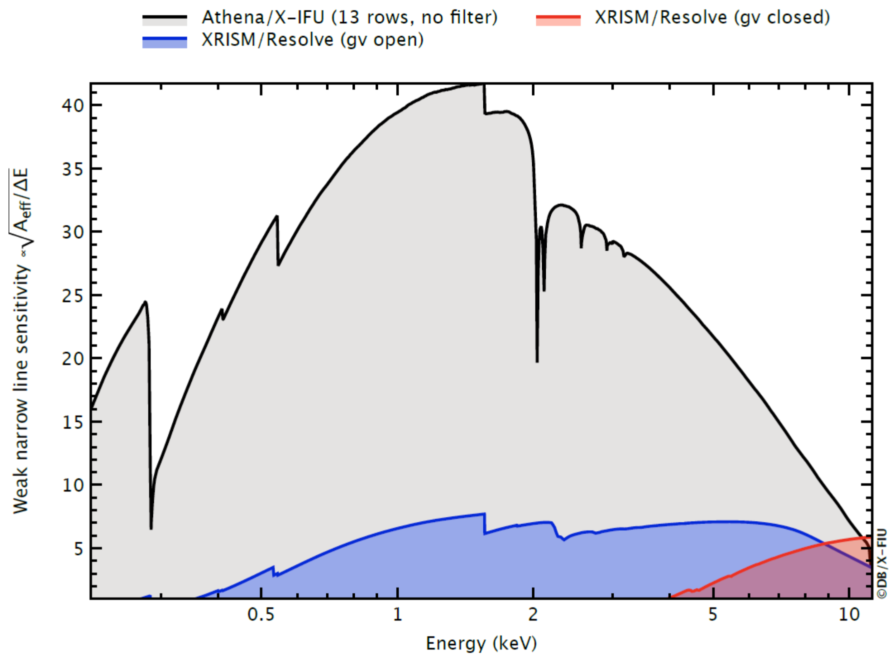

The X-IFU in the PLC

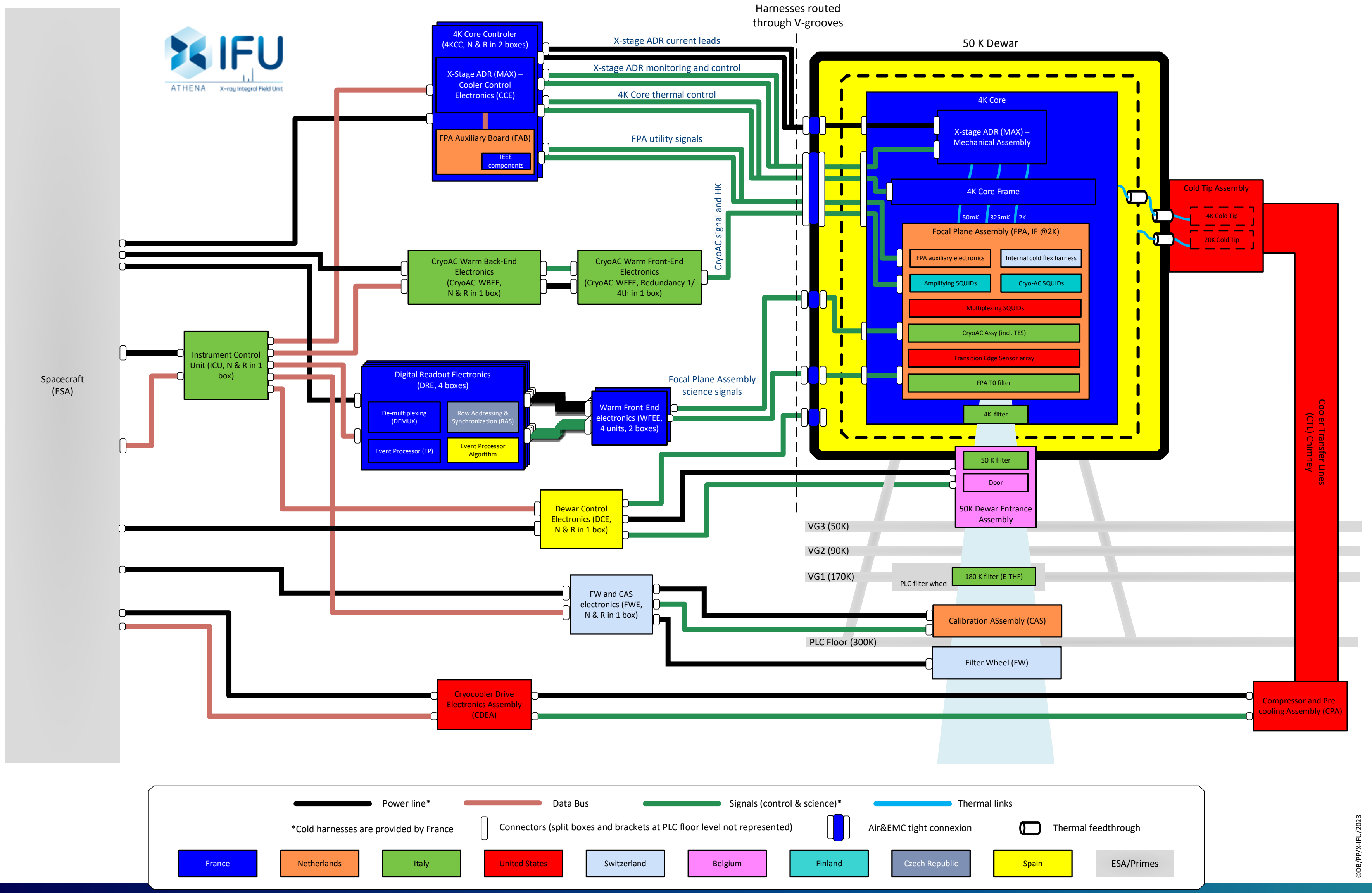

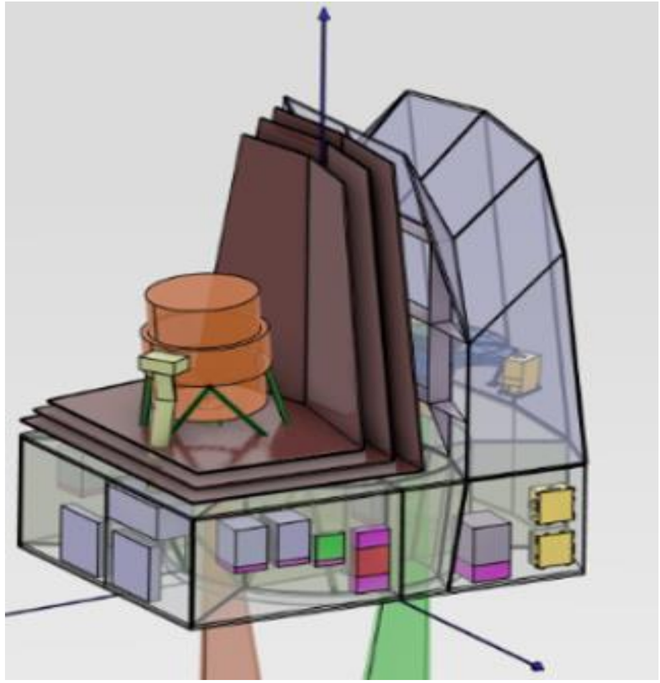

The X-IFU in the PLC

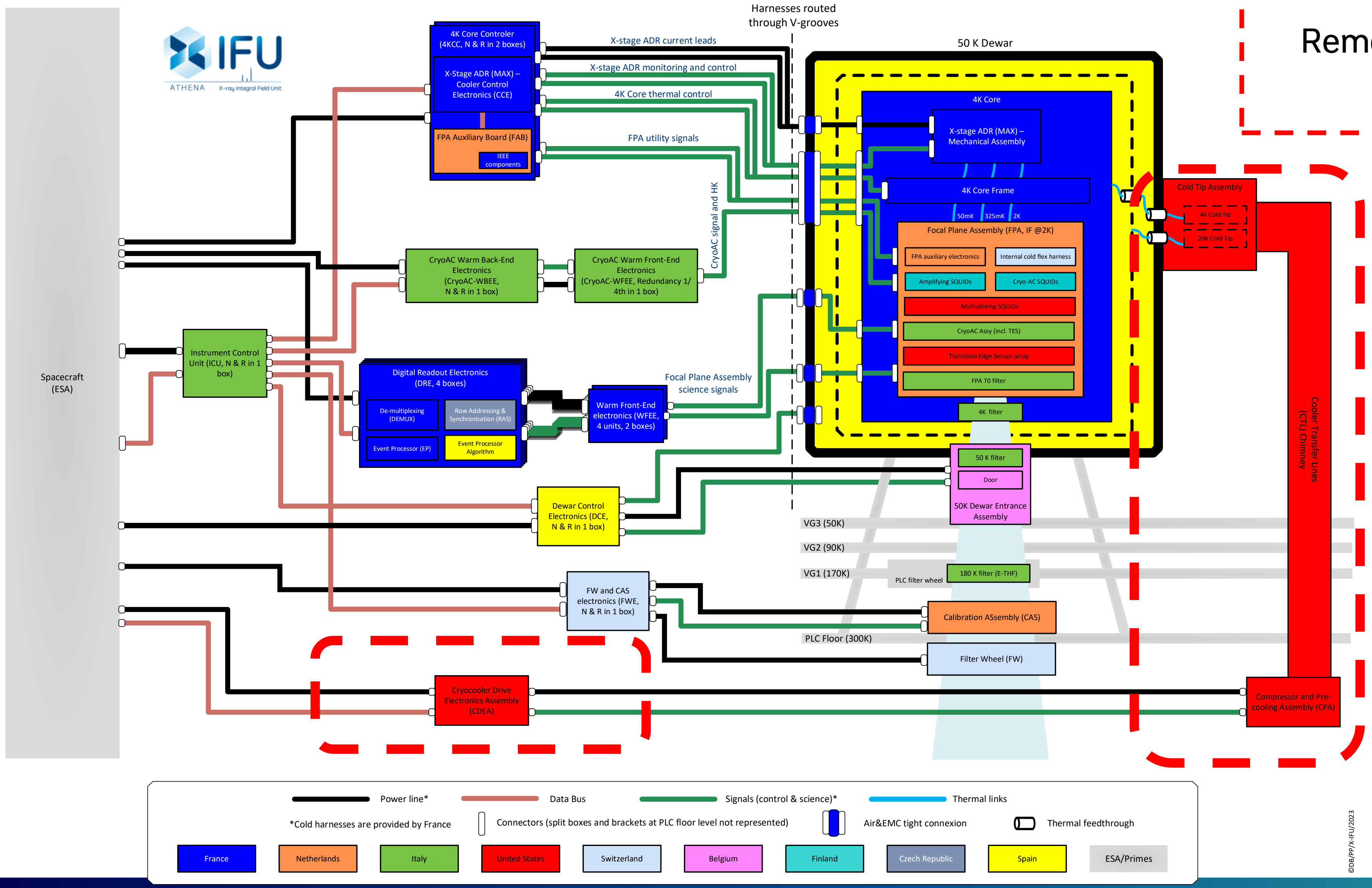

Remote US 4K cooler

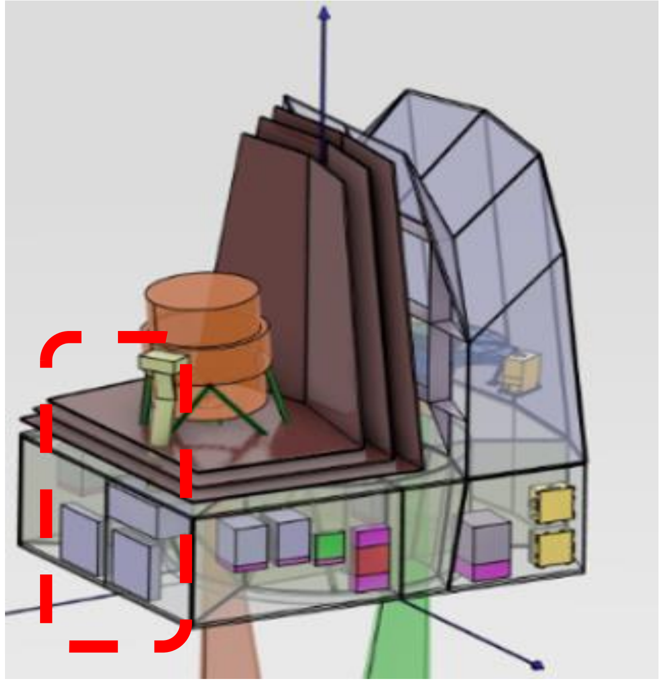

The X-IFU in the PLC

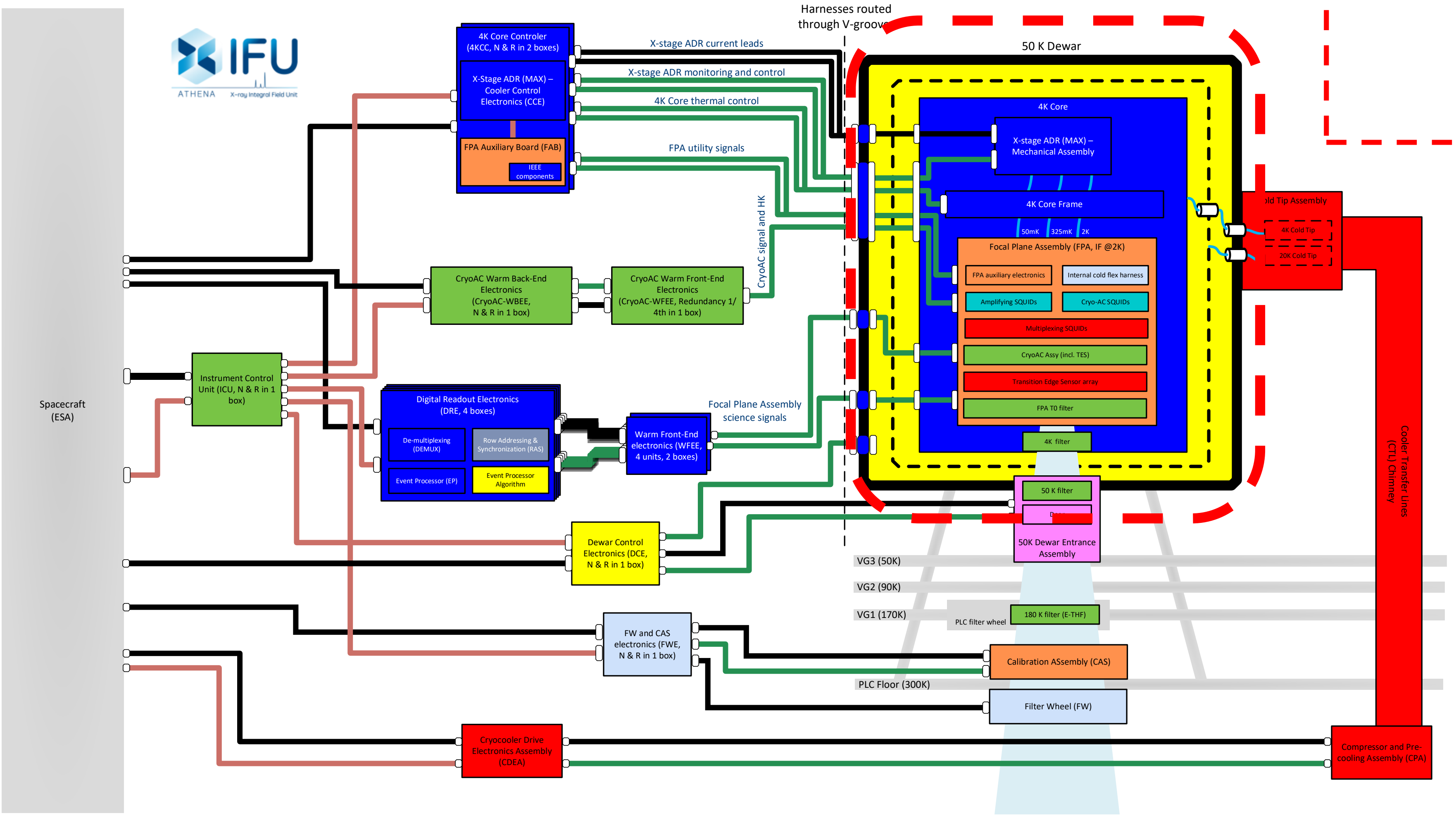

Power line*
Data Bus
Signals (control & science)*
Thermal links
*Cold harnesses are provided by France
Connectors (split boxes and brackets at PLC floor level not represented)
Air&EMC tight connexion
Thermal feedthrough

France	Netherlands	Italy	United States	Switzerland	Belgium	Finland	Czech Republic	Spain	ESA/Primes

50K Dewar (AVS)

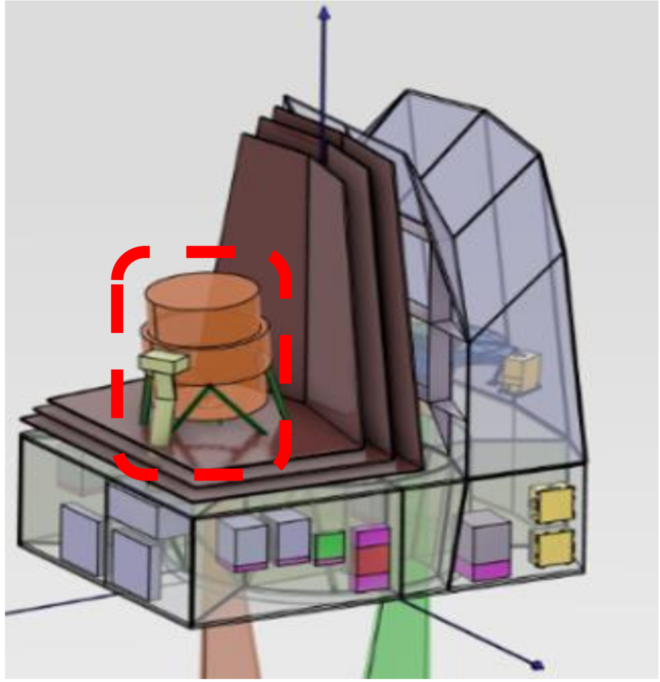

The X-IFU in the PLC

Warm electronics boxes in PLC « basement »

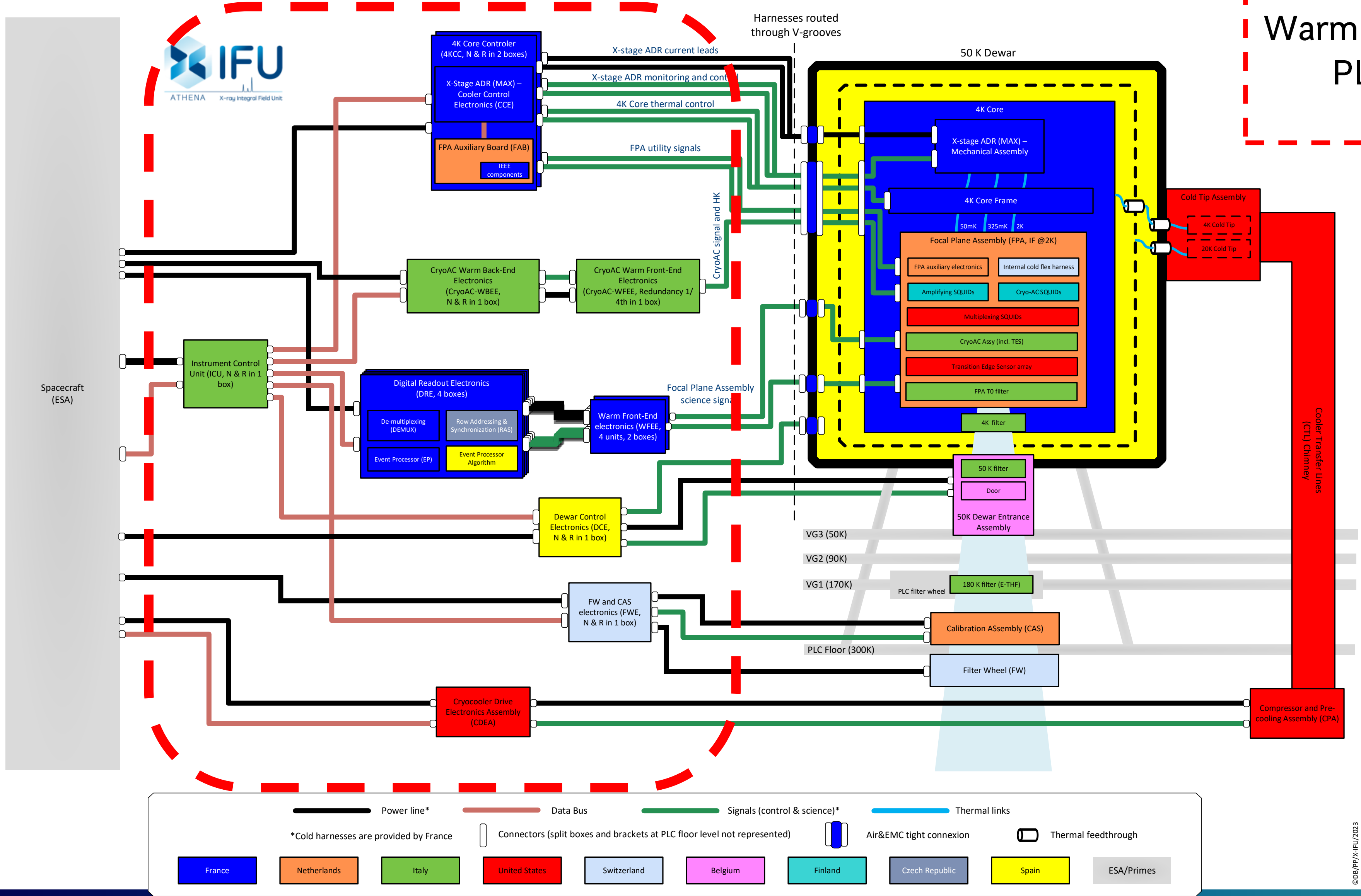

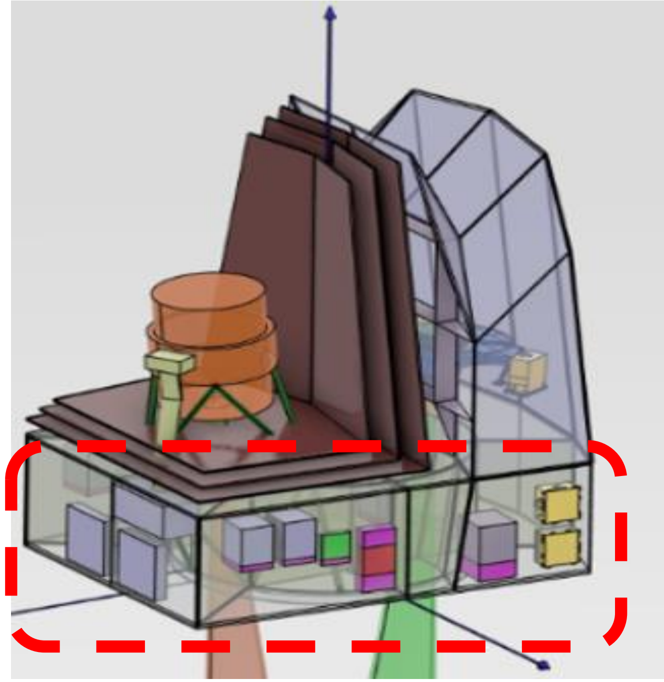

The X-IFU in the PLC

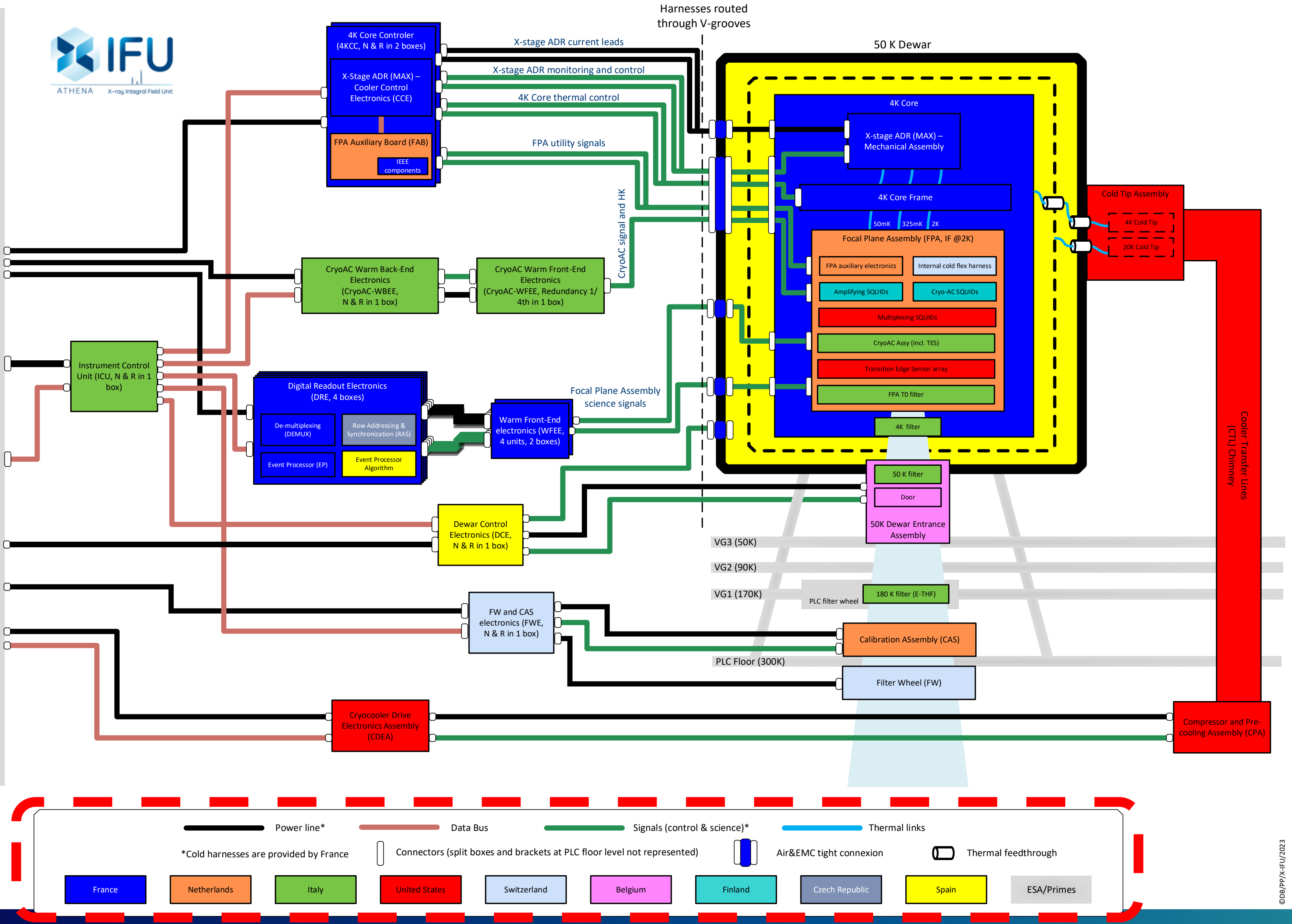

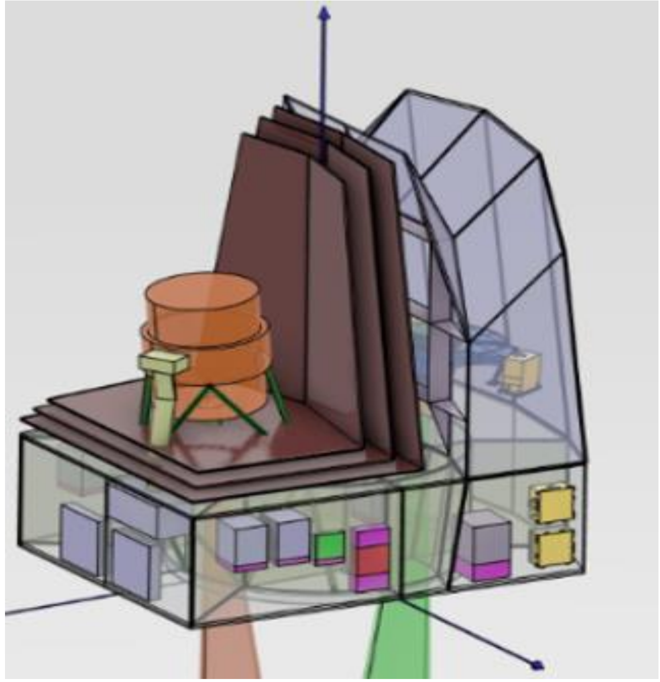

©DB/PP/X-IFU/2023

A large international collaboration

The new cryogenic architecture

- **New architecture following mission rescope**
  - **Dewar now under consortium responsibility (AVS). Passively cooled down to 50K via successive radiator panels**
  - **Active cooling down to 4.5K via remove US cooler**
    - Compressors and electronics in the « basement »
    - Competitive process in the US
- **Last stage cooling via multi-stage ADR (CEA SBT)**
  - **5 ADR pills**
    - ~ 1 mW at 2K
    - ~ 10 µW at 325 mK
    - ~ 1µW at 50 mK (~ 60 nW without margin from main detection chain cold electronics, ~ half in TES shunts, half in SQUIDs)

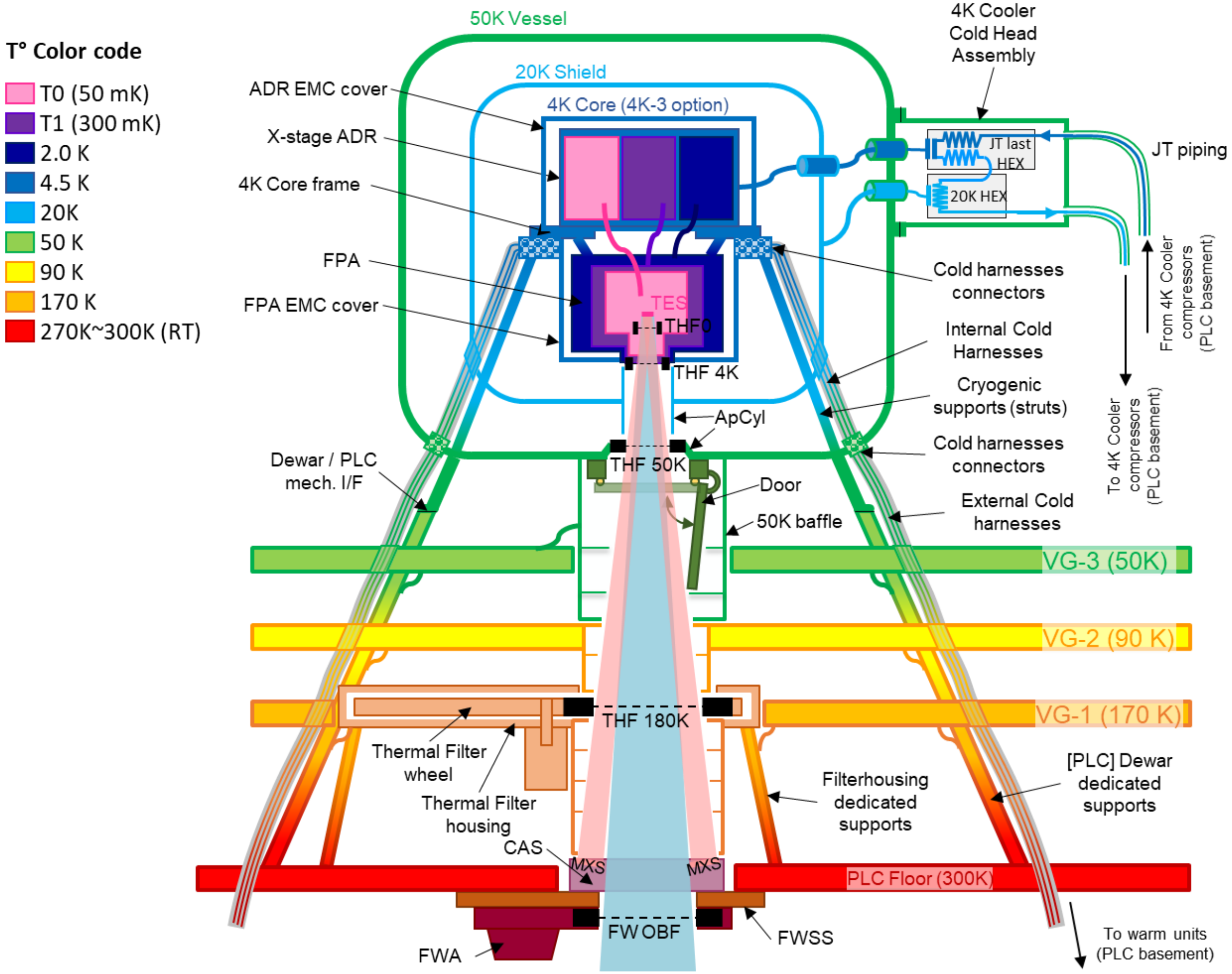

The new cryogenic architecture

- **New architecture following mission rescope**
  - **Dewar now under consortium responsibility (AVS). Passively cooled down to 50K via successive radiator panels**
  - **Active cooling down to 4.5K via remove US cooler**
    - Compressors and electronics in the « basement »
    - Competitive process in the US
- **Last stage cooling via multi-stage ADR (CEA SBT)**
  - **5 ADR pills**
    - ~ 1 mW at 2K
    - ~ 10 µW at 325 mK
    - ~ 1µW at 50 mK (~ 60 nW without margin from main detection chain cold electronics, ~ half in TES shunts, half in SQUIDs)

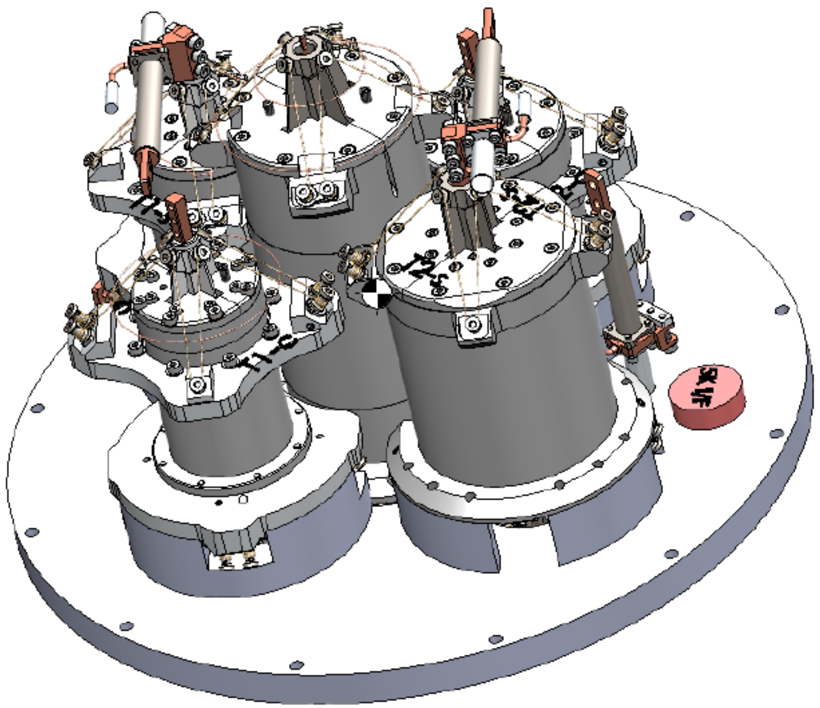

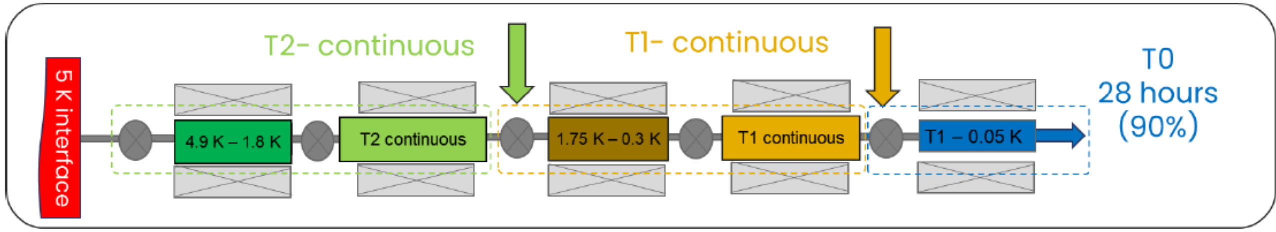

The 4K core

- **The « heart » of the instrument is organized in a 4K core**
  - **~ 45 kg, suspended inside 50 K dewar (likely via struts) with an interface at the green plate level**
  - **Faraday cage (on top of the 50 K dewar one) to protect scientific signals**
  - **Accommodates two main subsystems**
    - Focal Plane Assembly suspended at 2K by CFRP struts
    - Multistage ADR providing 2K, 325 mK (thermal intercept) and 50 mK cooling
  - **Superconducting looms between 4K and 2K**
  - **(« Tubes » are principle representations of harnesses to show interfaces)**

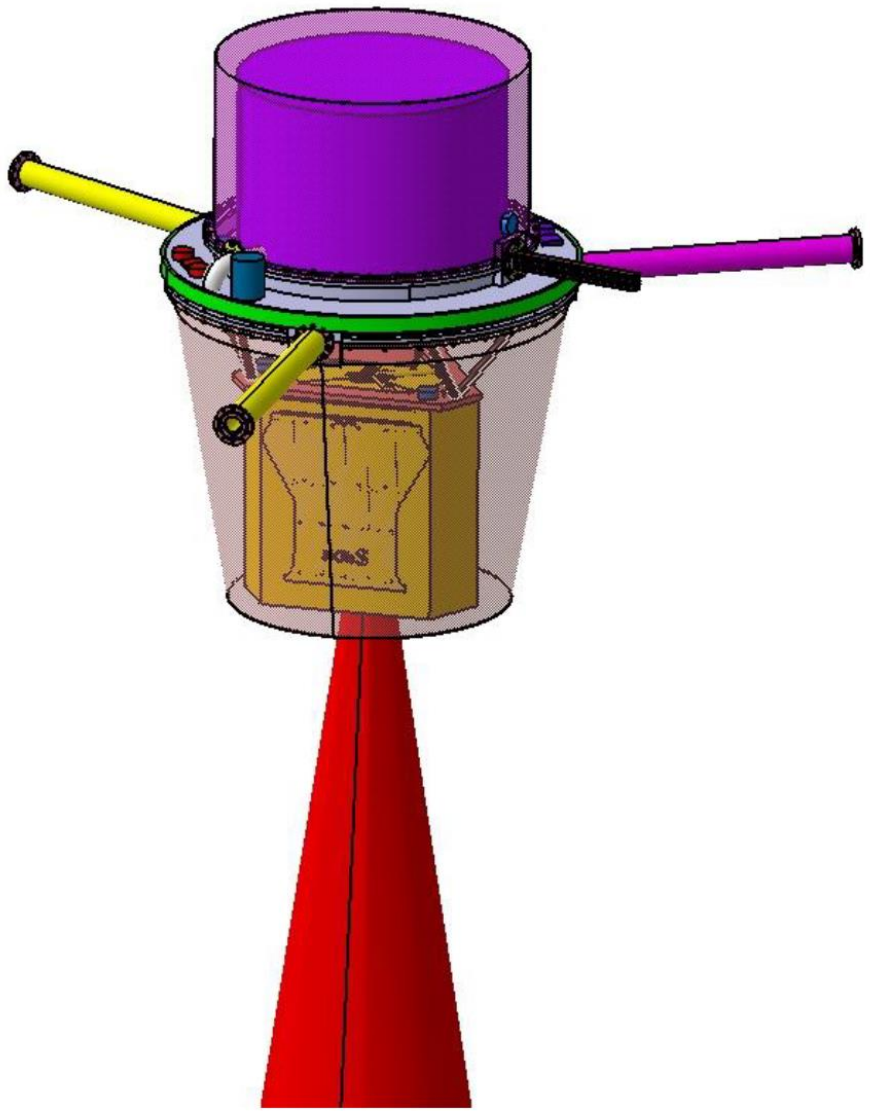

The 4K core

- **The « heart » of the instrument is organized in a 4K core**
  - **~ 45 kg, suspended inside 50 K dewar (likely via struts) with an interface at the green plate level**
  - **Faraday cage (on top of the 50 K dewar one) to protect scientific signals**
  - **Accommodates two main subsystems**
    - Focal Plane Assembly suspended at 2K by CFRP struts
    - Multistage ADR providing 2K, 325 mK (thermal intercept) and 50 mK cooling
  - **Superconducting looms between 4K and 2K**
  - **(« Tubes » are principle representations of harnesses to show interfaces)**

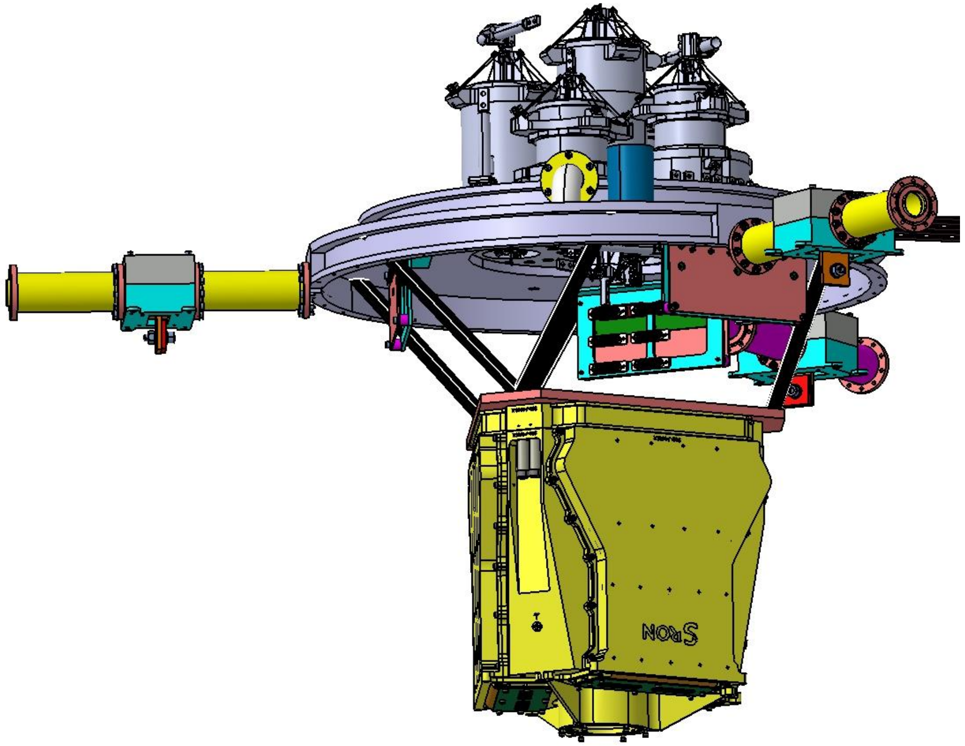

TES DETECTORS FOR X-IFU

cnes

Detection principle: Transition Edge Sensors (TES)

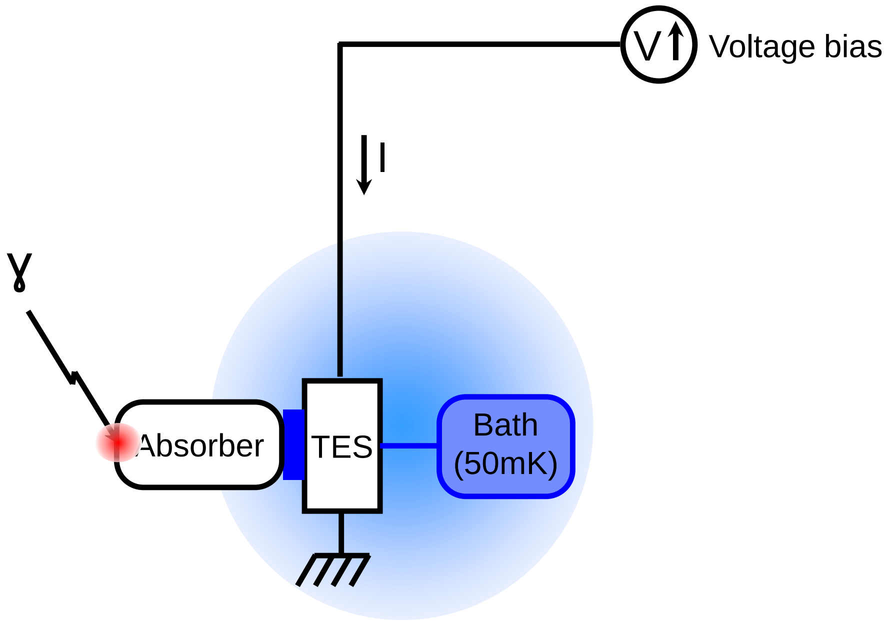

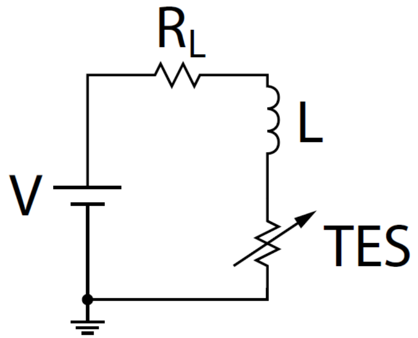

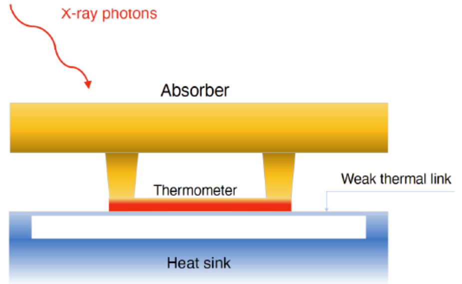

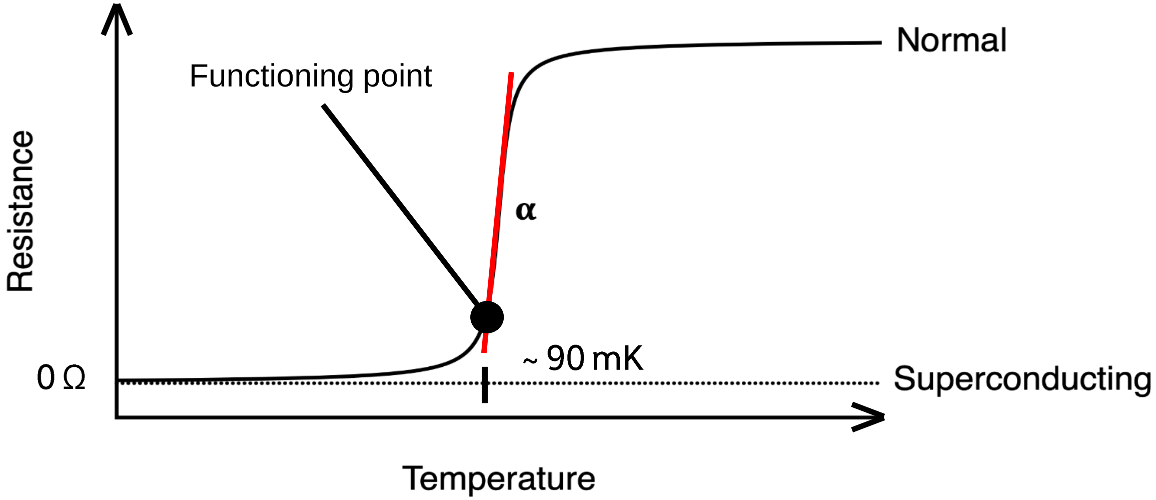

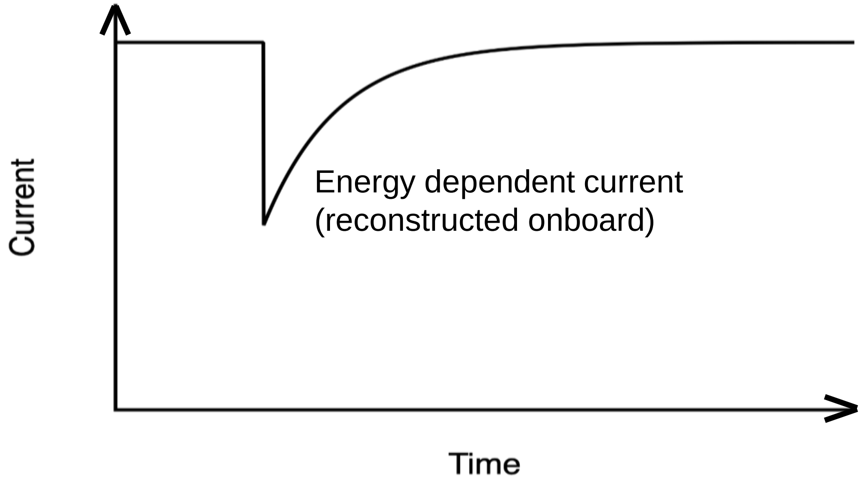

TES thermal equilibrium and electro-thermal feedback

- **The TES is maintained inside its transition by the Joule power provided by its bias**
- **Under (quasi) constant bias voltage, we have a negative electro-thermal feedback loop:**
  - $P_{Joule} = \dfrac{V^2}{R_{TES}(T,I)}$
  - $T \uparrow \Rightarrow R \uparrow \Rightarrow P_{Joule} \downarrow \Rightarrow T \downarrow$
- **Allows a stable operation of the TES in transition and speeds up the cooling of the TES after an X-ray impact => pushes the information towards higher frequency**
- **Note that devices with negative dR/dT (e.g. doped semiconductor detectors) in turn require being biased via a current**

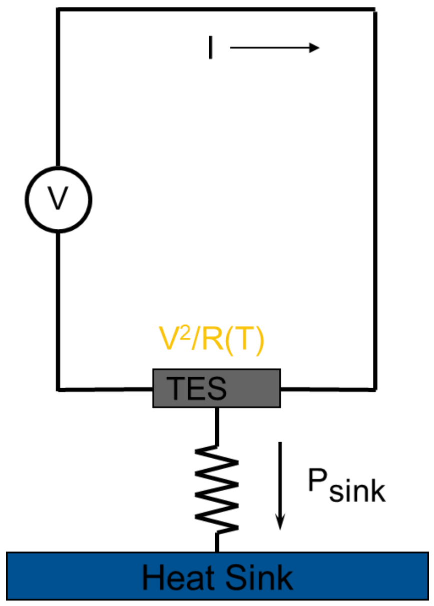

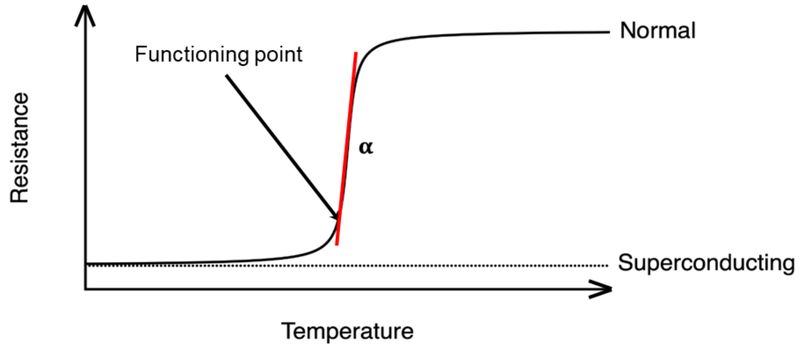

Main TES parameters and governing differential equations

- **The response of TES detectors is governed by two coupled differential equations**

$$L\frac{dI}{dt} = V_0 - IR_L - IR_{TES} + Noise$$

$$C\frac{dT}{dt} = -P_{sink} + R_{TES}I^2 + P_{Xray}$$

with $P_{sink} = K(T^n - T_{bath}^n) \approx P_{sink,0} + G\delta T$

$P_{Xray} = E_X/dt$

- **The TES transition itself is characterized locally by two main <u>unitless</u> parameters:**

$$\alpha = \left.\frac{\partial \log R}{\partial \log T}\right|_{I_0} \qquad \beta = \left.\frac{\partial \log R}{\partial \log I}\right|_{T_0}$$

$$R_{TES} \approx R_0 + \alpha\frac{R_0}{T_0} + \beta\frac{R_0}{I_0}$$

Pixel parameters definitions
R_n (mΩ) – TES normal resistance
T_0 (mK) – TES bias point temperature
G_b (pW/K) – Thermal conductance
C (pJ/K) – Total heat capacity
n – Thermal exponent
T_{bath} (mK) – Bath temperature
R_0 (mΩ) – TES bias point resistance
R_s (μΩ) – Shunt resistance
I_0 (μA) – TES current at bias point
α $(T/R\ \partial R/\partial T)$
β $(I/R\ \partial R/\partial I)$
$\mathcal{L}_I$ $(P_0\alpha/GT_0)$ – ETF loop gain
M – Unexplained Johnson noise factor
L (nH) – Damping inductance
τ_+/τ_- (μs) – Detector time constants at L
f_{eff}(Hz) – Effective frequency

Main TES parameters and governing differential equations

- The response of TES detectors is governed by two coupled differential equations

$$L\frac{dI}{dt} = V_0 - IR_L - IR_{TES} + Noise$$

$$C\frac{dT}{dt} = -P_{sink} + R_{TES}I^2 + P_{Xray}$$

with $P_{sink} = K(T^n - T_{bath}^n) \approx P_{sink,0} + G\delta T$

$P_{Xray} = E_X/dt$

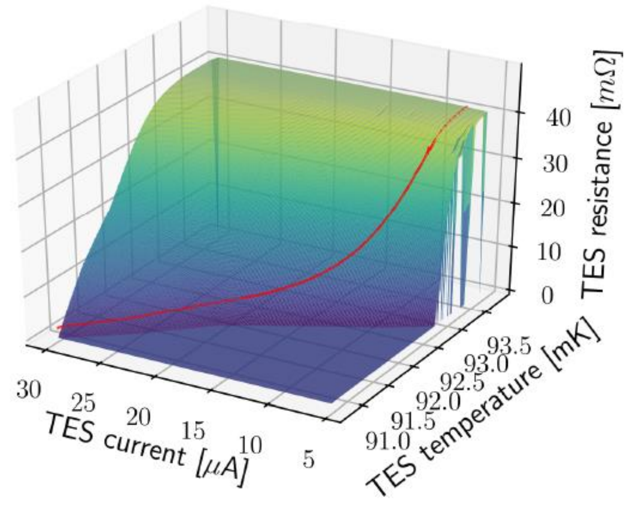

Gottardi&Nagayashi+21

- The TES transition itself is characterized locally by two main <u>unitless</u> parameters:

$$\alpha = \left.\frac{\partial \log R}{\partial \log T}\right|_{I_0} \qquad \beta = \left.\frac{\partial \log R}{\partial \log I}\right|_{T_0}$$

$$R_{TES} \approx R_0 + \alpha\frac{R_0}{T_0} + \beta\frac{R_0}{I_0}$$

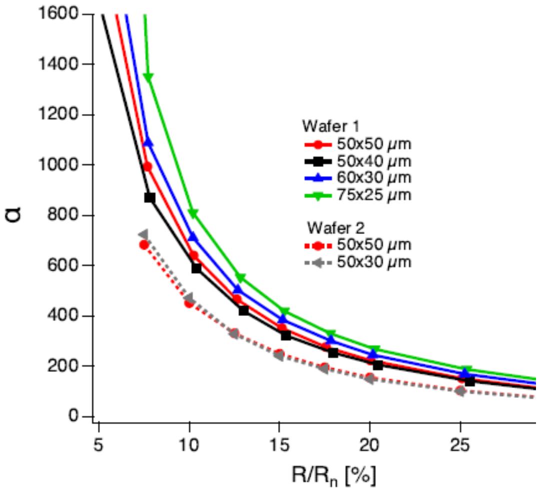

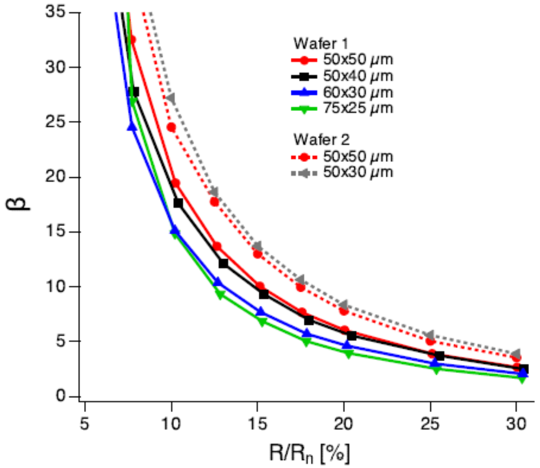

Wakeham+23

Main TES parameters and governing differential equations

- **The response of TES detectors is governed by two coupled differential equations**

$$L\frac{dI}{dt} = V_0 - IR_L - IR_{TES} + Noise$$

$$C\frac{dT}{dt} = -P_{sink} + R_{TES}I^2 + P_{Xray}$$

with $P_{sink} = K(T^n - T_{bath}^n) \approx P_{sink,0} + G\delta T$

$P_{Xray} = E_X/dt$

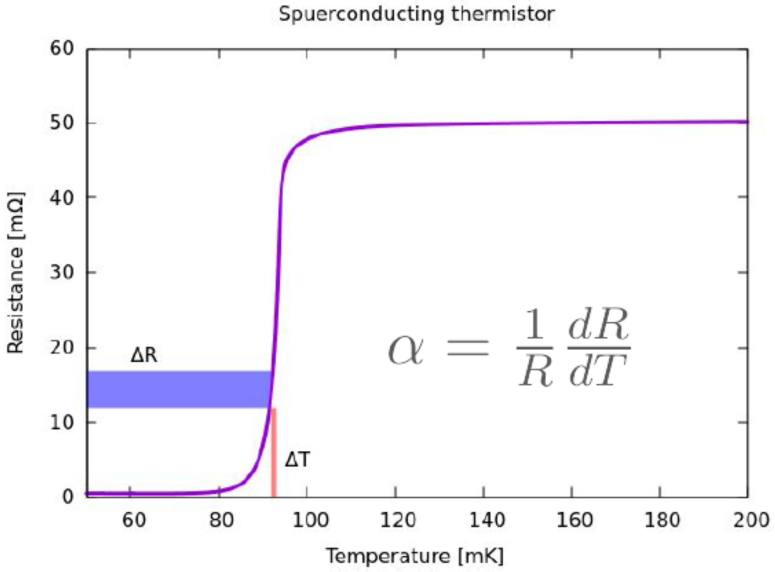

Plot from M. Gonzalez's LTD intro

- **The TES transition itself is characterized locally by two main <u>unitless</u> parameters:**

$$\alpha = \left.\frac{\partial \log R}{\partial \log T}\right|_{I_0} \qquad \beta = \left.\frac{\partial \log R}{\partial \log I}\right|_{T_0}$$

WARNING: Different convention from M. Gonzalez's ltd intro (see above)

$$R_{TES} \approx R_0 + \alpha\frac{R_0}{T_0} + \beta\frac{R_0}{I_0}$$

Small signal TES impulse response: an X-ray pulse

- **In the small signal limit (see Lindeman+00, Irwin&Hilton+05), the TES response follows**

$$\delta I \propto \left(e^{-t/\tau_+} - e^{-t/\tau_-}\right)$$

with $1/\tau_+$ and $1/\tau_-$ the eigen values of the differential system

- **The response is stable (critically or overdamped) if τ_+ and τ_- are real. This reduces to a constraint on the circuit inductance**
  - The circuit is underdamped (there are oscillations) if $L_{crit-} \leq L \leq L_{crit+}$
  - Typically, TES circuits are dimensioned such that $L \leq L_{crit-}$
- **In the low inductance and stiff bias voltage limit ($R_{shunt} \ll R_0$):**

$$\tau_+ \to \frac{L}{R_{shunt} + R_0(1+\beta)}$$ electrical time constant

$$\tau_- \to \tau_{eff} = \frac{C}{G}\frac{1+\beta}{1+\beta+\mathcal{L}_I}$$ thermal time constant, accelerated by ETF

- **The readout circuit has to cope with the initial sharp electrical rise whereas the pulse information is rather contained in the slower thermal response**
  - For a large part of the project, the circuit was thus optimized to operate near critical damping ($\tau_+ = \tau_-$)

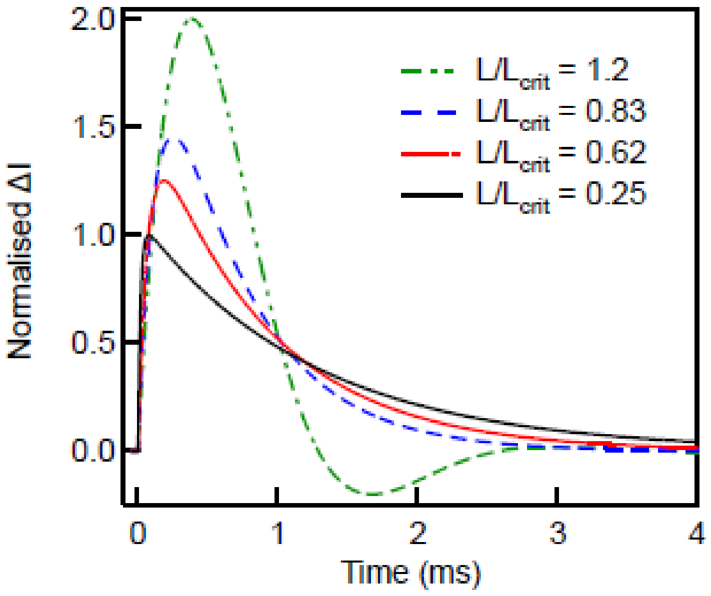

Gottardi&Smith+22

Main TES noise contributors

- **Phonon noise (aka thermal fluctuation noise)**
  - $S_{P_{TFN}} = 4k_B T_0^2 G F(T_0, T_{bath})$ **(fluctuations across the thermal link to the bath)**
- **Johnson noise from the load resistor**
  - $S_{V_{JN,L}} = 4k_B T_0 R_L$ **(electrical fluctuations in the shunt resistor)**
- **TES Johnson noise**
  - $S_{V_{JN,TES}} = 4k_B T_0 R_0 \zeta(I_0)$ **(electrical fluctuations in the TES resistance, but amplified by the TES non-linear response)**
  - **Without any other fluctuation mechanism than the impact of the TES current sensitivity, $\zeta(I_0) = 1 + 2\beta$ (I&H+00)**
  - **In practice, only really works at low β values. Most recent TESs for X-ray applications exhibit an "unexplained" noise in the TES electrical band: $S_{V_{TES}} = 4k_B T_0 R_0 (1 + 2\beta + M^2)$**
    - Hard to distinguish from internal thermal fluctuation noise (thermal fluctuations inside the TES, e.g. due to more than one heat capacity, imperfect thermalization, …). It has the same frequency response
  - **Each white thermodynamical fluctuations is transformed by the TES system and gets a distinct frequency response**

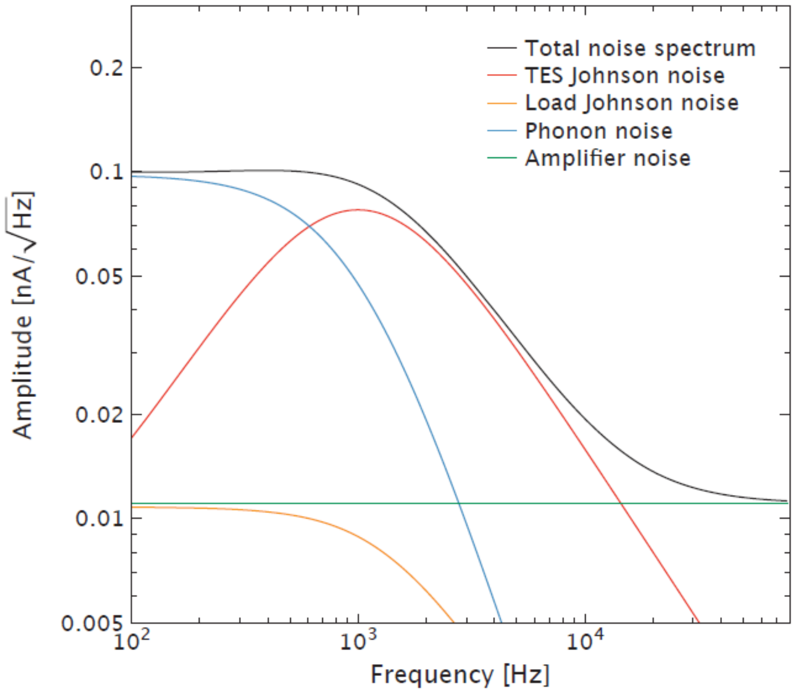

Main TES noise contributors

- **Phonon noise (aka thermal fluctuation noise)**
  - $S_{P_{TFN}} = 4k_B T_0^2 G F(T_0, T_{bath})$ **(fluctuations across the thermal link to the bath)**
- **Johnson noise from the load resistor**
  - $S_{V_{JN,L}} = 4k_B T_0 R_L$ **(electrical fluctuations in the shunt resistor)**
- **TES Johnson noise**
  - $S_{V_{JN,TES}} = 4k_B T_0 R_0 \zeta(I_0)$ **(electrical fluctuations in the TES resistance, but amplified by the TES non-linear response)**
  - **Without any other fluctuation mechanism than the impact of the TES current sensitivity, $\zeta(I_0) = 1 + 2\beta$ (I&H+00)**
  - **In practice, only really works at low β values. Most recent TESs for X-ray applications exhibit an “unexplained” noise in the TES electrical band: $S_{V_{TES}} = 4k_B T_0 R_0 (1 + 2\beta + M^2)$**
    - Hard to distinguish from internal thermal fluctuation noise (thermal fluctuations inside the TES, e.g. due to more than one heat capacity, imperfect thermalization, …). It has the same frequency response
  - **Each white thermodynamical fluctuations is transformed by the TES system and gets a distinct frequency response**

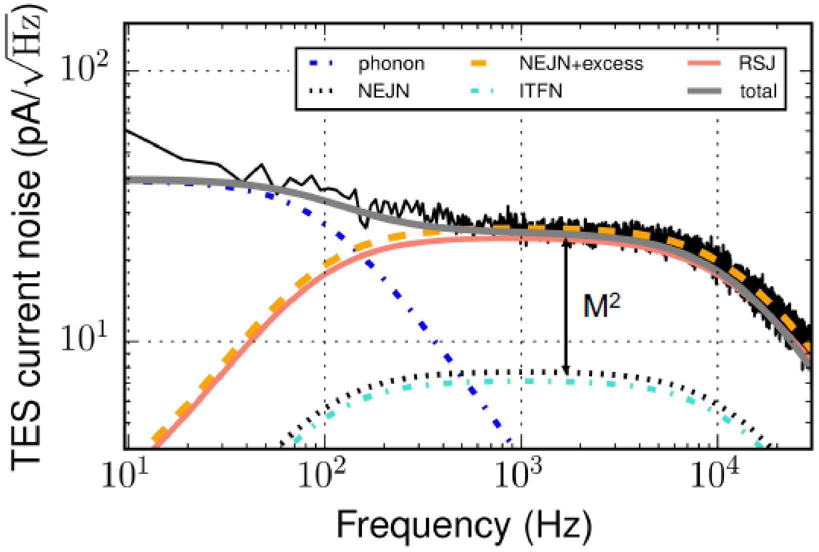

Gottardi&Smith+22

TES energy resolution and main driving parameters

- The TES energy resolution is given by the integrated signal to noise density:

$$\Delta E_{FWHM} = \sqrt{8\log(2)}\left(\int_0^\infty 4SNRD^2(f)df\right)^{-1/2}$$

$$= \sqrt{8\log(2)}\left(\int_0^\infty \frac{4}{NEP^2(f)}df\right)^{-1/2}$$

TES responsivity
(= FT of normalized pulse)

$$= \sqrt{8\log(2)}\left(\int_0^\infty \frac{4|s_I(f)|^2}{S_{I_{TFN}}(f) + S_{I_{JN,TES}}(f) + S_{I_{JN,L}}(f)}df\right)^{-1/2}$$

- In the small signal limit, without amplifier noise and in strong ETF case:

$$\Delta E_{FWHM} \propto \sqrt{\frac{4k_B T_0^2 C\sqrt{\zeta(I_0)}}{\alpha}}$$

Simplified TES model at high ETF and (very) low inductance
=> Information limited by Johnson noise

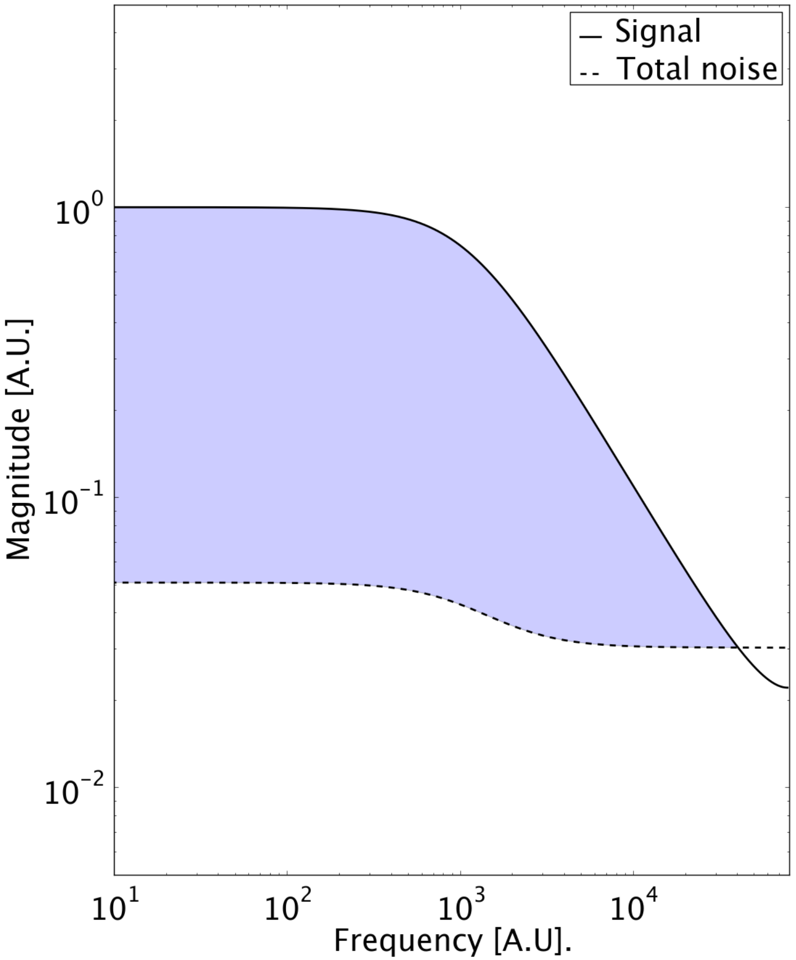

Impact of different TES parameters on performances: Temperature

$$\Delta E_{FWHM} \approx \sqrt{\frac{4k_B T_0^2 C\sqrt{\zeta(I_0)}}{\alpha}\sqrt{\frac{nF(T_0,T_{bath})}{1-(T_{bath}/T_0)^n}}}$$

~ 0.5

~3

for X-IFU TES

- **Usual « the colder the better » ($4k_BT_0^2$ noise scaling shared by all thermal detectors)**
  - **But need lower Tc and colder thermal bath (fluctuations become much stronger when trying to operate a TES close to the thermal bath temperature)**
  - **For X-IFU, $T_{bath} = 55\,mK$ (including ΔT in thermal link between last stage cooler and detector), $T_c \approx 90\,mK$**

Impact of different TES parameters on performances: Heat capacity

$$\Delta E_{FWHM} \approx \sqrt{\frac{4k_B T_0^2 C\sqrt{\zeta(I_0)}}{\alpha}\sqrt{\frac{nF(T_0,T_{bath})}{1-(T_{bath}/T_0)^n}}}$$

- **Reducing C (but keeping τ fixed):**
  - **Both sensitivity and transduced thermal noise increase linearly**
  - **Translates into a bandwidth increase => $\sqrt{C}$ impact on ΔE**
  - **Limited by intrinsic heat capacity of TES, heat capacity of absorber required for the X-ray stopping power and required energy range**
  - **X-IFU absorber made of a main bilayer of gold (good lateral thermal conductivity) and electroplated bismuth (better stopping power to heat capacity ratio)**
    - Small gold cap on top of absorber to increase IR reflectivity and protect absorber (Bi) from humidity

Simplified TES model at high ETF and (very) low inductance
=> Information limited by Johnson noise

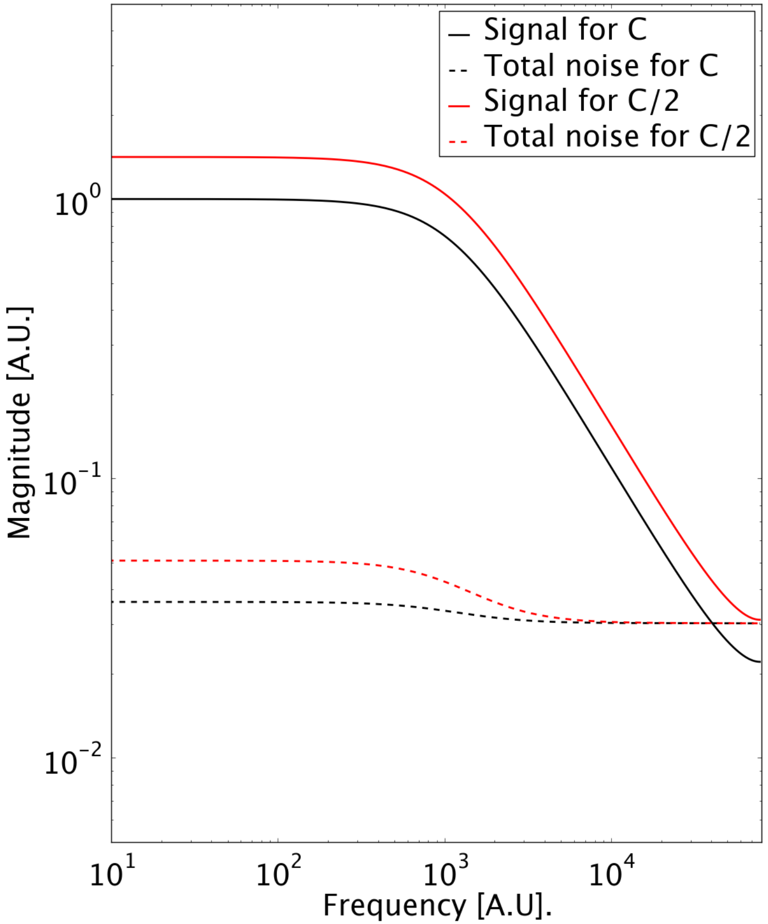

Impact of different TES parameters on performances: Heat capacity

$$\Delta E_{FWHM} \approx \sqrt{\frac{4k_B T_0^2 C\sqrt{\zeta(I_0)}}{\alpha}\sqrt{\frac{nF(T_0,T_{bath})}{1-(T_{bath}/T_0)^n}}}$$

- **Reducing C (but keeping τ fixed):**
  - **Both sensitivity and transduced thermal noise increase linearly**
  - **Translates into a bandwidth increase => $\sqrt{C}$ impact on ΔE**
  - **Limited by intrinsic heat capacity of TES, heat capacity of absorber required for the X-ray stopping power and required energy range**
  - **X-IFU absorber made of a main bilayer of gold (good lateral thermal conductivity) and electroplated bismuth (better stopping power to heat capacity ratio)**
    - Small gold cap on top of absorber to increase IR reflectivity and protect absorber (Bi) from humidity

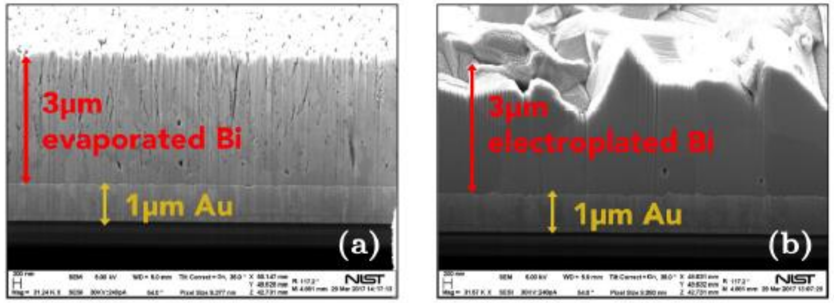

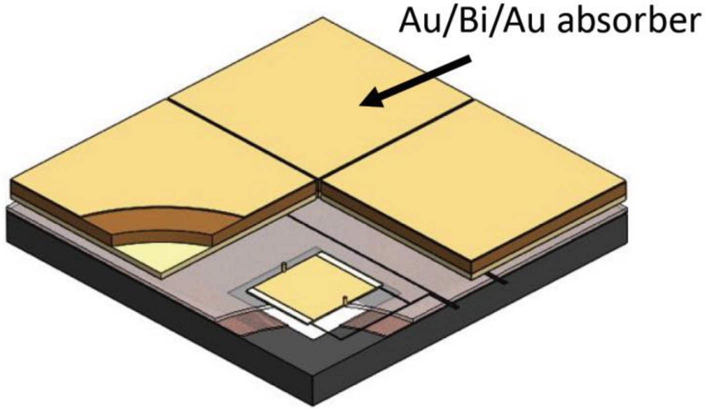

Impact of different TES parameters on performances: alpha

$$\Delta E_{FWHM} \approx \sqrt{\frac{4k_B T_0^2 C\sqrt{\zeta(I_0)}}{\alpha}\sqrt{\frac{nF(T_0, T_{bath})}{1-(T_{bath}/T_0)^n}}}$$

- **Increasing alpha:**
  - **In strong ETF limit, manifests itself as a bandwidth increase => $1/\sqrt{\alpha}$ scaling**

Simplified TES model at high ETF and (very) low inductance
=> Information limited by Johnson noise

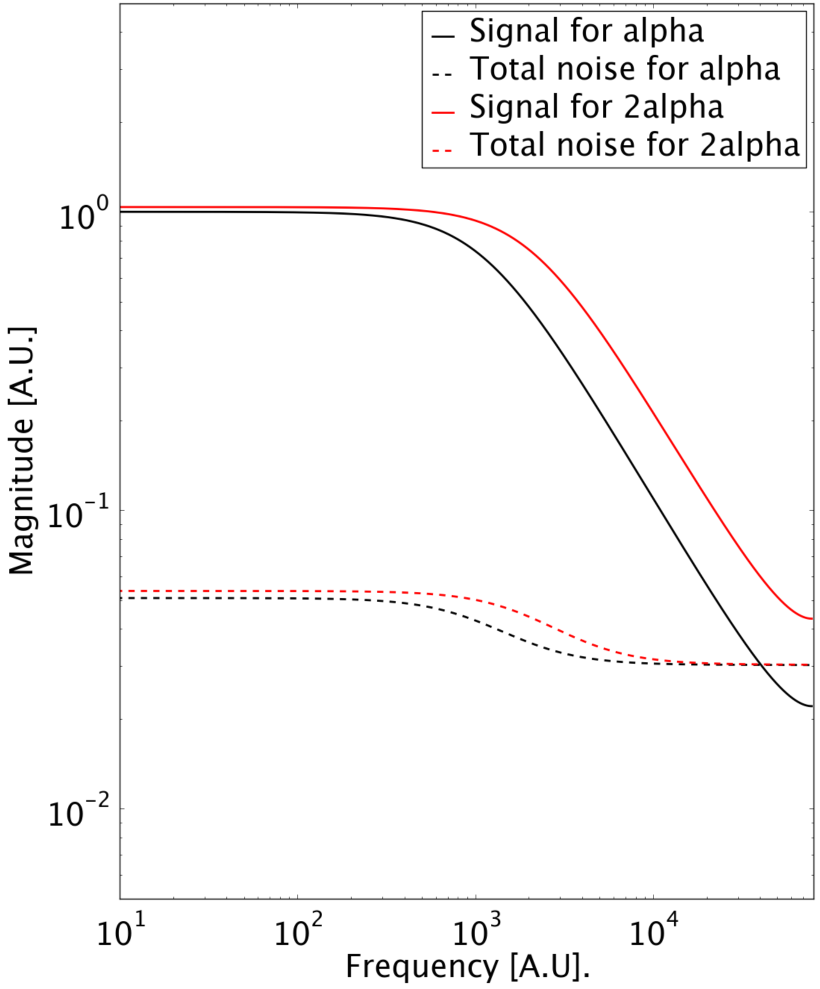

What about pixel speed/bath conductivity?

$$\Delta E_{FWHM} \approx \sqrt{\frac{4k_B T_0^2 C\sqrt{\zeta(I_0)}}{\alpha}\sqrt{\frac{nF(T_0, T_{bath})}{1-(T_{bath}/T_0)^n}}}$$

- What happens when we change G? Warning: « rough arguments »
  - The low frequency response density scales as $1/G$
  - Phonon noise amplitude scales as $\sqrt{G}$
- BUT… to recover same TES setpoint temperature, need to decrease Joule power and thus current scales as $1/\sqrt{G}$ => overall signal range scales as $1/\sqrt{G}$. In total:
  - Response scales as $1/\sqrt{G}$
  - Phonon noise does not change
  - Johnson noise does not change
- And bandwidth scales as G
- Overall $SNR \times \sqrt{BW}$ is conserved => ΔE does not depend on G at first order

Note Fourier transform scaling: if x(t)→X(w), then x(at)→X(w/a)/|a|

Simplified TES model at high ETF and (very) low inductance
=> Information limited by Johnson noise

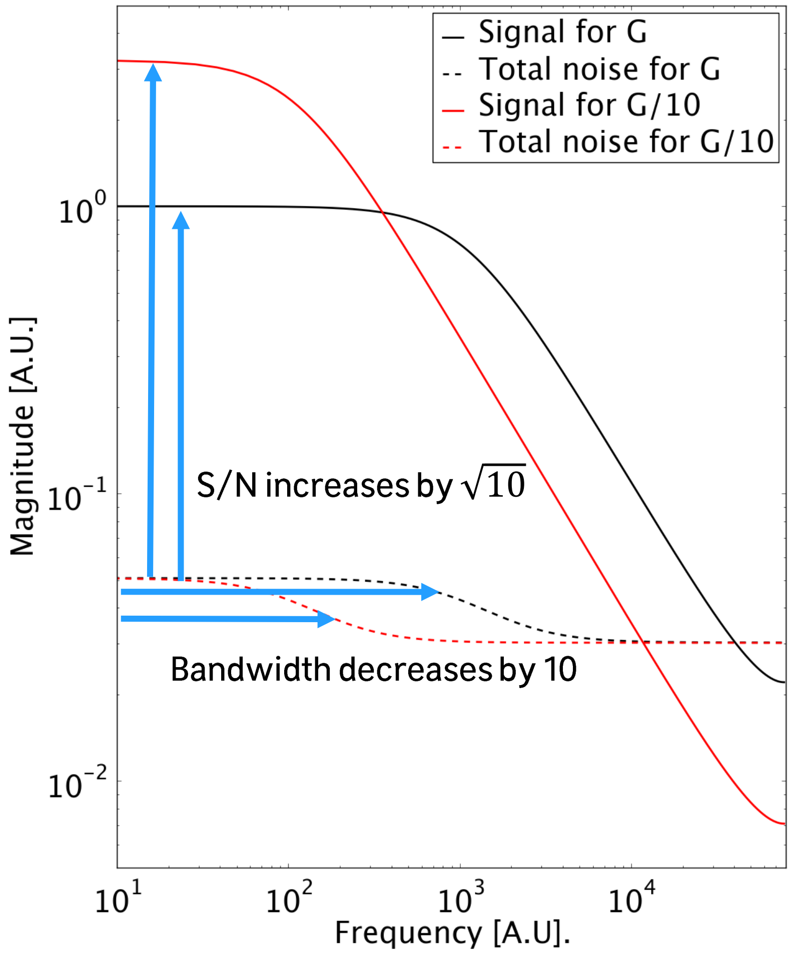

Optimal filtering (matched filter)

- **The energy of each X-ray pulse needs to be measured on board**
  - At 2 cps/pxl and ~ 50 ms pulse records sampled on 16 bits at 130 kHz, the current useful X-IFU data rate ≈ 300 Mbits/s…
- **Most X-ray calorimeters use *Optimal Filtering*. It assumes (as an approximation – both are wrong! But it works):**
  - Pulses are linear with energy : $d(t) = E \times s(t)$
  - Noise is stationary: noise PSD $N^2(f)$ is sufficient to describe the full system noise
- **χ^2 minimization problem in the Fourier Space:**

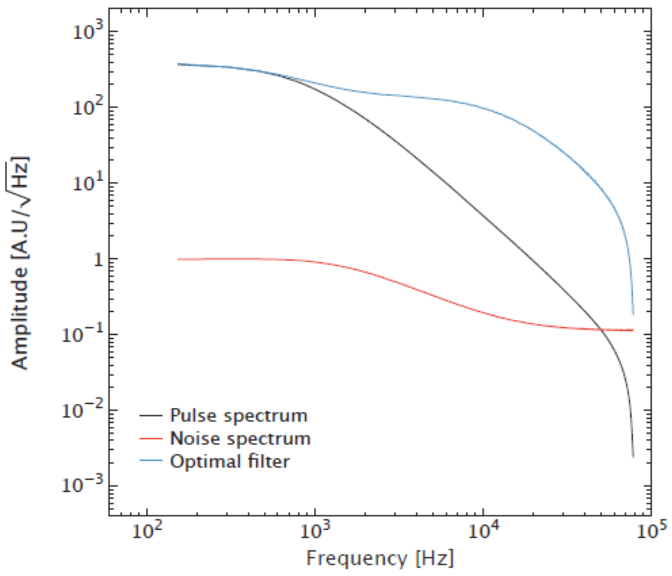

$$\min\left(\sum \frac{|D(f) - E \times S(f)|^2}{|N^2(f)|}\right) \Rightarrow \hat{E} = \frac{\langle D(f), S^*(f)/N^2(f)\rangle}{\sum |S(f)|^2/N^2(f)}$$

Weighting by Noise Spectral Density

Equivalent in time domain: $$\hat{E} = \frac{\left\langle d(t), \mathcal{FFT}^{-1}\left\{\frac{S(f)}{N^2(f)}\right\}\right\rangle}{\sum |S(f)|^2/N^2(f)}$$

The time domain optimal filter

Optimal filtering (matched filter)

- The energy of each X-ray pulse needs to be measured on board
  - At 2 cps/pxl and ~ 50 ms pulse records sampled on 16 bits at 130 kHz, the current useful X-IFU data rate ≈ 300 Mbits/s…
- Most X-ray calorimeters use *Optimal Filtering*. It assumes (as an approximation – both are wrong! But it works):
  - Pulses are linear with energy : $d(t) = E \times s(t)$
  - Noise is stationary: noise PSD $N^2(f)$ is sufficient to describe the full system noise
- χ^2 minimization problem in the Fourier Space:

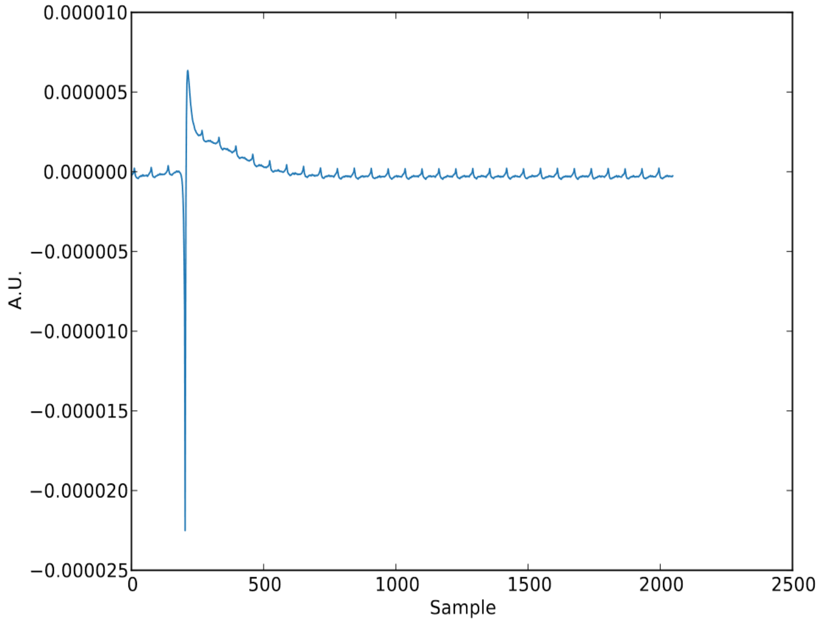

$$\min\left(\sum \frac{|D(f) - E \times S(f)|^2}{|N^2(f)|}\right) \Rightarrow \hat{E} = \frac{\langle D(f), S^*(f)/N^2(f)\rangle}{\sum |S(f)|^2/N^2(f)}$$

Weighting by Noise Spectral Density

Equivalent in time domain: $$\hat{E} = \frac{\left\langle d(t), \mathcal{FFT}^{-1}\left\{\frac{S(f)}{N^2(f)}\right\}\right\rangle}{\sum |S(f)|^2/N^2(f)}$$

The time domain optimal filter

Record length degradation

- **The 0Hz bin of the OF is usually removed (the filter becomes zero-summed)**
  - **Energy reconstruction becomes insensitive to offsets and in general less sensitive to low frequency noise (e.g. 1/f)**
    - Not to low frequency gain variation though (e.g. temperature, bias, drifts)!
  - **Information is lost. The shorter the filter (record), the larger the degradation (Doriese+09):**

$$\Delta E = \sqrt{8\log(2)}\left(\int_{1/2t_{rec}}^{\infty} 4SNRD^2(f)df\right)^{-1/2} = \frac{\lim_{t_{rec}\to\infty} \Delta E}{\sqrt{1-1/(2t_{rec}f_{eff})}}$$

with $f_{eff} = \frac{\int_0^\infty SNRD^2(f)df}{\lim_{f\to 0} SNRD^2(f)}$

- **Slower (easier to readout) pixels lead to larger degradation**

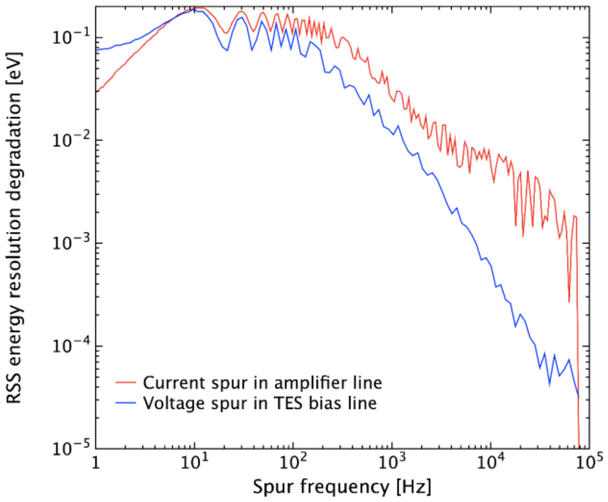

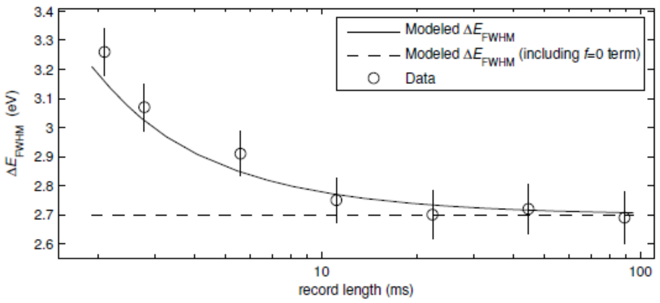

Count rate capability

- **X-ray photons arrival times are governed by Poisson statistics**
  - **Depending on time separation, the quality of the energy reconstruction can be degraded**
  - **Grading scheme used to identify high (and lower grade) resolution events. Creates branching ratios as a function of count rate**
- **An X-ray calorimeter count rate capability is thus usually defined as a fraction of high resolution events to be met at a given count rate**
- **This C.R. requirement, yields a maximum total time period Δt_{tot} that is permitted to process an X-ray event:**

For uniform count rate: $$P(HR) = P(no\ evt\ in\ \Delta t_{tot}) = e^{-c\Delta t_{tot}} \Rightarrow \Delta t_{tot} = -\frac{\log P(HR)}{c}$$

For non-uniform count rate (e.g. point sources) : $$P(HR) = \sum_{pixels} f_i P(HR)_i = \sum_{pixels} f_i\, e^{-c_i \Delta t_{tot}} \Rightarrow \Delta t_{tot} = \cdots$$

$$\Delta t_{tot} = 10\,\tau_{fall} + t_{rec}$$

Simplified secondaries exclusion

Available time for pulse processing

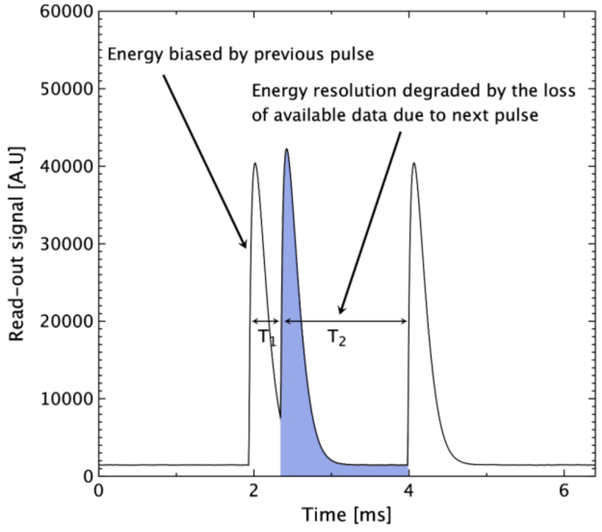

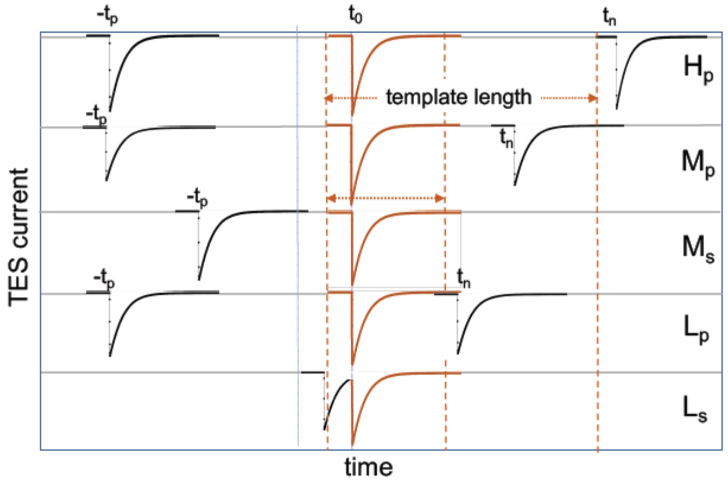

SXS event grading

What about X-IFU? On focus constraint

- **Two main types of count rate capability requirements:**
  - **Point source: 80% throughput at 1 mCrab, goal at 10 mCrab**
  - **Extended source: 80% throughput on Perseus cluster, goal at CasA**
- **Without defocusing, in the original X-IFU concept (250µm pixel pitch), 1mCrab lead to ~ 42 cps on central pixel (also larger mirror)!**
  - **80% throughput criterion yields $\Delta T_{tot} = 11\text{ms}$**
  - **Much tighter constraint than extended source goal (2.3 cps/pxl => $\Delta T_{tot} = 97\text{ms}$)**
- **Which pixel speed is required to make this work?**
  - **As a simplification, $\tau_{fall} \approx \tau_{eff}$ and f_{eff} scaled together with respect to original « Large Pixel Array » pixel parameters (Smith+16) ⬄ scaling G without changing other parameters**
  - **For a 2 eV intrinsic detector, need f_{eff} in the range of 1 kHz**

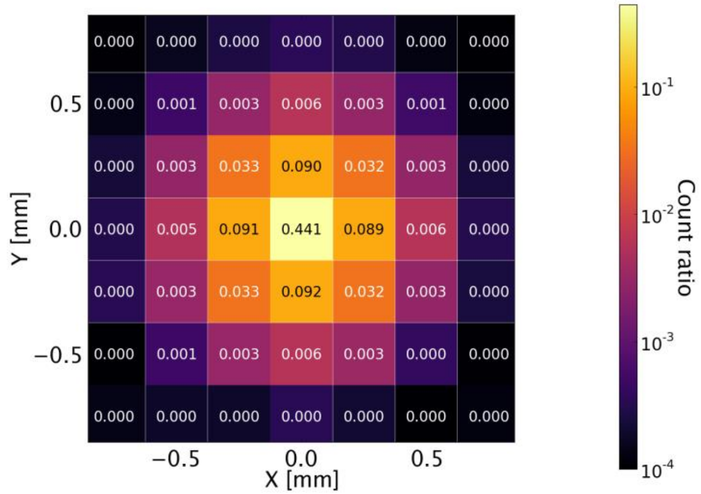

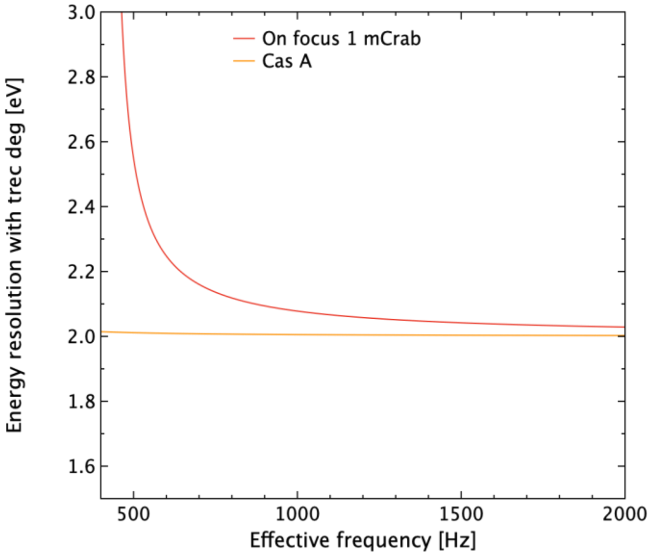

What about X-IFU? Introduction of defocusing

- **Early in the program, ability to defocus the mirror was introduced (same mechanism as for instrument selection)**
  - **Spreads point source flux over several hundreds of pixels**
  - **1 mCrab constraint becomes $\Delta T_{tot} = 1.45\ s \gg \Delta T_{tot,ext\ goal}$**
- **Instrument can simply be dimensioned on extended source count rate goal**
  - **Count rate constraint becomes much less stringent**
  - **Can "spend" associated margin to either:**
    - Decrease the pixel speed => easier to read out (see later)
    - Increase the pixel size => lower number of required pixels to populate the field of view
      - Of course, still need to "properly" sample the PSF
      - Still reasonable imaging with pixel size ~ telescope HEW
      - Athena HEW = 5" (now 10") ⇔ 291 µm with 12 m focal length
  - **We did both**

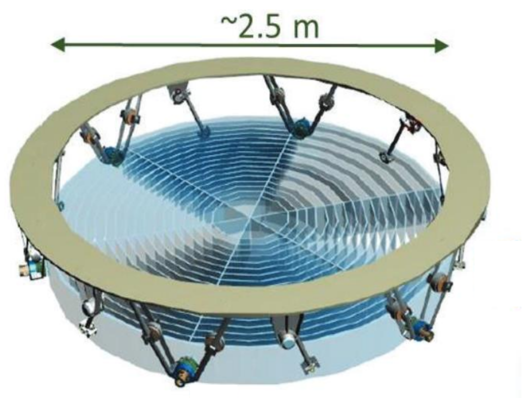

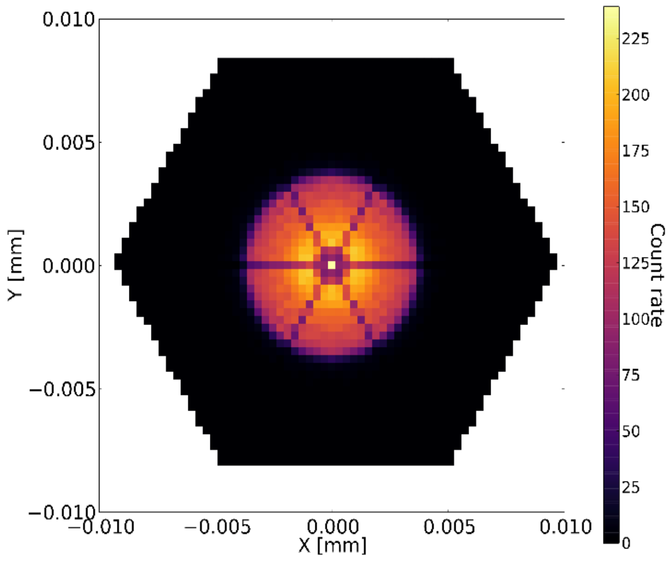

Evolution of TES array design over X-IFU study

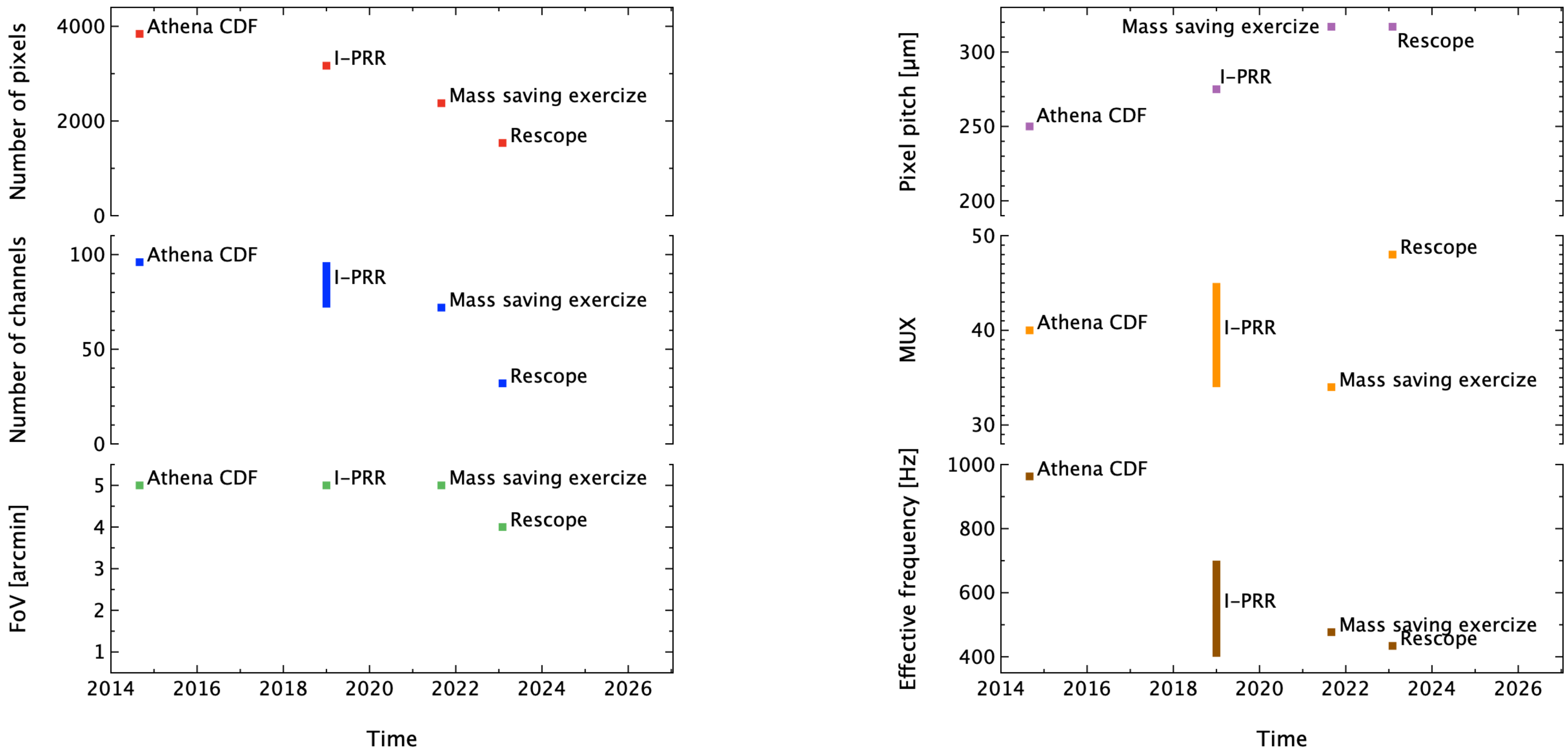

❖ **Preserved instrument performance for most of the study while significantly decreasing demands on the cryogenic system**

Evolution of TES array design over X-IFU study

[1] Smith+16
[2] No published reference, design principles similar to Nagayoshi+20
[3] Smith+21
[4] Wakeham+23

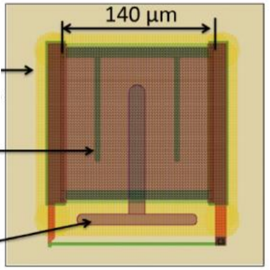

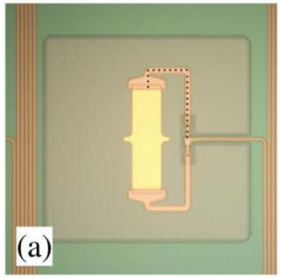

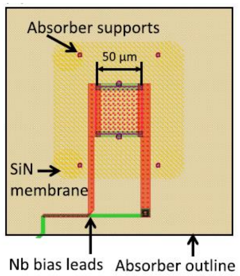

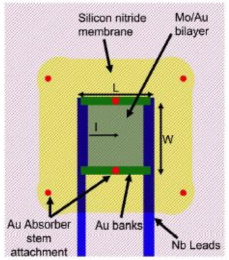

Parameter	LPA1 [1] Start of phase A baseline	LPAa 75 AR:0.5 [2] End of phase A baseline (FDM)	LPA2.5a [3] First TDM baseline pixel	LPA 50x30 µm [4] Current optimization
Pixel pitch (µm)	249	275	317	317
T_0 (mK) – TES bias point T°	90	88	89	89
G_b (pW/K) – Thermal cond.	200	60	72	66
C (pJ/K) – Total heat capacity	0.8	1.0	0.73	0.73
R_0 (mΩ) – TES bias point resistance	1	7.1	0.97	1.4
P_0 (pW) – TES bias power	4.63	1.31	1.55	1.41
$\alpha\,(T/R\;\partial R/\partial T)$	75	532	619	619
$\beta\,(I/R\;\partial R/\partial I)$	1.25	8	22	22
M – Unexplained Johnson noise factor	0	1.73	1.88	1.88
L/L_{crit}	1	1	0.64	0.74
f_{eff}(Hz) – Effective frequency	962	421	477	435
$\Delta E_{smallsig}$ – Small sig resolution	1.7	1.68	1.72	1.72

TES optimization for AC bias

- **Original X-IFU concept used FDM multiplexing (see D. Prêle's presentation tomorrow) with TESs operated under AC bias**

- **Two main degradations observed wrt. DC bias**
  - **AC losses from Eddy currents generated in the normal metal structures**
    - Prevents biasing low in the transition, spoils alpha, adds an additional noise source
  - **AC Josephson effects**
    - Relatively large non-linear Josephson inductance in parallel with the TES resistance
    - Generates step-like structures in the TES transition

- **Joint NASA/GSFC and SRON effort to optimize TES design**
  - **Remove normal metal features as much as possible (notably stripes)**
  - **Reduce non microstip area loop formed by TES and leads**
  - **Increase Rn, notably via increased aspect ratio**
    - Higher Rn at the same power reduces the weak link effect
  - **Reduction of pixel speed to mitigate carrier leakage**

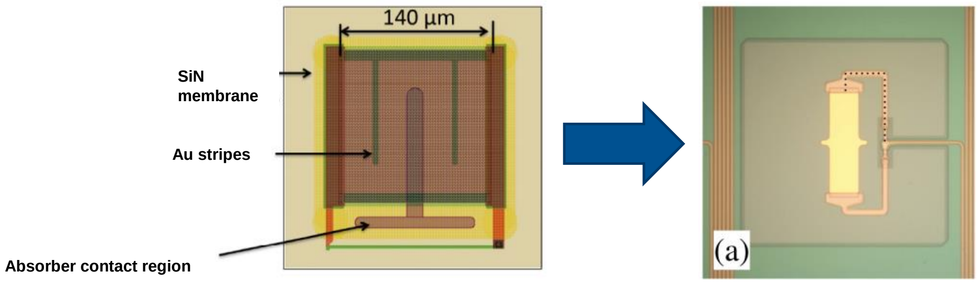

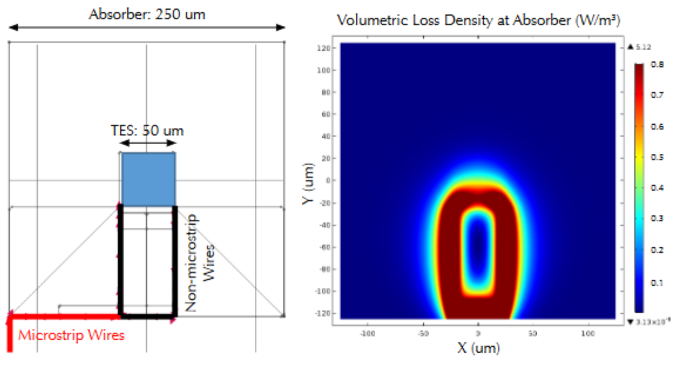

TES Modeling and Dissipative Loss Simulation with FEM

Sakai+17

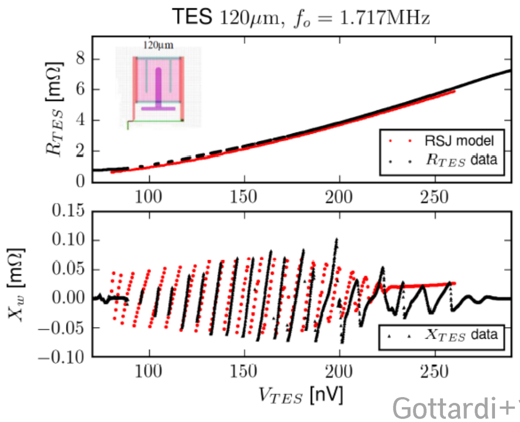

Gottardi+17

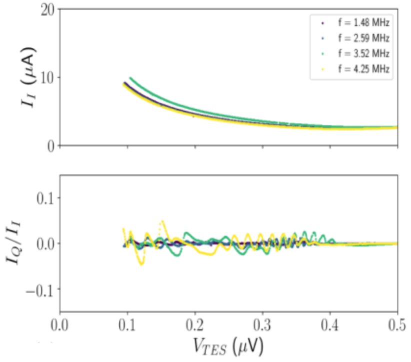

de Wit+20

THE X-IFU TDM DETECTION CHAIN: PRINCIPLE AND DIMENSIONING RULES

· · · · cnes · · · ·

SQUID readout

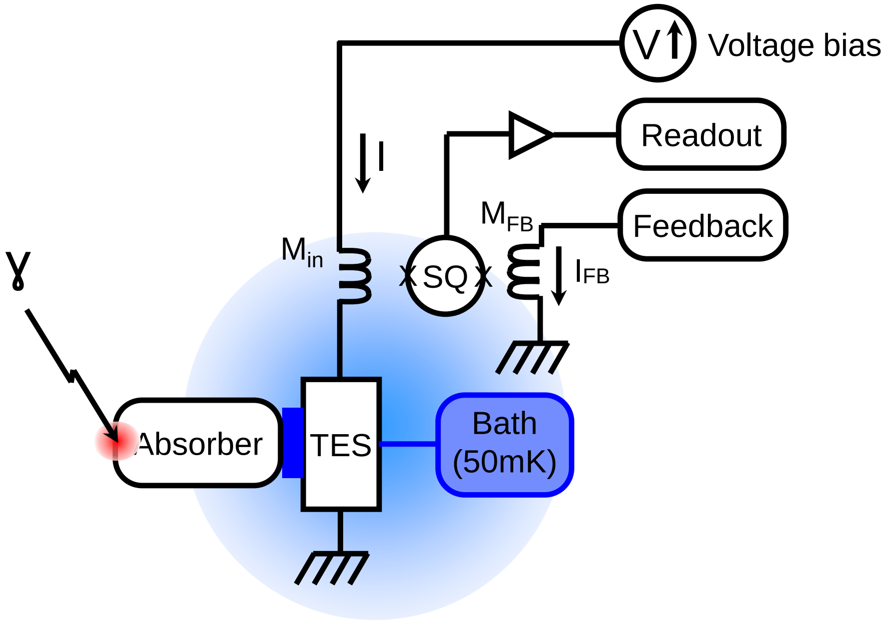

- **TES current is readout by SQUIDs (Superconducting Quantum Interference Devices)**
  - **The current flows through a coil to create a magnetic field**
  - **The SQUID transduces the magnetic field into a measurable voltage signal**

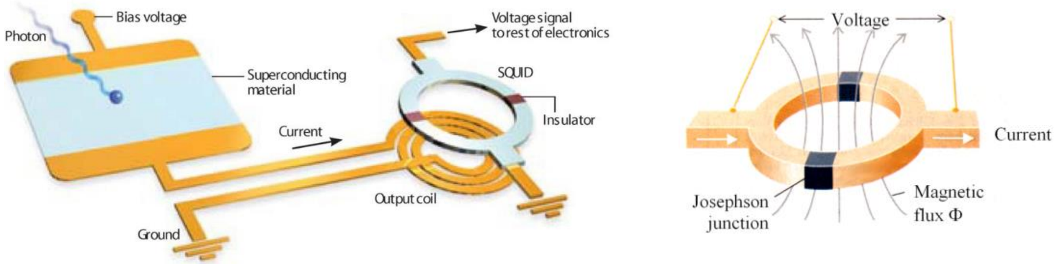

- **A SQUID characteristic is very non-linear (almost a sine wave)**
  - **Its linear readout requires a feedback signal generated in the warm electronics**
  - **Operated in a so-called « Flux Locked Loop » aka FLL**

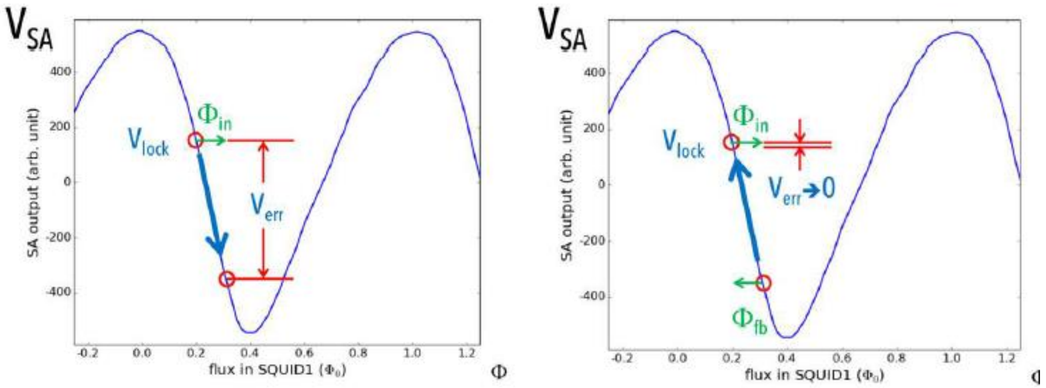

Time Domain Multiplexing (see also D. Prêle's presentation)

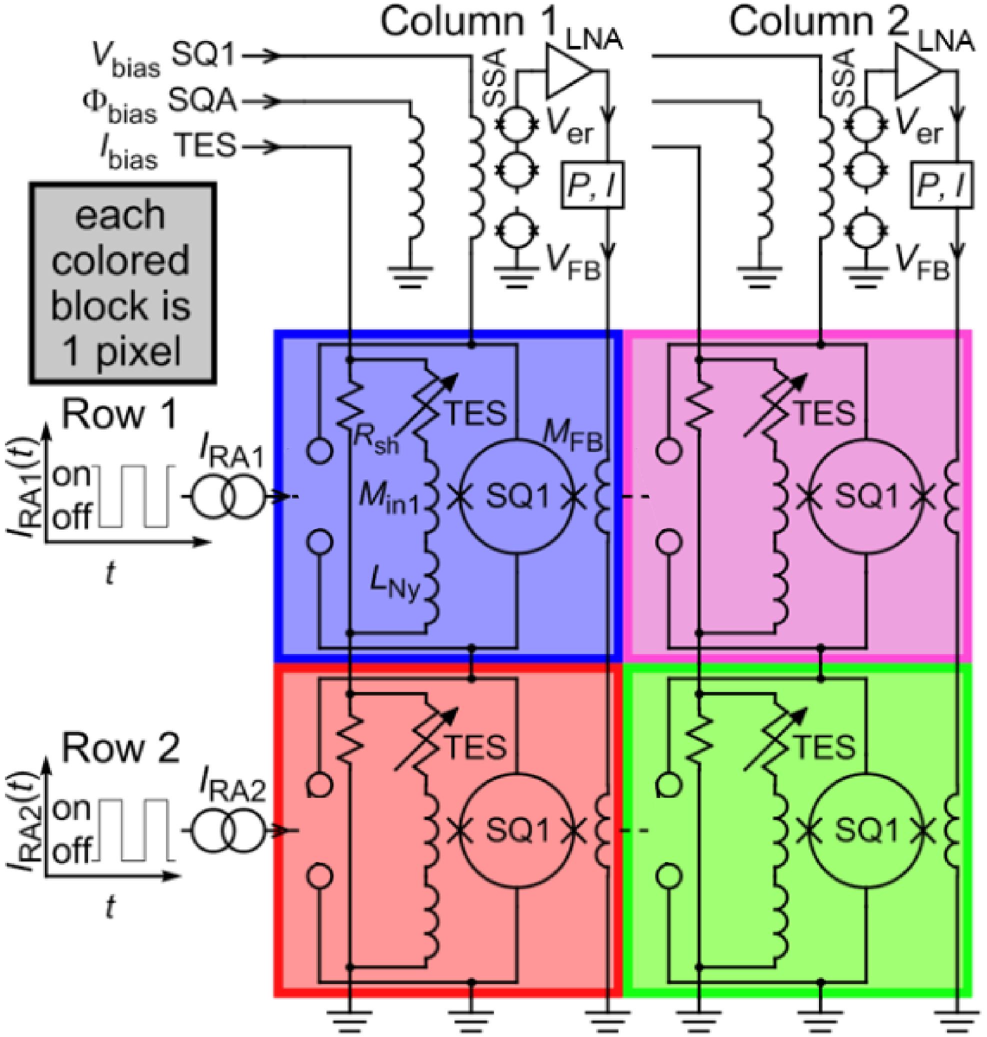

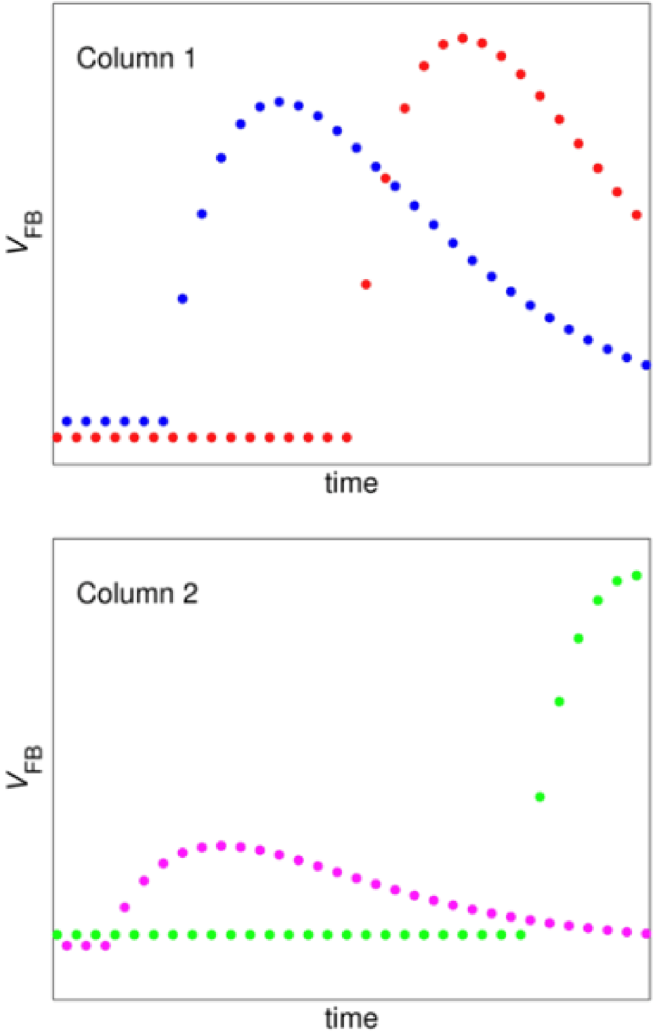

- t_{row}: time between two rows/pixels (160 ns for X-IFU)
- $t_{frame} = N_{MUX} \times t_{row}$: time between two reading of the same row/pixel (=48x160 ns =7.68 µs for X-IFU)
- X-IFU operated in 4 independent (but synchronized) 8x48 TDM schemes

The overall X-IFU readout architecture

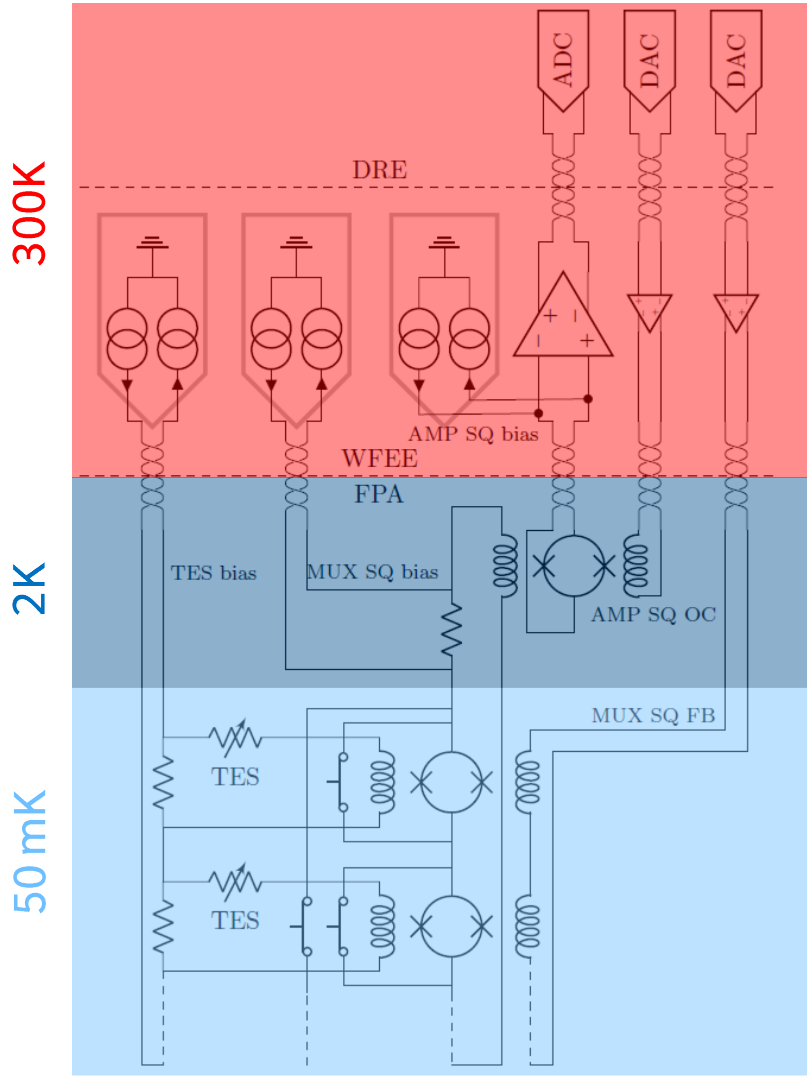

Gonzalez+24

The overall X-IFU readout architecture

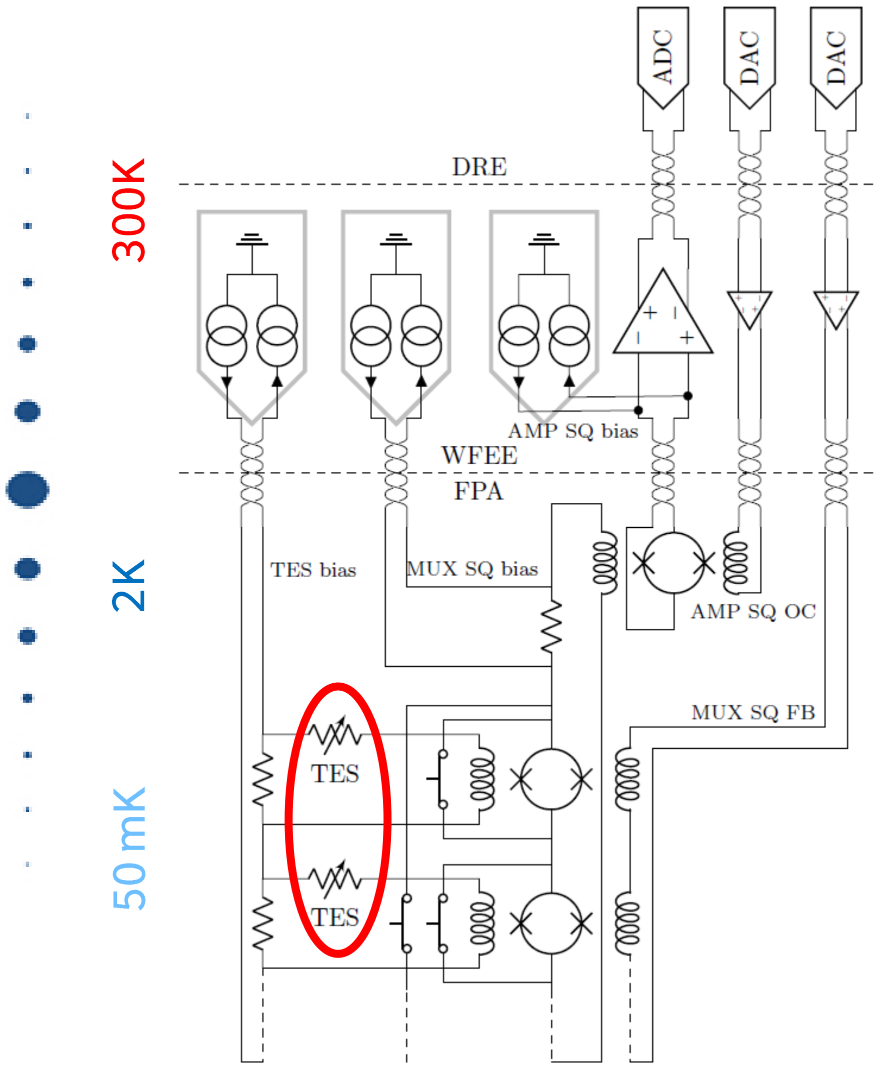

Gonzalez+24

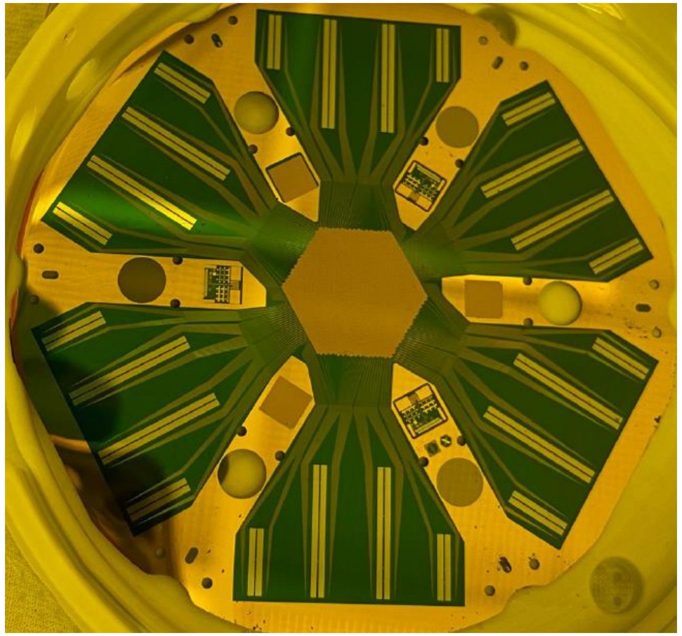

Credit: NASA/GSFC

- **Array of 1504 TES detectors (NASA/GSFC)**

The overall X-IFU readout architecture

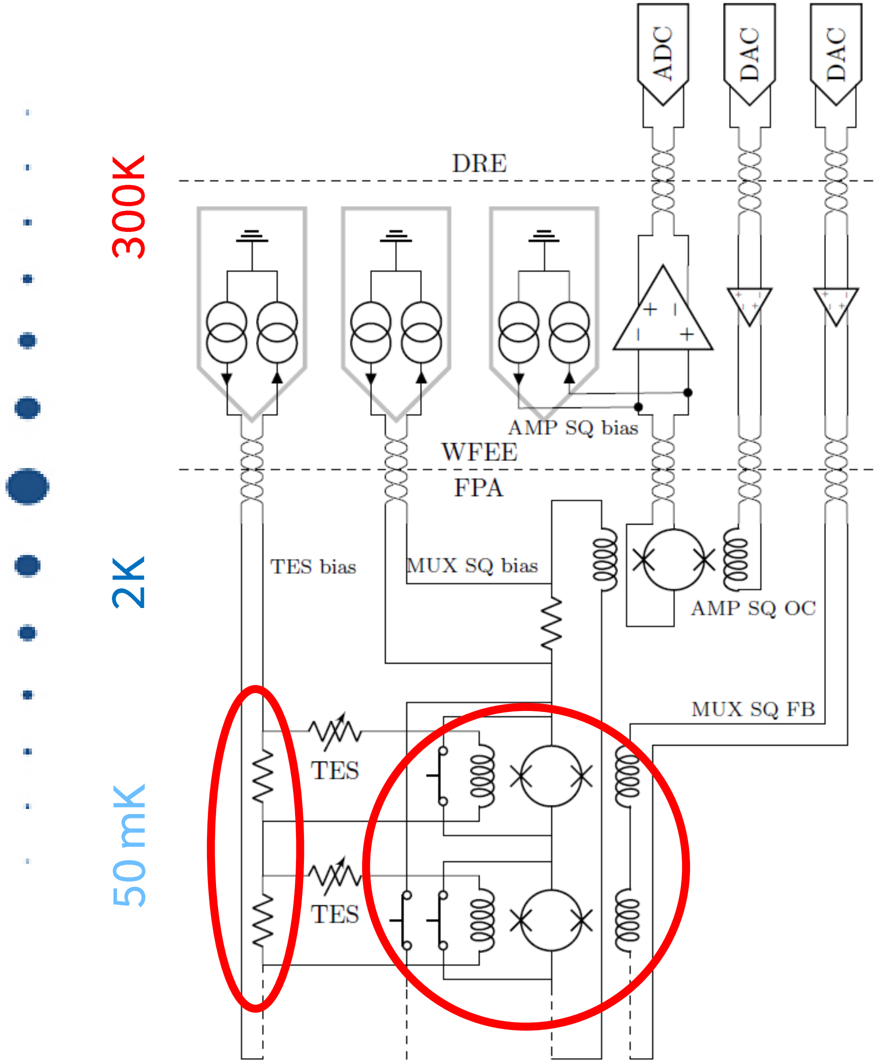

Gonzalez+24

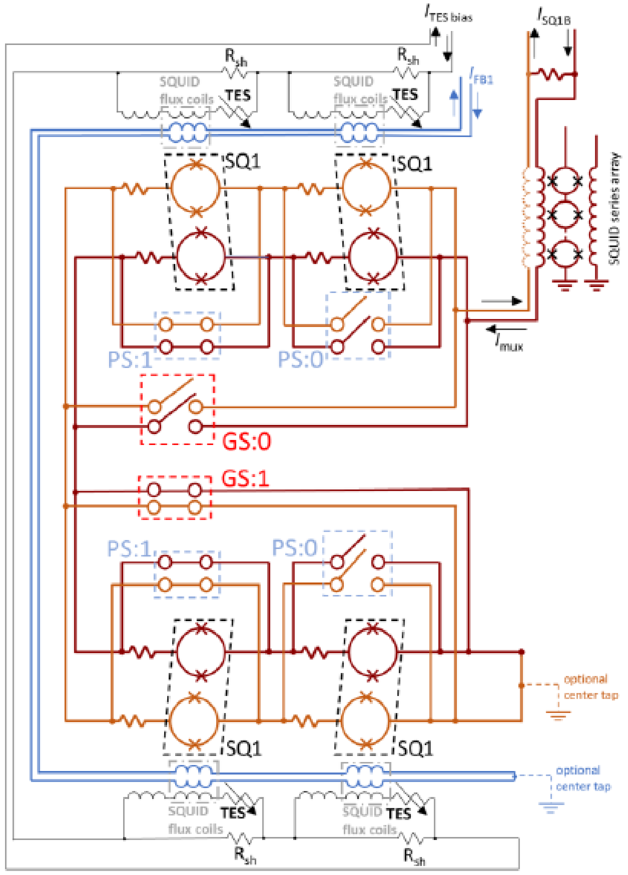

Durkin+23

- **Fully differential MUX SQUID chip (NIST)**
  - **Two level FAS to limit wiring for RA signals**
  - **Also contains shunt and Nyquist L for TES**

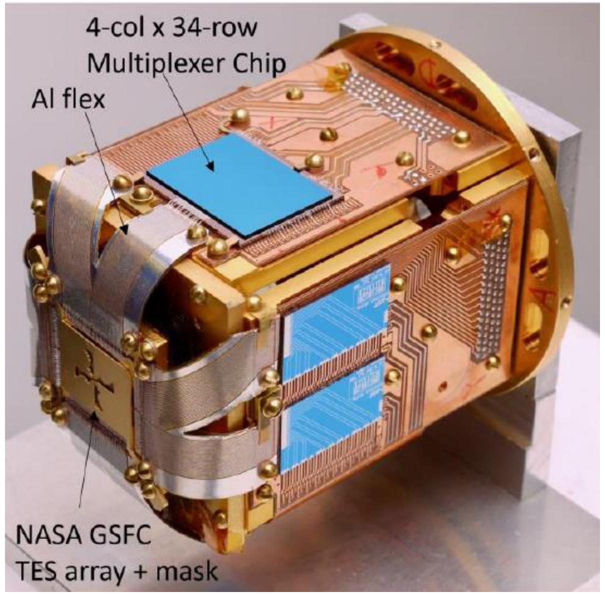

The overall X-IFU readout architecture

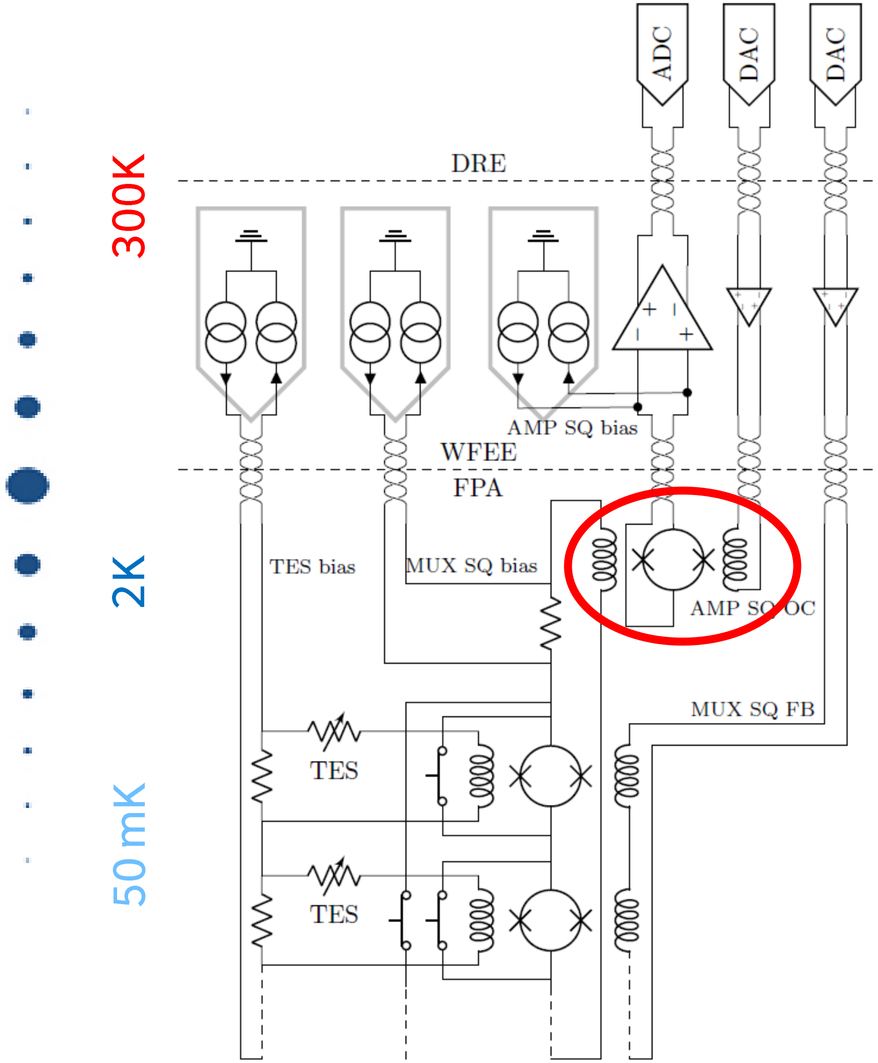

Gonzalez+24

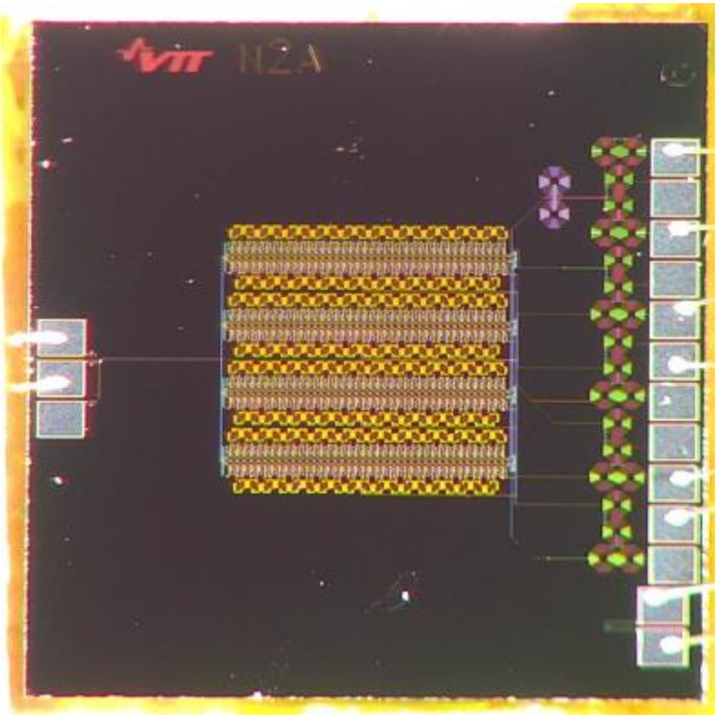

Credit: VTT

- **Differential AMP SQUID (VTT)**
  - **Most of the cold gain (~600 Ω transresistance)**
  - **Located at 2K**

The overall X-IFU readout architecture

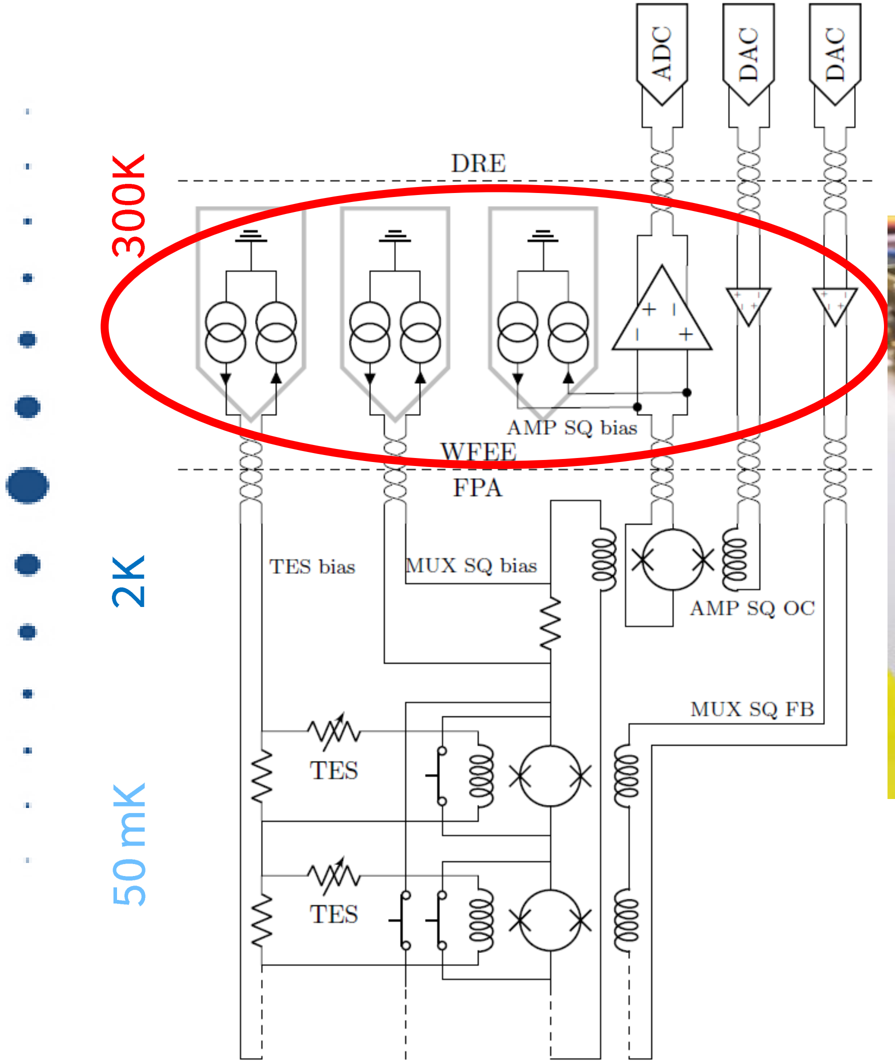

Gonzalez+24

Credit: APC

- **Warm Front-End Electronics (APC)**
  - **Located in PLC basement at 300 K**
  - **Differential LNA and current sources for cold electronics bias implemented in dedicated ASIC**
  - **Implements buffers on DRE dynamic lines**

The overall X-IFU readout architecture

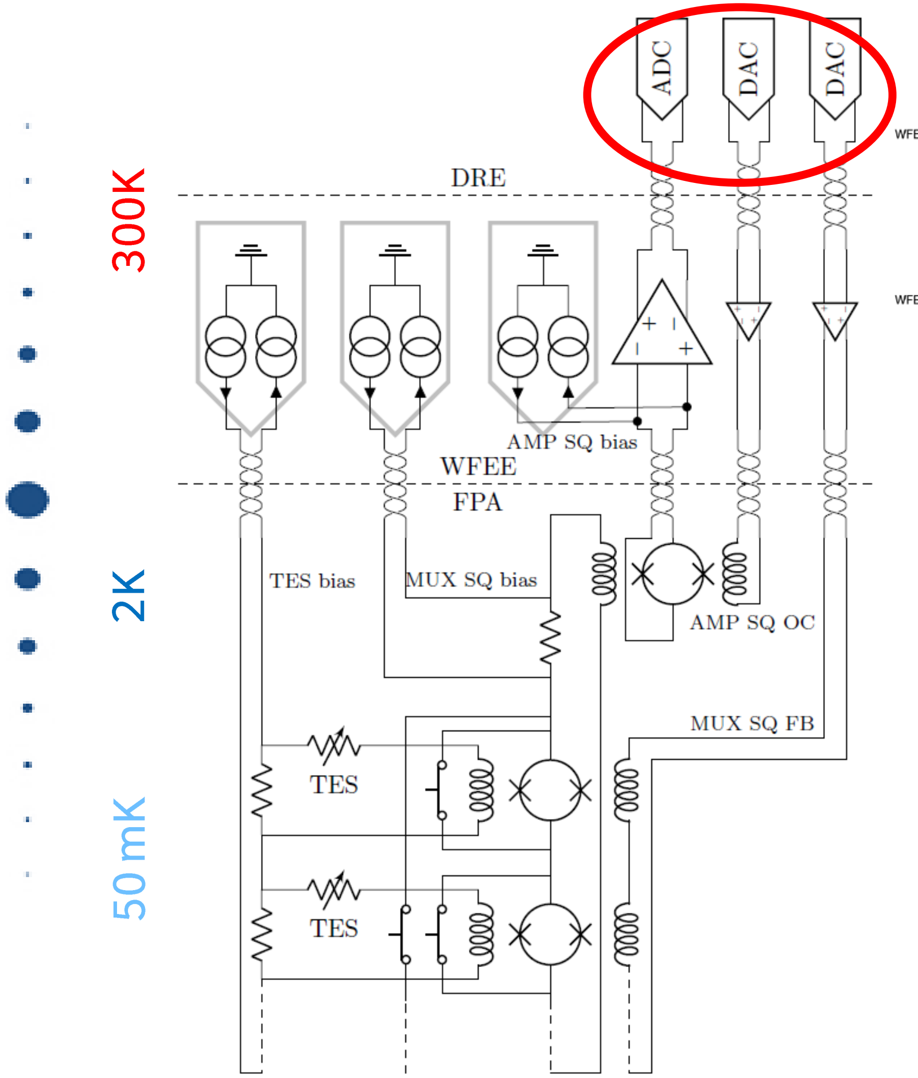

Gonzalez+24

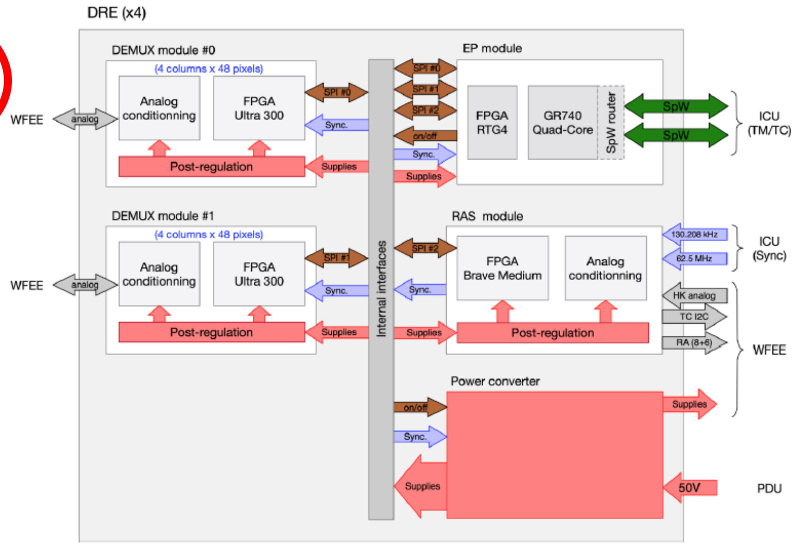

DRE block diagram

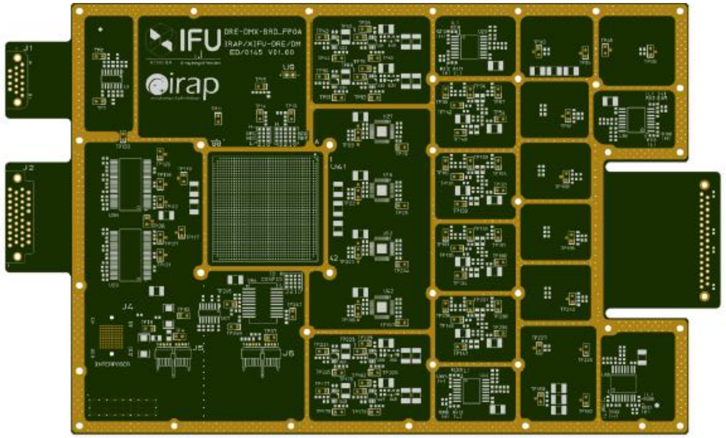

Credit: IRAP

❖ **Digital Readout Electronics (IRAP)**

- **Digitalization and demultiplexing of TDM signals**
- **Feedbacks generation for both SQUID stages**
  - Not a closed loop for AMP SQUIDs
  - Regular pattern to compensate varying offset from one MUX SQUID to another
- **Row address signals generation**
- **On-board processing**

The overall X-IFU readout architecture

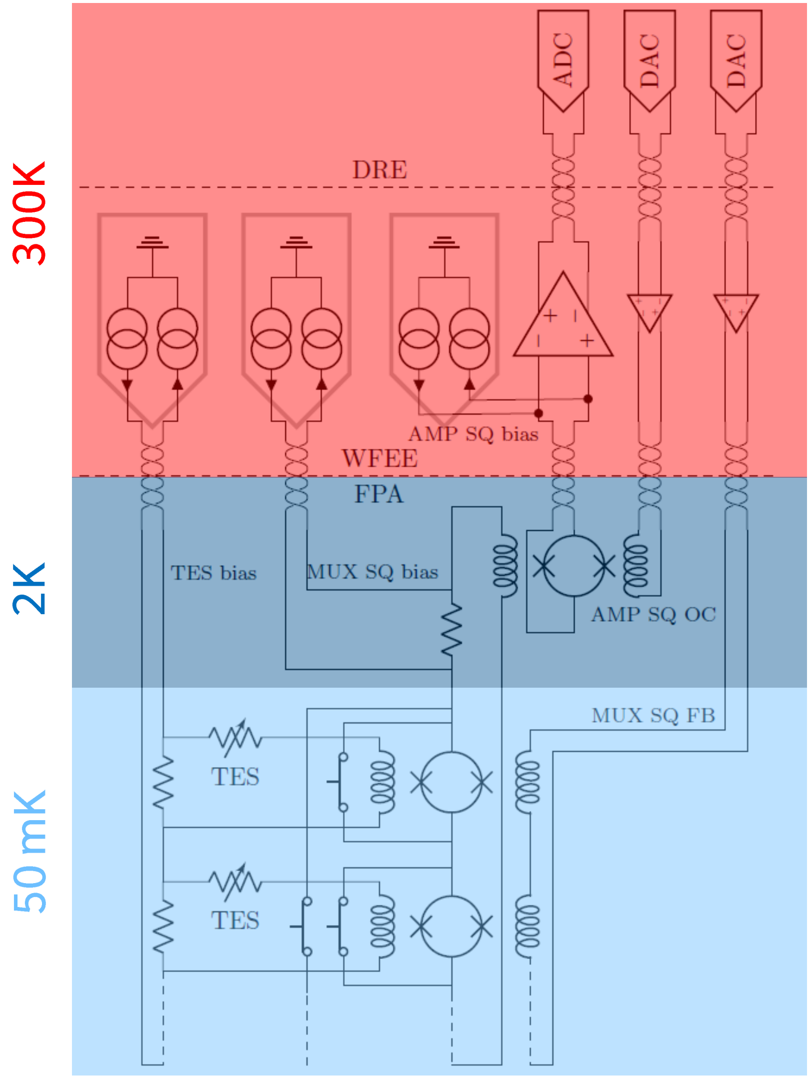

Gonzalez+24

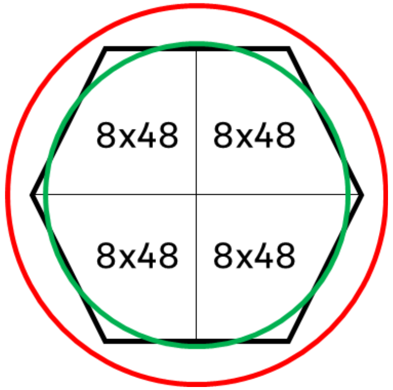

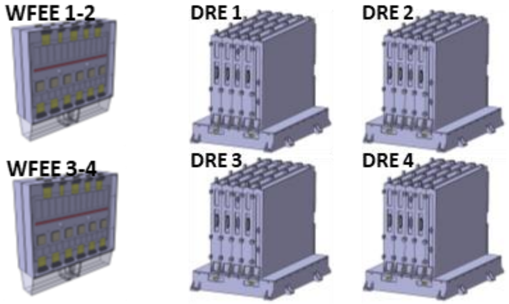

Number of channels	32
MUX	48
Pixels	1504 (+32)
FoV	3.98' ~ 4'
RA signals	6 + 8
FPA T0 panels	4
FPA T2 panels	2
Science harness	2
Wires per science harness	~ 500 (with isolation pairs)
WFEE physical box	2
WFEE functional units	4
Columns per ASIC	2
ASICs per WFEE unit	4
DRE physical boxes	4
DRE functional units	4
Columns per FPGA	4
DEMUX module per DRE unit	2

TDM dimensioning rules: FLL operation

- **FLL algorithm:**
  - $I_{FB}[n] = I_{FB}[n-1] + K_I(I_{TES}[n] - I_{FB}[n-1]) + I_{offset}$
- **Feedback signal generated at the previous frame**
- **TES signal change between two frames should not exceed the SQUID monotonous/linear range for the most energetic event in the band (12 keV)**
  - In practice, pulse slew rate decay makes it so that one could tolerate an overshoot on the pulse onset without loosing stability
  - Not used for now in dimensioning

$$\Delta\phi_{max} = \left.\frac{dI}{dt}\right|_{max} M_{in} N_{MUX} t_{row} \leq \phi_{range} \approx 0.3\ \phi_0$$

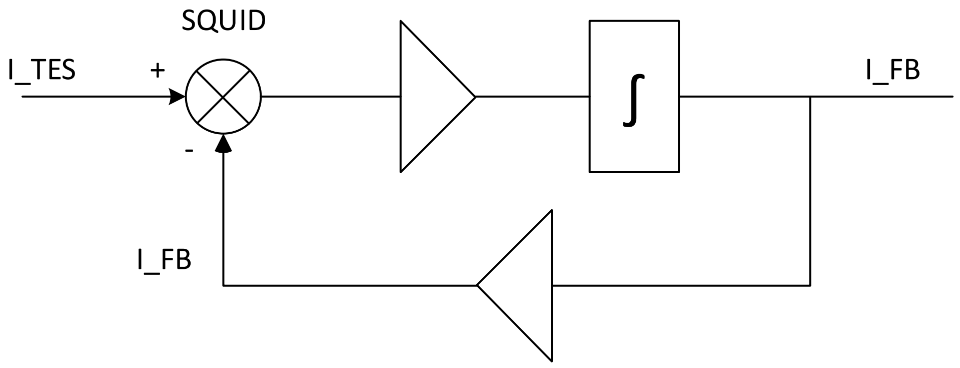

FLL architecture

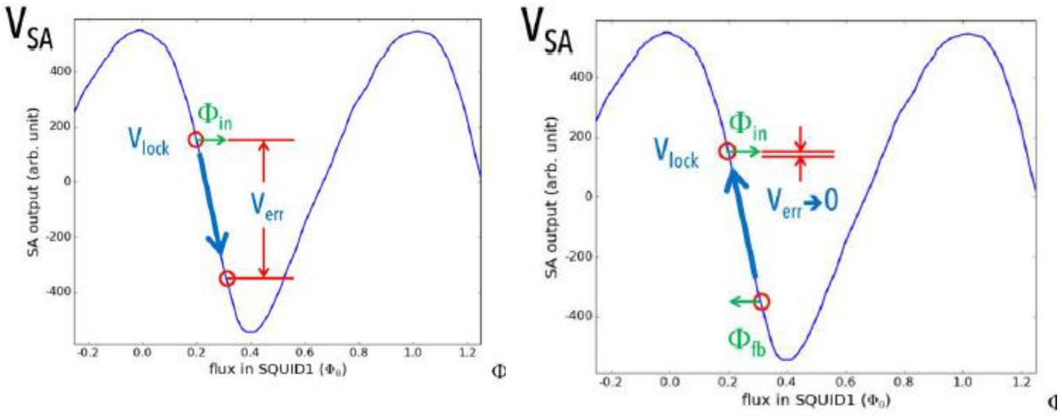

TDM dimensioning rules: aliasing

- **Each pixel is only read out every N_{MUX} row**
- **Mismatch between the open-loop bandwidth…**
  - **Needs to allow the system to respond on the timescale of a row: $f_{OL} > 1/t_{row}$ (6.25 MHz for X-IFU)**
- **… and the readout frequency**
  - $f_{sample} = \frac{1}{t_{frame}} = \frac{1}{N_{MUX} t_{row}}$ **(130 kHz for X-IFU)**
- **Readout noise gets aliased $2N_{MUX}$ times:**

$$M_{in}\sqrt{S_{I_{MUX}}} = \sqrt{\pi N_{MUX} S_{\phi}}$$

Assumes open loop has an equivalent 1st order roll-off at $1/t_{row}$ => factor $\pi/2$

with $\sqrt{S_{I_{MUX}}}$ multiplexed readout noise referred to TES (unit: A/√Hz)
M_{in} mutual inductance coupling I_{TES} to MUX SQUID (unit: H)
$\sqrt{S_{\phi}}$ non-multiplexed readout noise, referred to MUX SQUID (unit: ϕ_0/√Hz)
N_{MUX} multiplexing factor = number of TDM rows

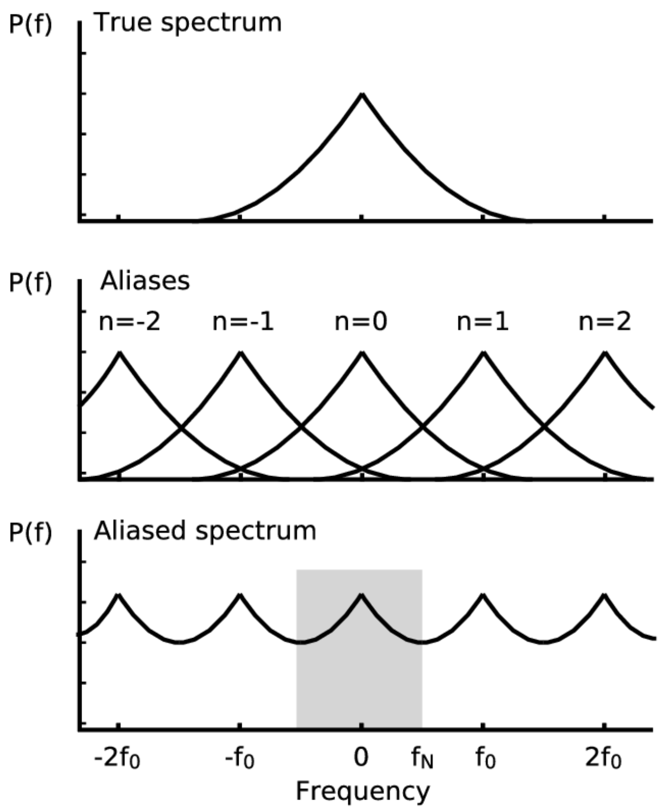

Dimensioning exercise (small signal model)

Question: which TDM performance is required as a function of pixel speed?

- **Target performance:**
  - **2 eV (for a 3 eV instrument) at detector + readout chain level**
    - Actual pixel + readout allocation ~ 2.25 eV, but would lead to unrealistic constraints. 2 eV taken to somewhat compensate the fact that the small signal model underpredicts resolutions
  - **Target throughput before rescope: 90% at 2.5 cps/pxl (extended source count rate goal, setting aside 10 % for crosstalk rejection – see later):** $\Delta T_{tot} = 42ms$
  - **Post rescope focal plane population: 4' equivalent diameter, populated by 317 µm pitch pixels in 32 TDM columns => MUX 47(+1: one pure resistive pixel per column to monitor gain drifts)**
- **First done with LPA1 pixel (phase A design). Then pixel speed modified only via G**
  - **Setpoint current rescaled to keep same working temperature**
  - **L modified to remain at critical damping**
  - **All other parameters kept the same**
- **Disclaimers**
  - **Use simplified dimensioning rules here for ease of description and small signal model**
  - **Will highlight after how TES non-linearity (among others) modifies the dimensioning for the latest X-IFU design point**

Maximum allowed readout (white) noise for LPA1

$$t_{rec} = \Delta t_{\text{tot}} - 10\tau_{eff} = 37.8\ ms$$

$$\Delta E_{FWHM} = \sqrt{8\log(2)}\left(\int_{1/2t_{rec}}^{\infty} \frac{4|s_I(f)|^2}{S_{I\,TFN}(f) + S_{I\,JN,TES}(f) + S_{I\,JN,L}(f) + S_{I_{MUX}}}\,df\right)^{-1/2} \leq 2\ eV$$

=> Gives a limit on the maximum allowed (multiplexed) readout noise at TES level $S_{I_{MUX,max}}$

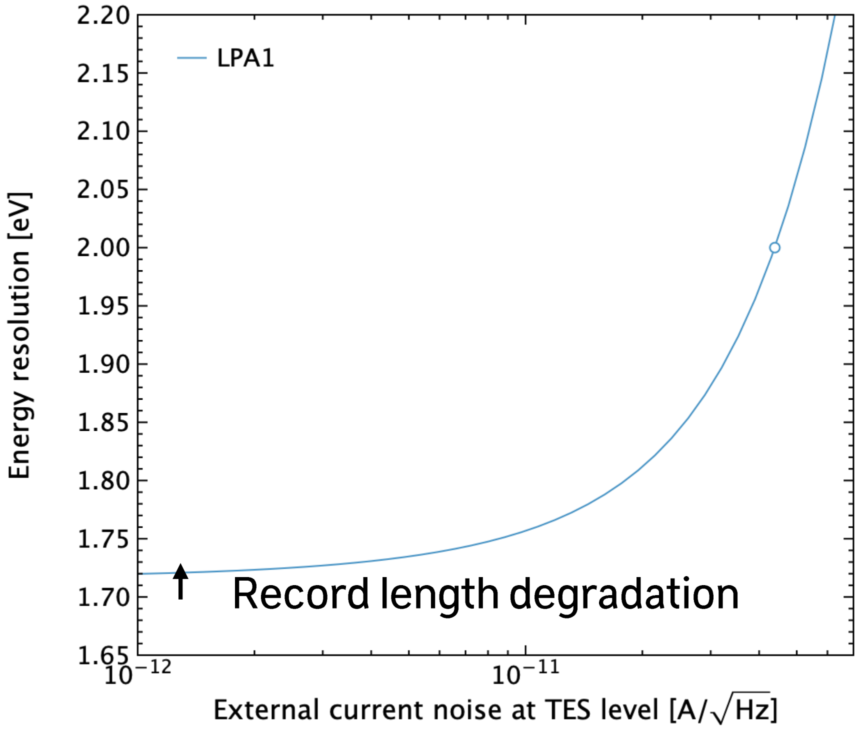

$$S_{I_{MUX,max}} = 43.9\text{pA}/\sqrt{Hz}$$

Optimization of SQUID input mutual inductance

- **Two main TDM dimensioning relations**
  - **SQUID linear flux range :** $\left.\frac{dI}{dt}\right|_{max} M_{in} N_{MUX} t_{row} \leq 0.3\ \phi_0$
  - **Maximum TES ref'd noise to reach performance :** $\frac{\sqrt{\pi N_{MUX} S_\phi}}{M_{in}} \leq \sqrt{S_{I_{MUX,max}}}$

- **Min is a free parameter that can (needs to) be optimized for each array model**
  - **Min ↑**
    - Readout noise ↓ wrt. TES noise
    - Required linear flux range ↑
  - **Min ↓**
    - Readout noise ↑ wrt. TES noise
    - Required linear flux range ↓

TDM allowed parameter space

- **Two main TDM dimensioning relations**
  - **SQUID linear flux range :** $\left.\frac{dI}{dt}\right|_{max} M_{in} N_{MUX} t_{row} \leq 0.3\ \phi_0$
  - **Maximum TES ref'd noise to reach performance :** $\frac{\sqrt{\pi N_{MUX} S_\phi}}{M_{in}} \leq \sqrt{S_{I_{MUX,max}}}$
- **Combine with Min (free parameter): provides the allowed parameter space for the multiplexing scheme (t_{row} and N_{MUX})**

$$t_{row} \frac{\sqrt{S_\phi}}{0.3\phi_0} \leq \frac{\sqrt{S_{I_{MUX,max}}}}{\left.\frac{dI}{dt}\right|_{max}} \times \frac{1}{N_{MUX}^{3/2}\sqrt{\pi}}$$

1/« dynamic range density » of SQUID readout system
Characterizes the performance of the readout system

1/« dynamic slew density » (Doriese+12) of the TES
Characterizes the constraint from the TES detector

For LPA1:

$$S_{I_{MUX,max}} = 43.9\text{pA}/\sqrt{Hz}$$

$$\left.\frac{dI}{dt}\right|_{max} = 1\ A/s$$

$$DSR = 23.7 \times 10^9\ \sqrt{Hz}$$

TDM allowed parameter space

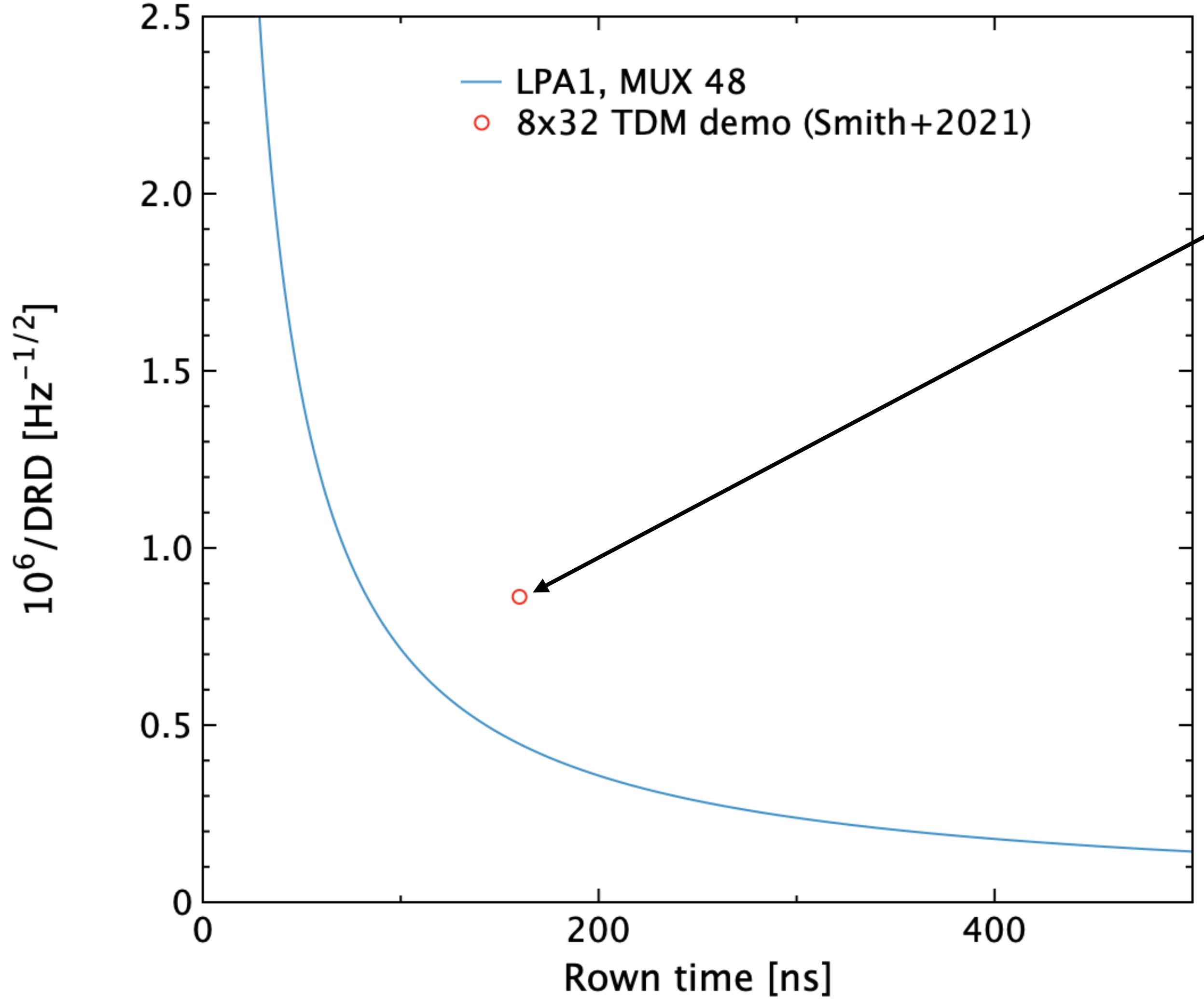

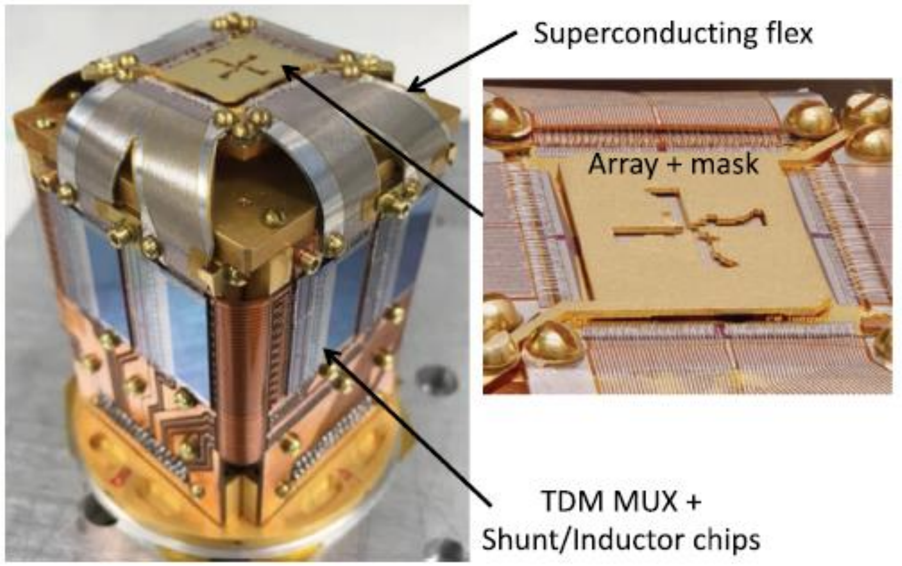

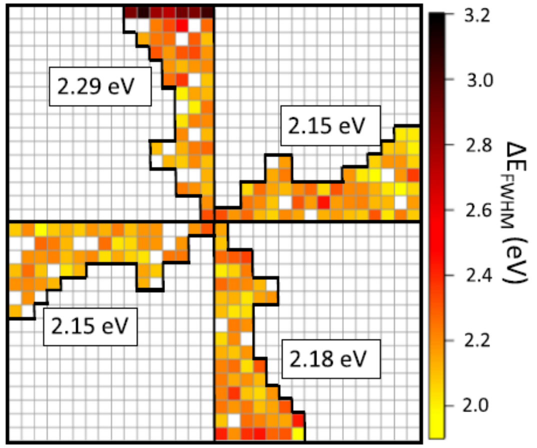

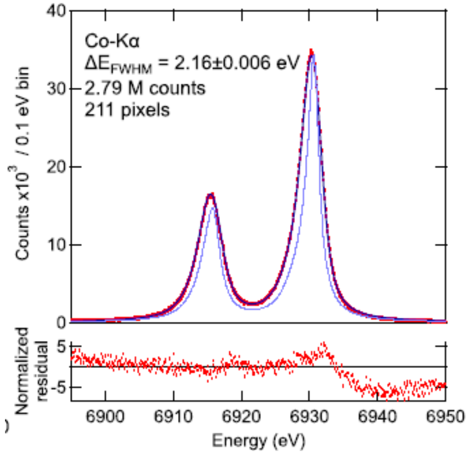

TDM allowed parameter space

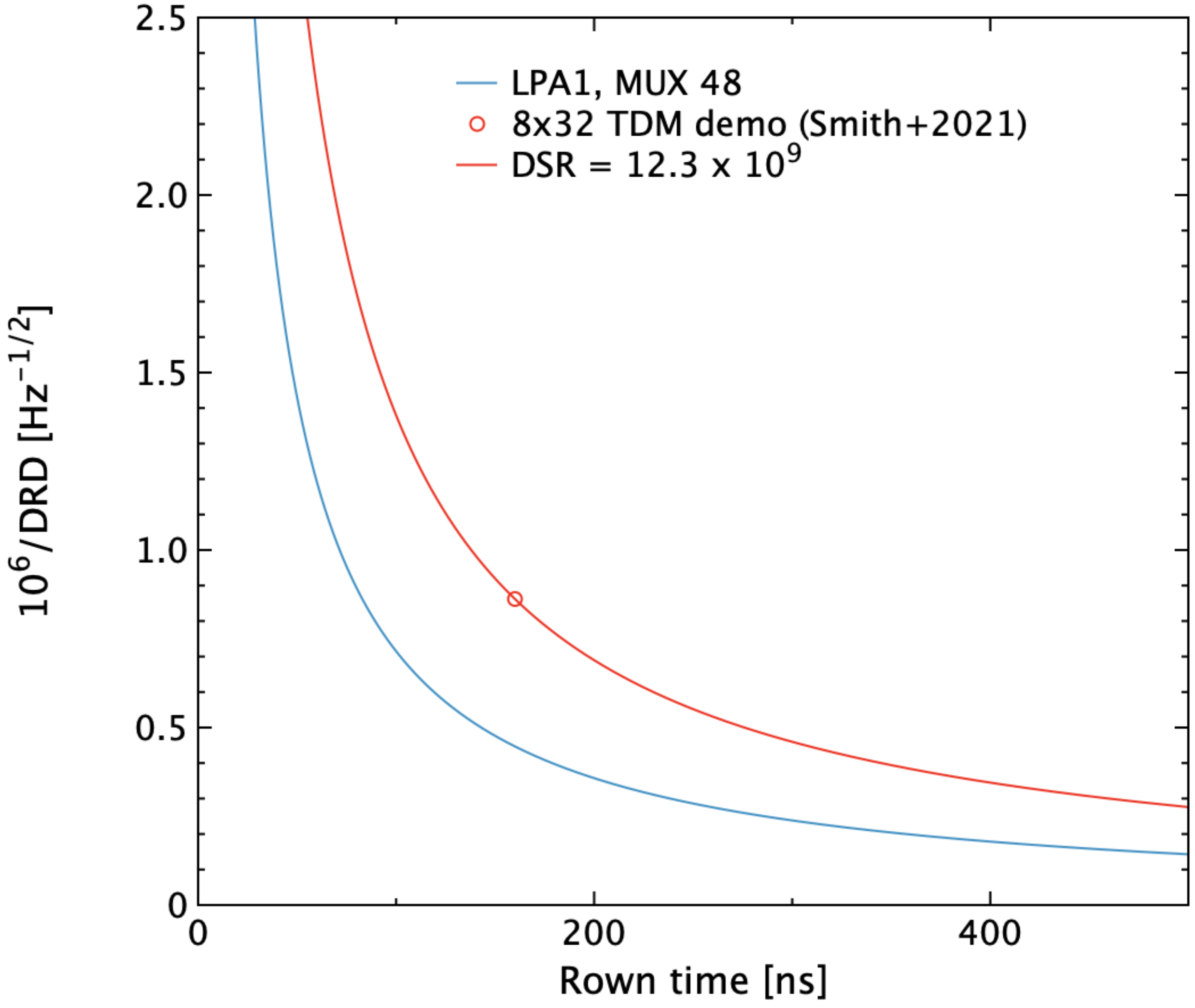

- **Would not be able to implement the X-IFU with the original pixel design by almost a factor 2 on either (or a combination)**
  - **Noise amplitude spectral density**
  - **Squid dynamic**
  - **Row time**
- **But… We know that original pixel concept was largely too fast. What happens when we slow down the pixel?**

Dimensioning exercise (small signal model): Slowing down the pixel

- Reminder: simple scaling of G as a toy exercise

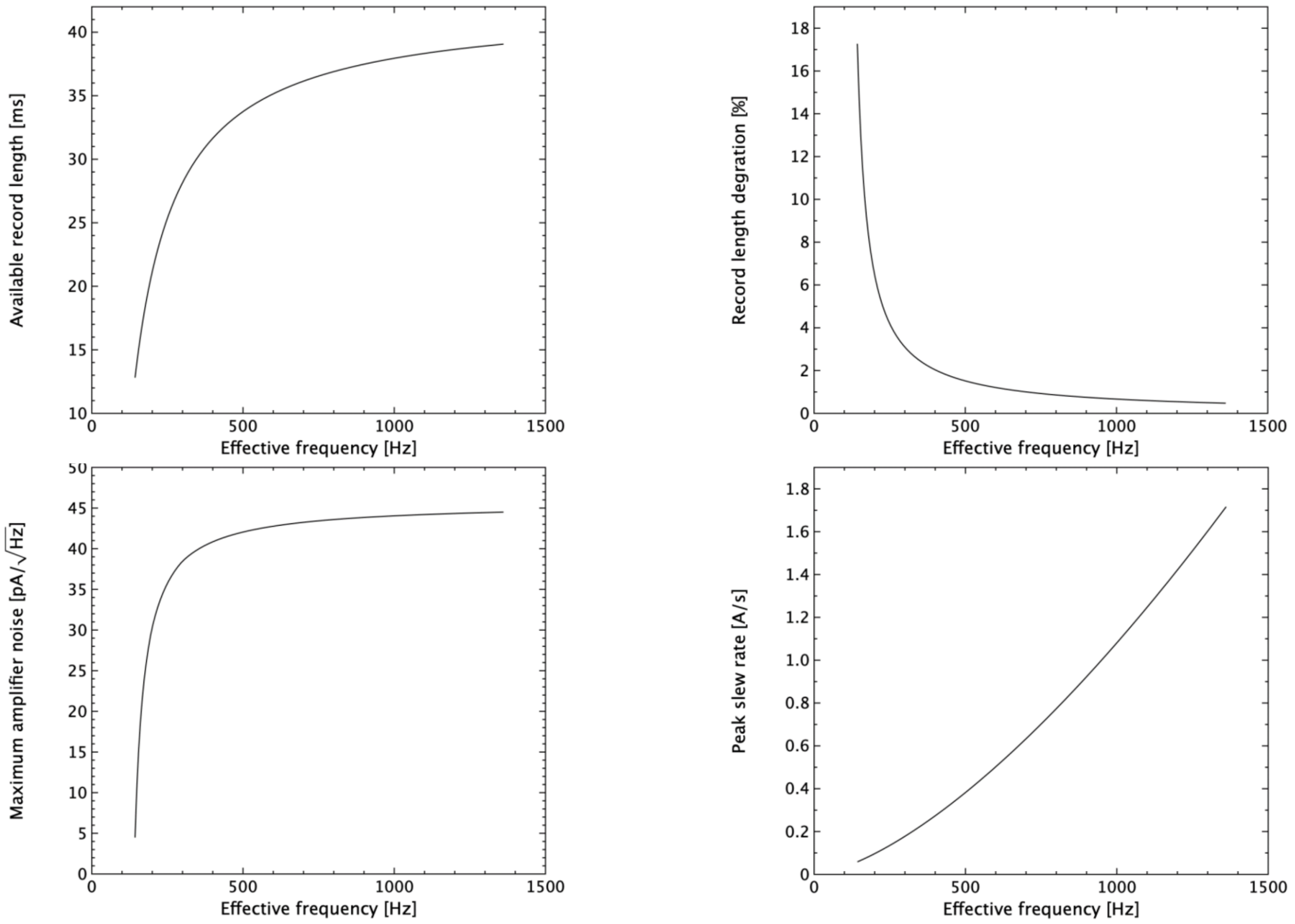

Dimensioning exercise (small signal model): Slowing down the pixel

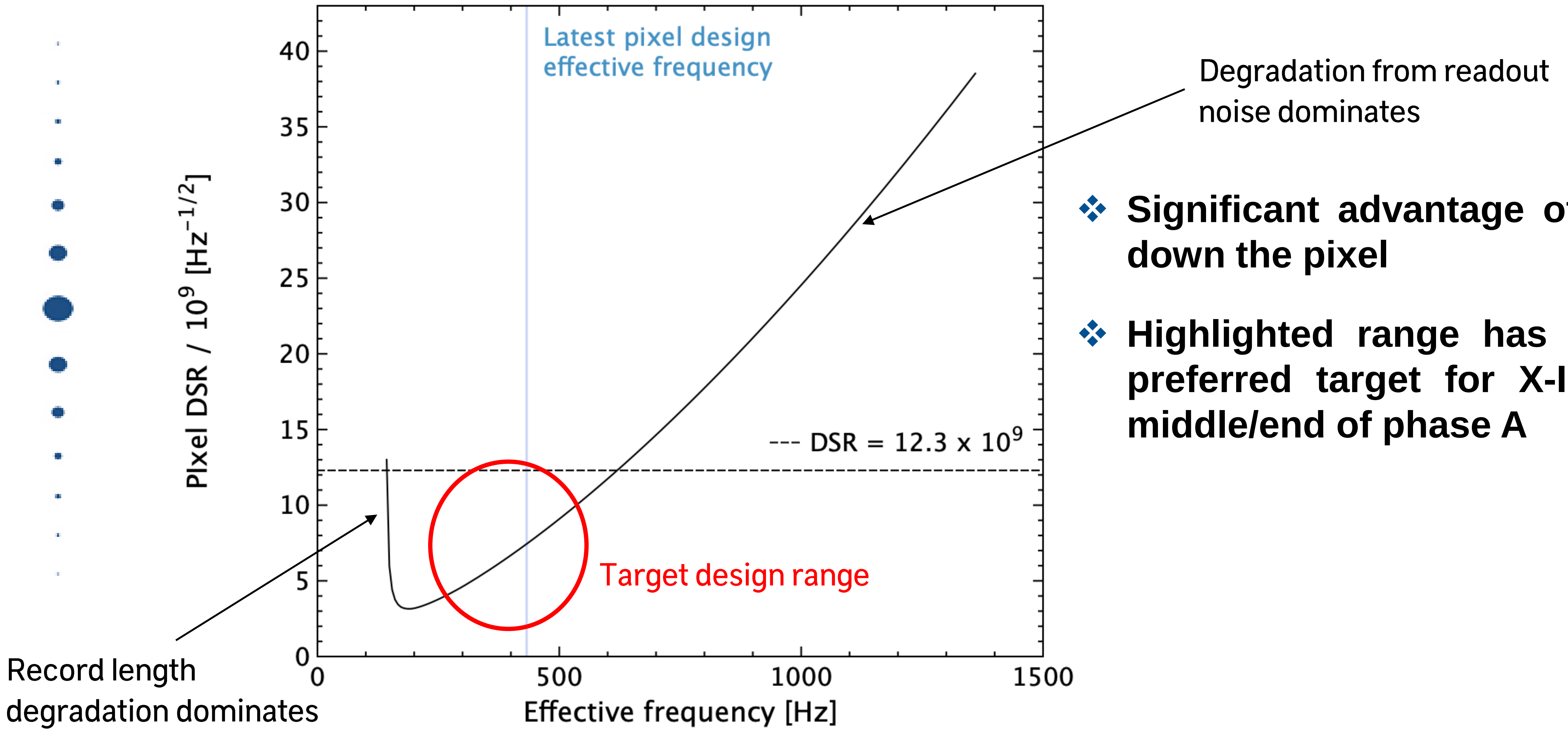

- Significant advantage of slowing down the pixel
- Highlighted range has been the preferred target for X-IFU since middle/end of phase A

Impact of non-linearity

- **Whereas useful to describe trends, the small signal is certainly not reliable to dimension an X-IFU like readout**
  - **Especially true for stripe-less high alpha TESs as those foreseen for X-IFU**
- **Intrinsic energy resolution is largely underestimated**
  - **Need to rather dimension the impact of readout noise as a quadrature term on top of the pixel intrinsic resolution**
  - **Also allows having a less ambiguous share of requirements between subsystems…**
- **Maximum slew rate is overestimated by a factor of a few**
- **Note that operation slightly below L_{crit} may also be favored when taking into account non-linearity**

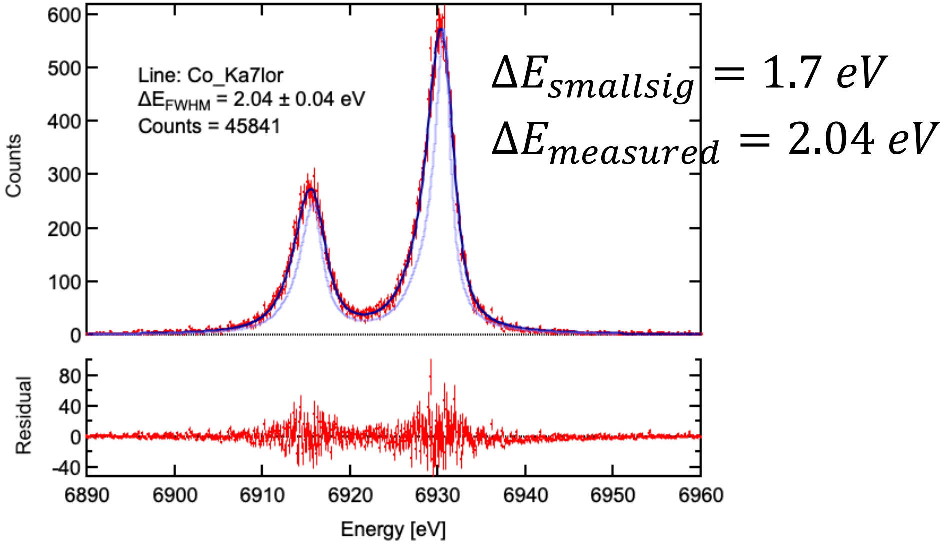

Courtesy data from same pixels as Smith+21

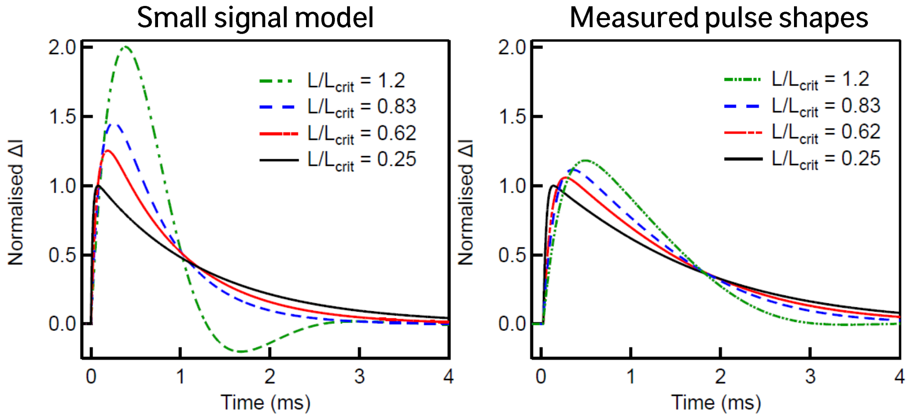

Gottardi&Smith+22

Application to latest target pixel design

- **Current target pixel is an adaptation of the 8x32 TDM demo pixel**
- **Aim at higher aspect ratios (Wakeham+23) to**
  - **Further decrease the pixel speed**
  - **Reduce the pixel sensitivity to magnetic field (among the main source of gain drifts)**
- **Latest measurements predict**
  - **A slew rate at 12 keV of ~ 0.17 A/s**
  - **An acceptable readout noise of 25 pA/√Hz at TES level for the budgeted ~ 0.8 eV quadratic degradation from readout**
  - **=>** $DSR = 6.8 \times 10^{9}\sqrt{Hz}$

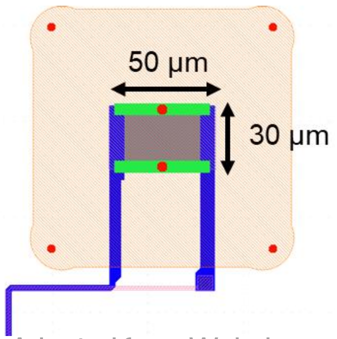

Adapted from Wakeham+23

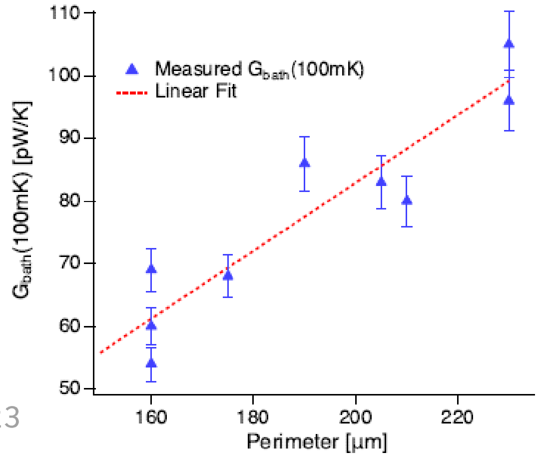

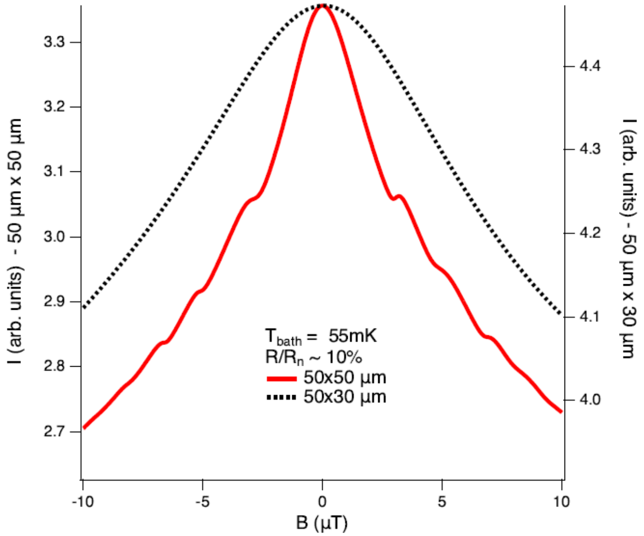

Application to latest target pixel design

- **Current target pixel is an adaptation of the 8x32 TDM demo pixel**
- **Aim at higher aspect ratios (Wakeham+23) to**
  - **Further decrease the pixel speed**
  - **Reduce the pixel sensitivity to magnetic field (among the main source of gain drifts)**
- **Latest measurements predict**
  - **A slew rate at 12 keV of ~ 0.17 A/s**
  - **An acceptable readout noise of 25 pA/√Hz at TES level for the budgeted ~ 0.8 eV quadratic degradation from readout**
  - **=> $DSR = 6.8 \times 10^9 \sqrt{Hz}$**

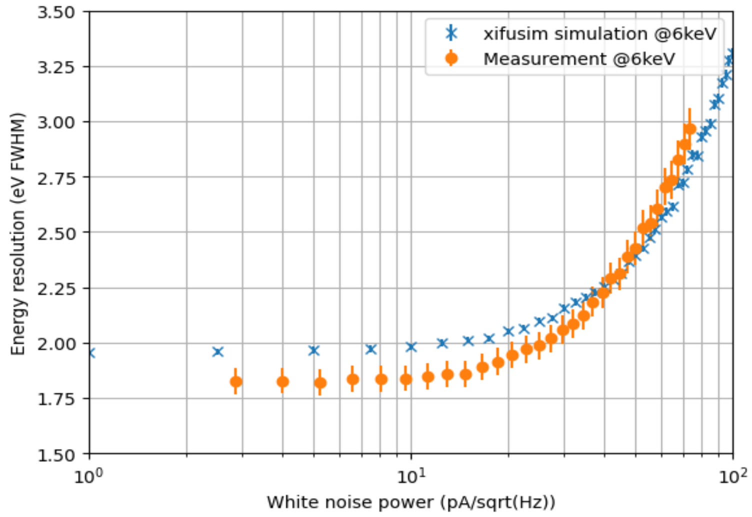

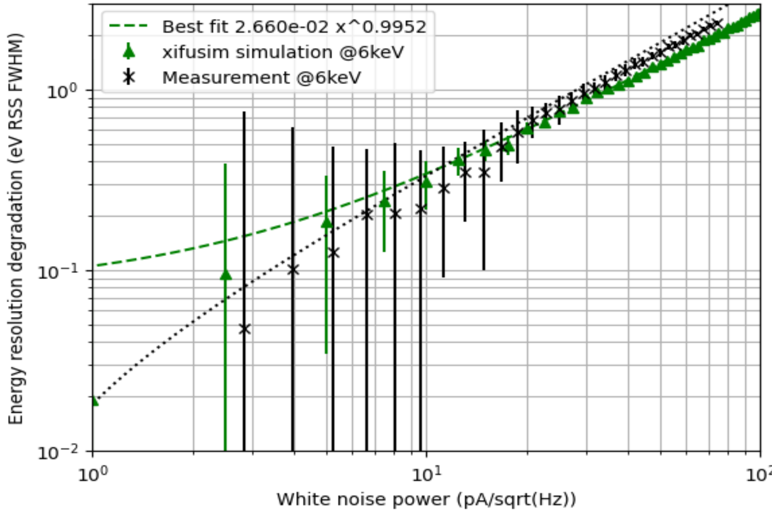

Application to latest target pixel design

- **Current target pixel is an adaptation of the 8x32 TDM demo pixel**
- **Aim at higher aspect ratios (Wakeham+23) to**
  - Further decrease the pixel speed
  - Reduce the pixel sensitivity to magnetic field (among the main source of gain drifts)
- **Latest measurements predict**
  - A slew rate at 12 keV of ~ 0.17 A/s
  - An acceptable readout noise of 25 pA/√Hz at TES level for the budgeted ~ 0.8 eV quadratic degradation from readout
  - => $DSR = 6.8 \times 10^9 \sqrt{Hz}$

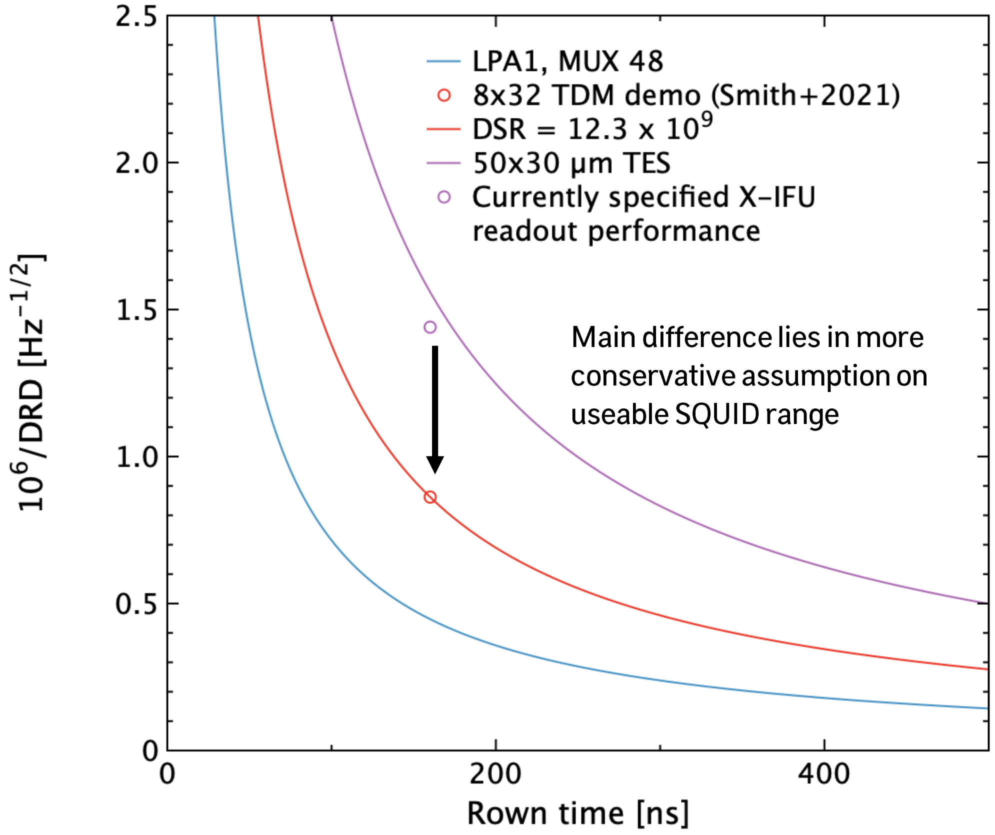

GOING BEYOND SIGNAL TO NOISE RATIO OPTIMIZATION

cnes

TDM bandwidths optimization

- **At each TDM row, a settling transient occurs when the system switches from one signal level (pixel) to the other**
- **Its shape depends on:**
  - **The physics of the MUX SQUID (including FAS)**
  - **The relative timing between the different TDM signals (FB and RA) and their filtering by the system, therefore on the system bandwidths**
- **It creates:**
  - **Crosstalk**
  - **Gain scale distortions**

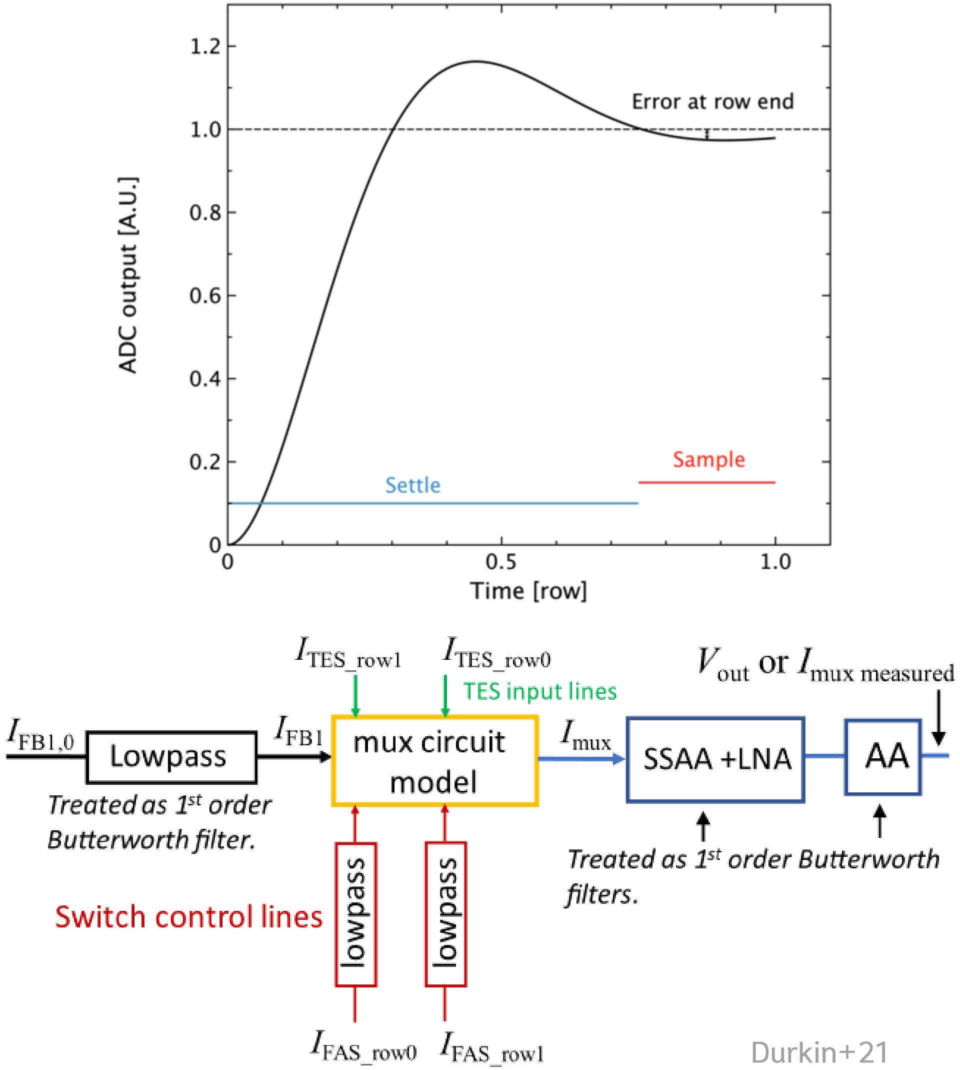

Durkin+21

TDM bandwidths optimization

- **At each TDM row, a settling transient occurs when the system switches from one signal level (pixel) to the other**
- **Its shape depends on:**
  - **The physics of the MUX SQUID (including FAS)**
  - **The relative timing between the different TDM signals (FB and RA) and their filtering by the system, therefore on the system bandwidths**
- **It creates:**
  - **Crosstalk**
  - **Gain scale distortions**

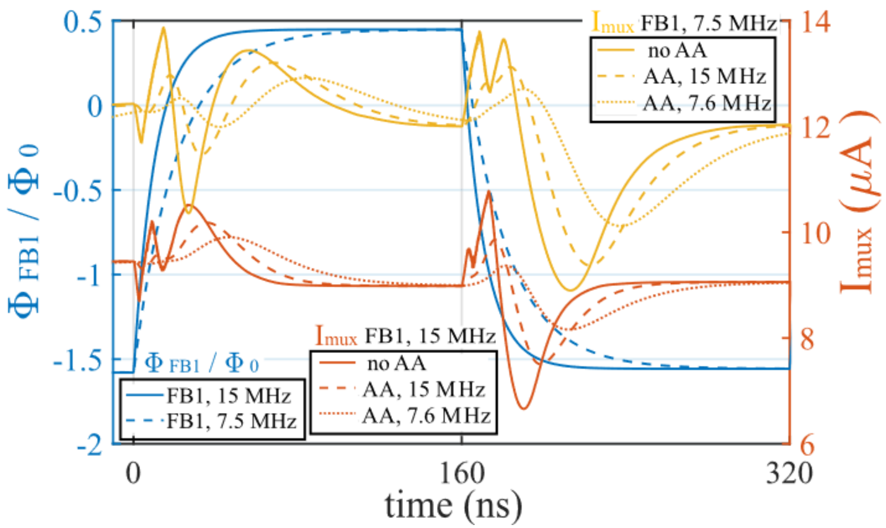

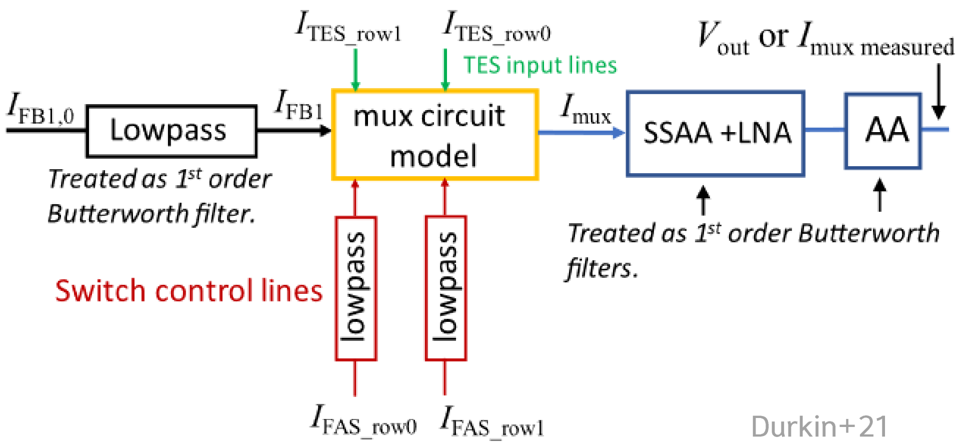

Durkin+21

TDM bandwidths optimization: crosstalk vs. bandwidth

- **The amplitude of the end of row residual depends on the signal from the previous row**
- **Different frequency cut-offs lead to different crosstalk types. At first order:**
  - **A cut-off in the pre-modulation bandwidth will slow the settling of the FB signal (~ pulse) => creates proportional crosstalk**
  - **A cut-off in the post-modulation bandwidth will slow the settling of the error signal (~ pulse derivative) => creates derivative crosstalk**
- **Simulations of this effect for X-IFU showed that most bandwidths need to be in the range of at least 10 MHz, i.e. quite higher than the "canonical" 6.25 MHz given by 1/trow**

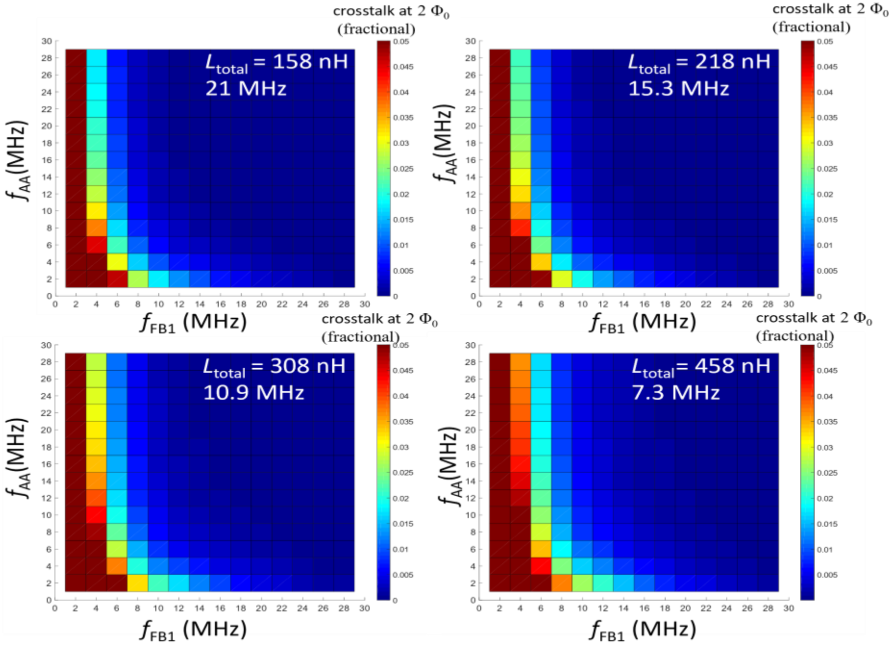

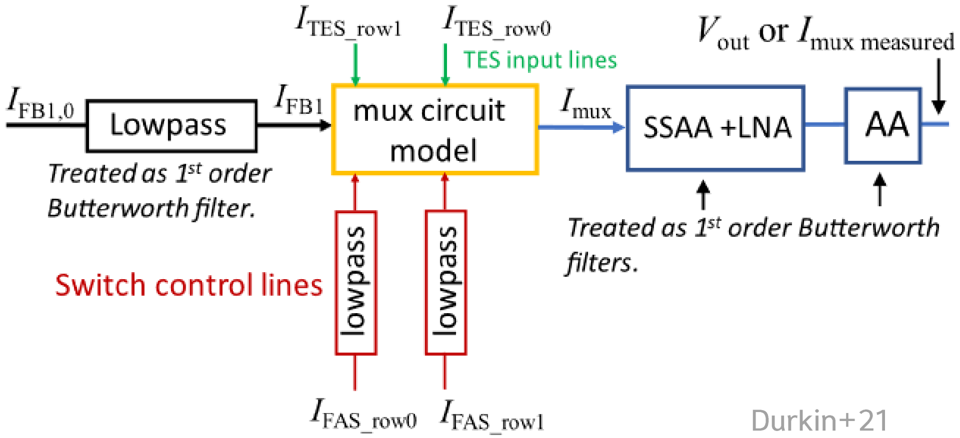

Durkin+21

TDM bandwidths optimization: gain scale effect

- As the settling shape is non-linear (notably because full FB signal spans several ϕ_0), the end of row residual, even in absence of a pulse in the previous row, depends on the signal level
- This creates gain scale distortions that can be significant with respect to the "main gain scale", which is dominated by the TES response
- Simulations show that BWs need to be more open than to respect the previous crosstalk criterion
  - SQUID-level model shows very good match to measurements
  - End-to-end measurement performed using linear pulse injections show similar distortions as simulations (quantitative comparison in progress)
- Will increase the Noise Equivalent Bandwidth of the readout noise
  - In practice, combination of bandwidths leads to similar NEB as $\frac{\pi}{2} f_{row}$

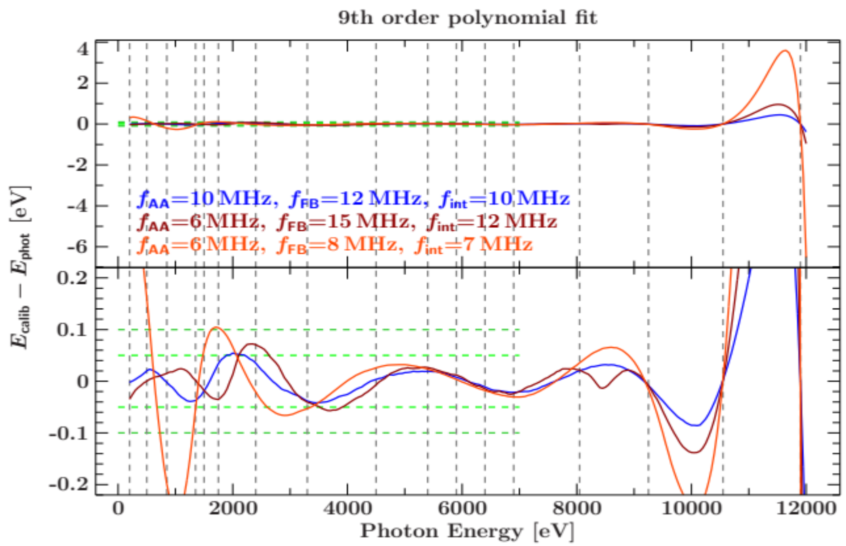

Simulations performed by C. Kirsch with xifusim (Kirsch+22)

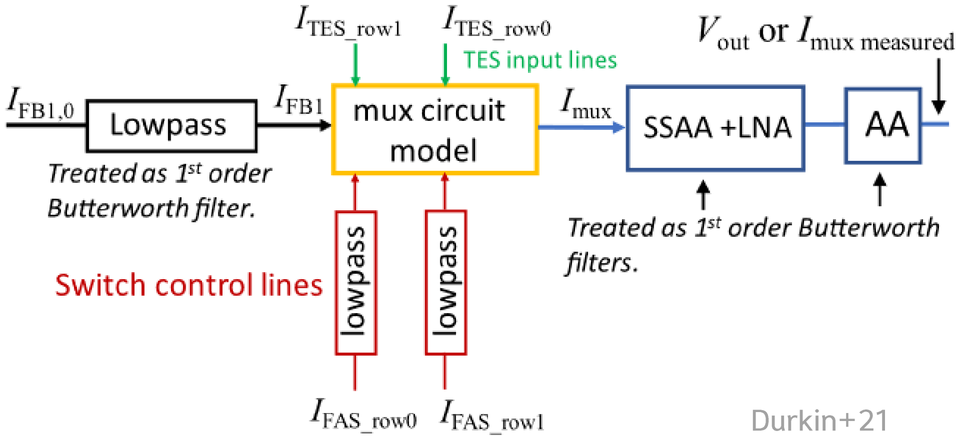

Durkin+21

Other crosstalk mechanisms and how they influence the performance

- Crosstalk = small fraction of a perpetrator pulse leaking onto a victim pulse
- Creates energy offsets as a function of time separation and the match between the crosstalk pulse shape and the optimal filter
  - E.g. proportional crosstalk will create a much larger effect than derivative crosstalk
- Main sources of crosstalk in X-IFU
  - TDM transients
  - Thermal crosstalk (largely mitigated by backside gold coating of TES wafer – few µm thickness)
  - Inductive coupling (in MUX SQUID chip, harnesses, between TES wires, ..)
- Advantage = it is a fully deterministic process
  - Can create exclusion rules to reject from the science the most impacted events
  - In principle, could try to correct for it (even if not very accurately)
- Overall, in pre-rescope design, expected ~ 10% additional (on top of grading) throughput loss from crosstalk

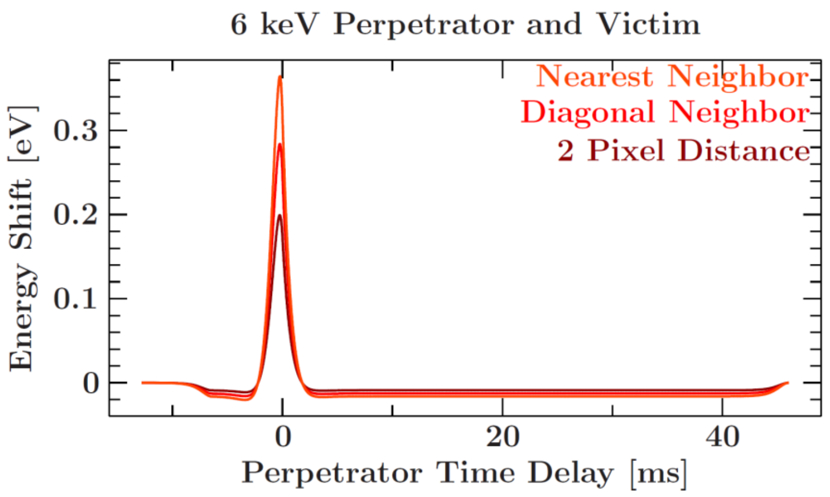

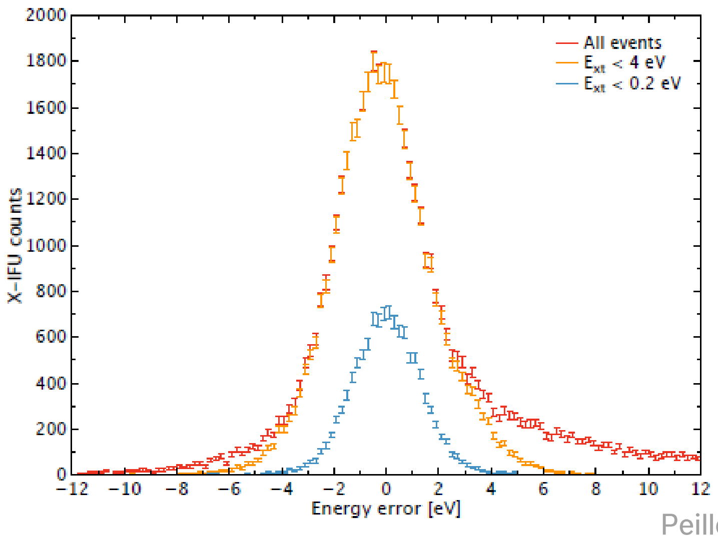

Peille+18

Other crosstalk mechanisms and how they influence the performance

- **Crosstalk = small fraction of a perpetrator pulse leaking onto a victim pulse**
- **Creates energy offsets as a function of time separation and the match between the crosstalk pulse shape and the optimal filter**
  - E.g. proportional crosstalk will create a much larger effect than derivative crosstalk
- **Main sources of crosstalk in X-IFU**
  - TDM transients
  - Thermal crosstalk (largely mitigated by backside gold coating of TES wafer – few µm thickness)
  - Inductive coupling (in MUX SQUID chip, harnesses, between TES wires, ..)
- **Advantage = it is a fully deterministic process**
  - Can create exclusion rules to reject from the science the most impacted events
  - In principle, could try to correct for it (even if not very accurately)
- **Overall, in pre-rescope design, expected ~ 10% additional (on top of grading) throughput loss from crosstalk**

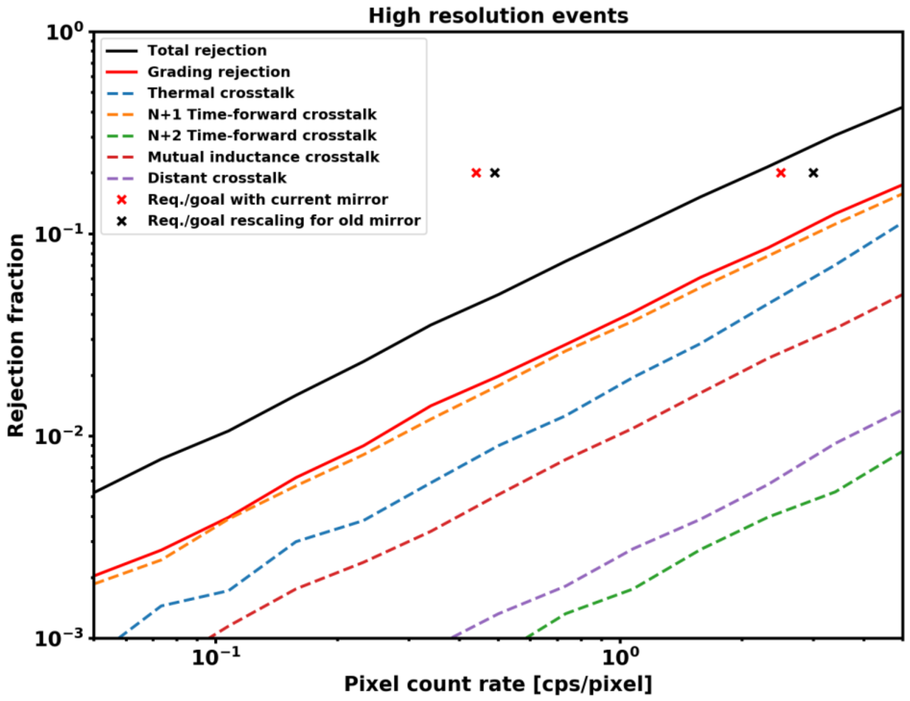

Environmental drifts

Parameter	Assumed SSR sensitivity requirements	ΔE = 0.1 eV equivalent
Temperature	$\partial E/\partial T$ = 150 meV/μK	0.28 μK rms
Bias voltage	$\partial E/(\partial V/V)$ = 15 meV/ppm	2.8 ppm rms
Magnetic field	$\partial E/\partial B$ = 3 eV/nT	15 pT rms

- **TESs are very performant but sensitive detectors**
- **Drifts of the environment will modulate the X-ray response**
  - **Degrades the resolution on short time scales**
  - **Creates non-linear modifications of the instrument gain scale on longer timescales**
- **Requires**
  - **~ 1μK rms thermal stability**
  - **10^5 – 10^6 shielding towards external magnetic fields**
  - **Electronics gain stability in the TES bias and FB lines of the order of few 10 ppm/K**

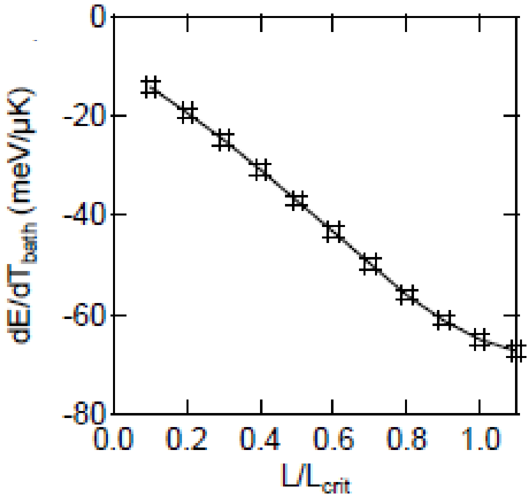

Gottardi&Smith+22

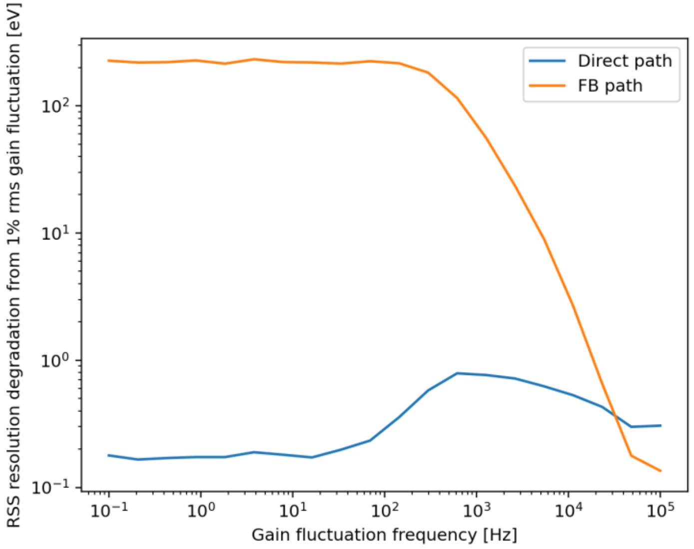

Environmental drifts

Parameter	Assumed SSR sensitivity requirements	ΔE = 0.1 eV equivalent
Temperature	$\partial E/\partial T$ = 150 meV/μK	0.28 μK rms
Bias voltage	$\partial E/(\partial V/V)$ = 15 meV/ppm	2.8 ppm rms
Magnetic field	$\partial E/\partial B$ = 3 eV/nT	15 pT rms

- **TESs are very performant but sensitive detectors**
- **Drifts of the environment will modulate the X-ray response**
  - Degrades the resolution on short time scales
  - Creates non-linear modifications of the instrument gain scale on longer timescales
- **Requires**
  - ~ 1μK rms thermal stability
  - 10^5 – 10^6 shielding towards external magnetic fields
  - Electronics gain stability in the TES bias and FB lines of the order of few 10 ppm/K

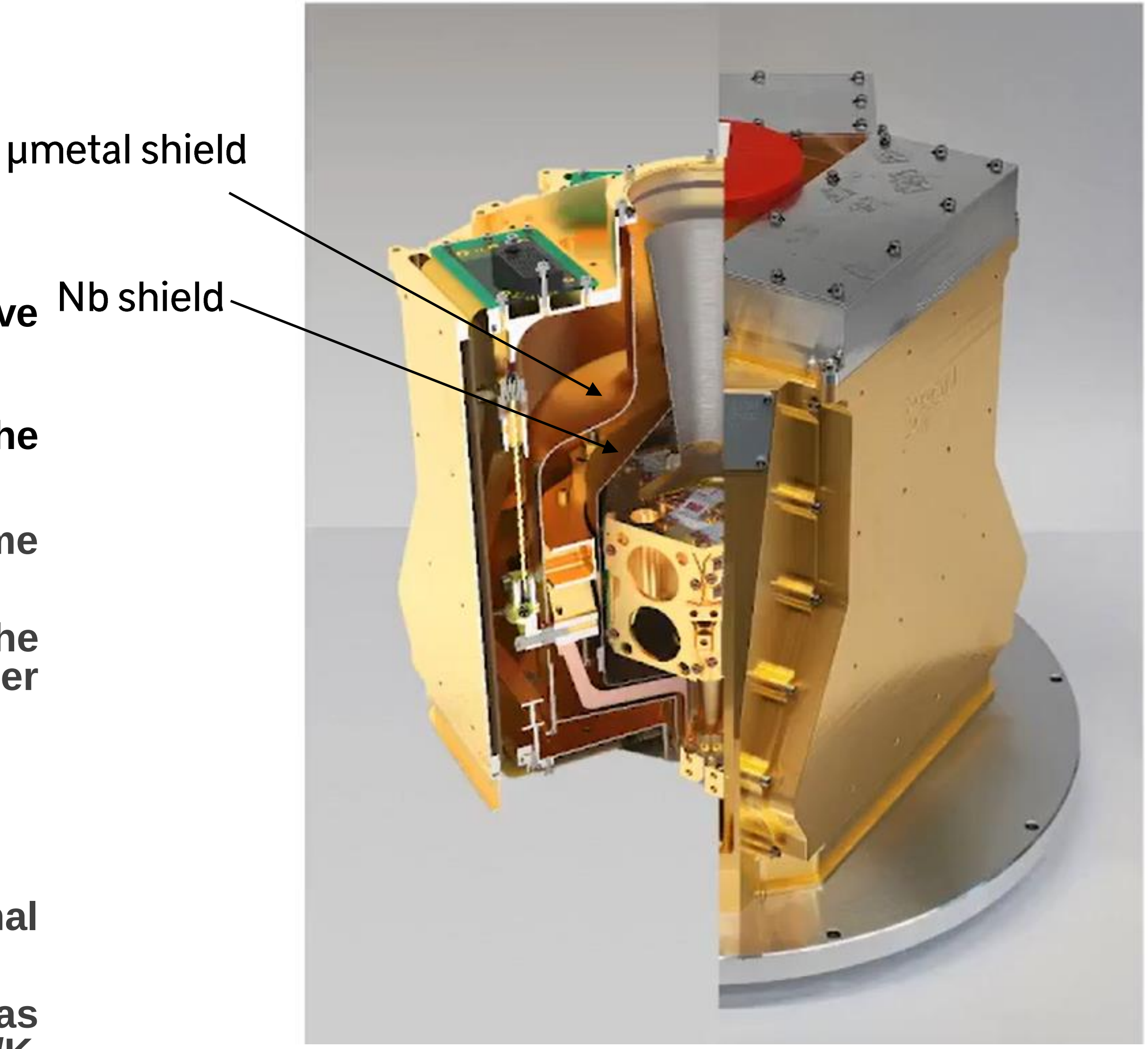

FPA DM1.0, credit SRON

Long timescale drift: gain drift correction algorithms

- **Similar to XRISM, the X-IFU will implement a modulated X-ray source to track the pixels' gains in a set of fiducial lines**
  - Will shine for 1-1.5 s every few tens of s
- **Due to the non-linear nature of the TES gain scale (and of its modification by an external parameter), linear correction is not sufficient**
  - Rather interpolate in a non-linear manner between calibrated gain scales
  - Higher order corrections also being tested using the pre-pulse baseline as an additional fiducial

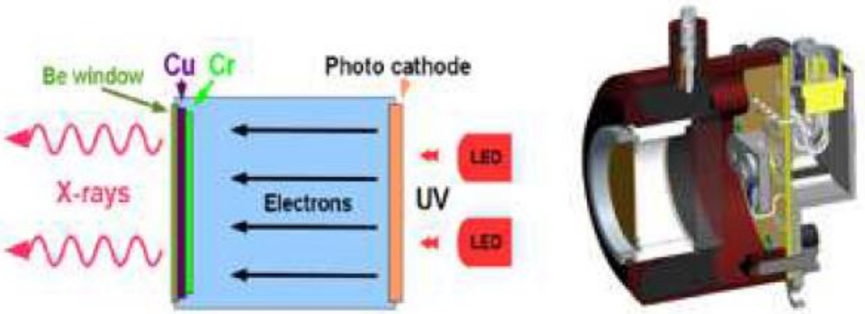

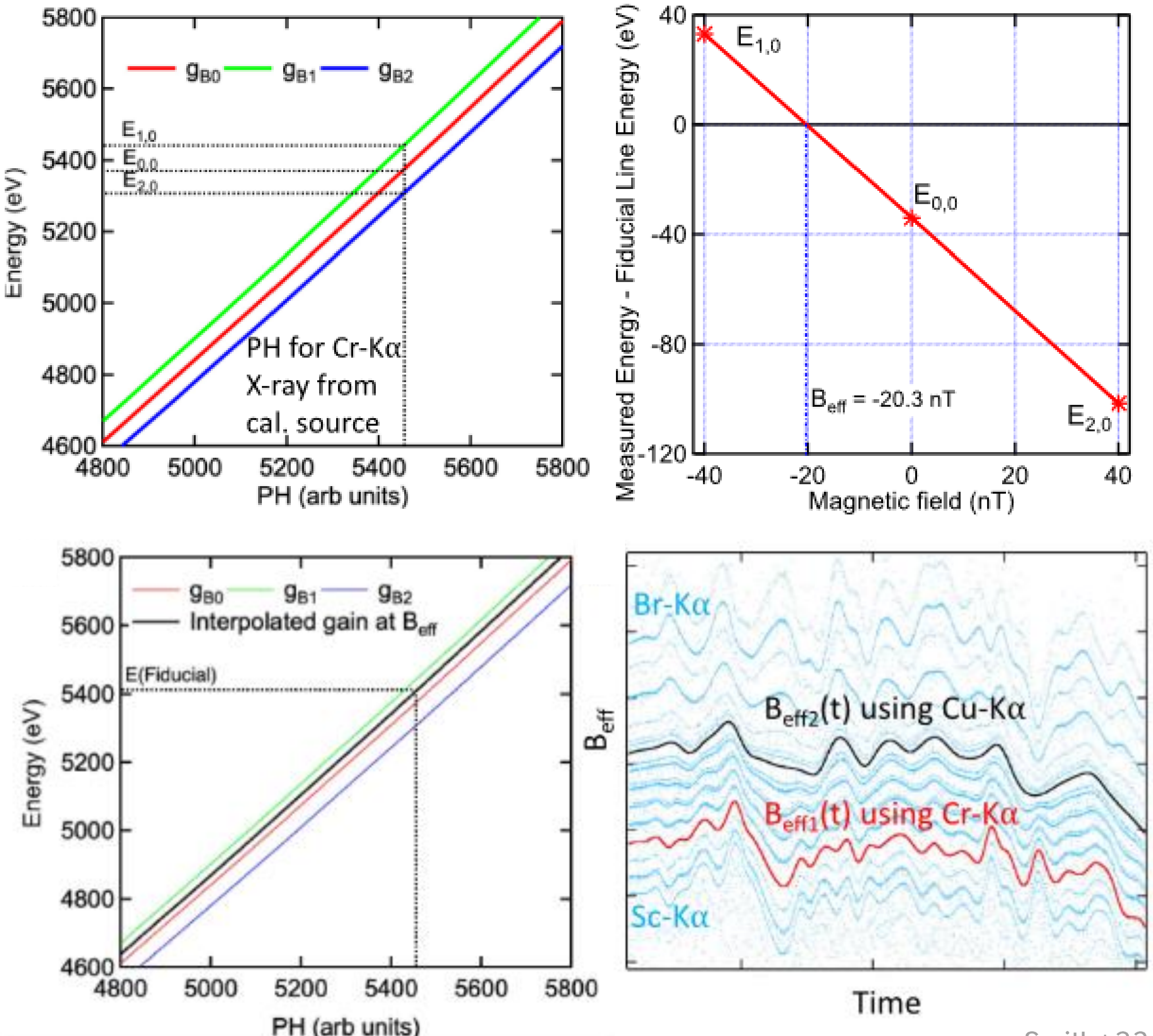

Smith+23

Long timescale drift: gain drift correction algorithms performance

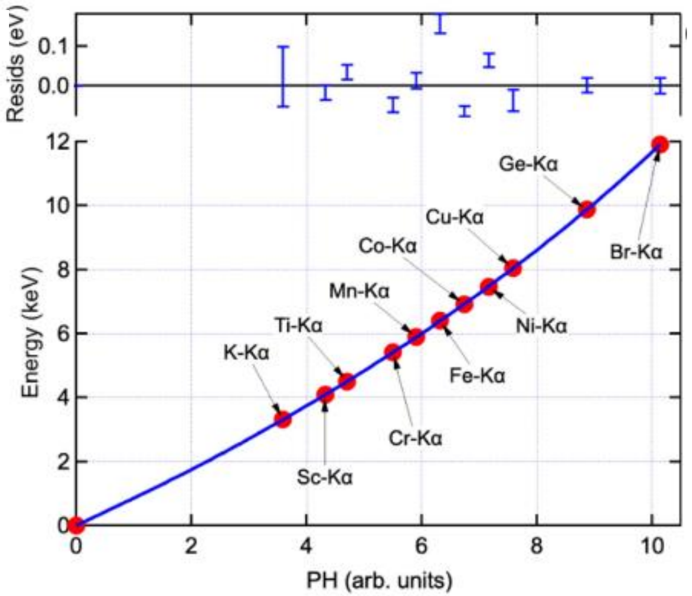

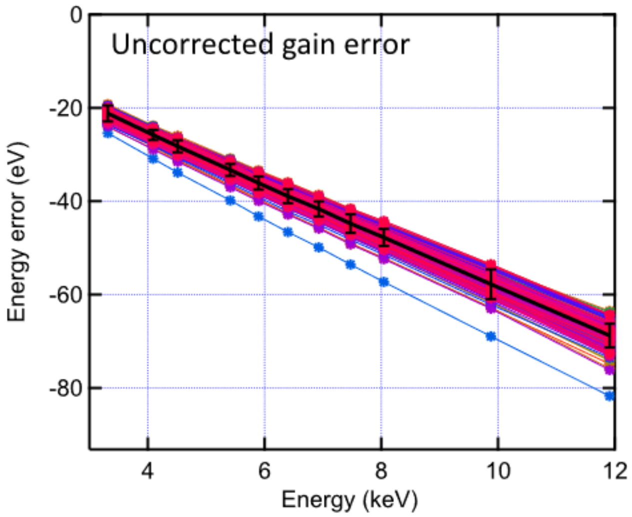

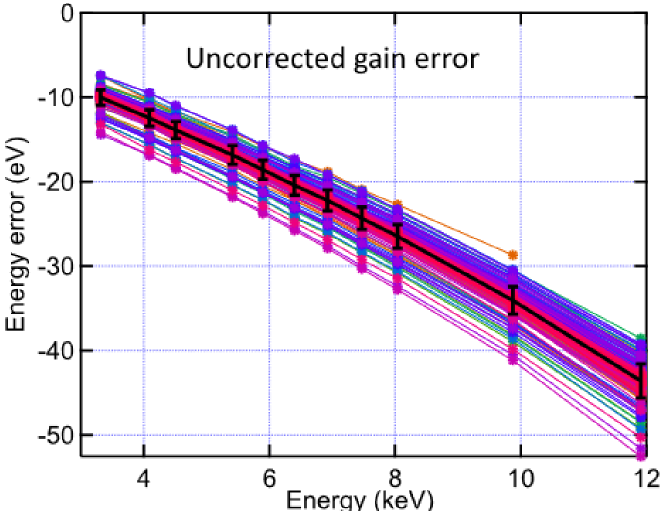

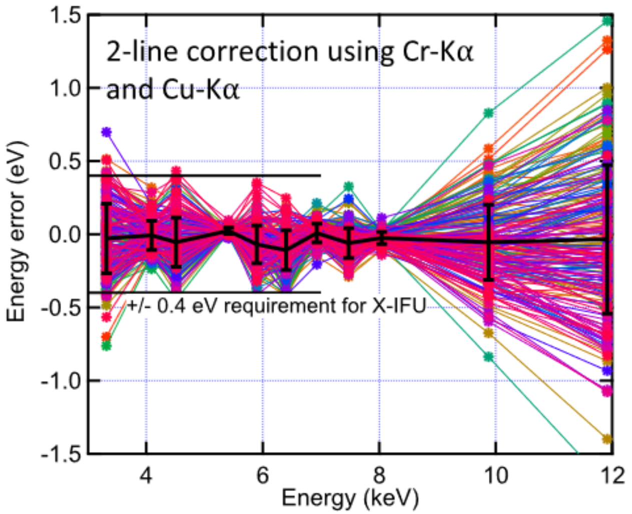

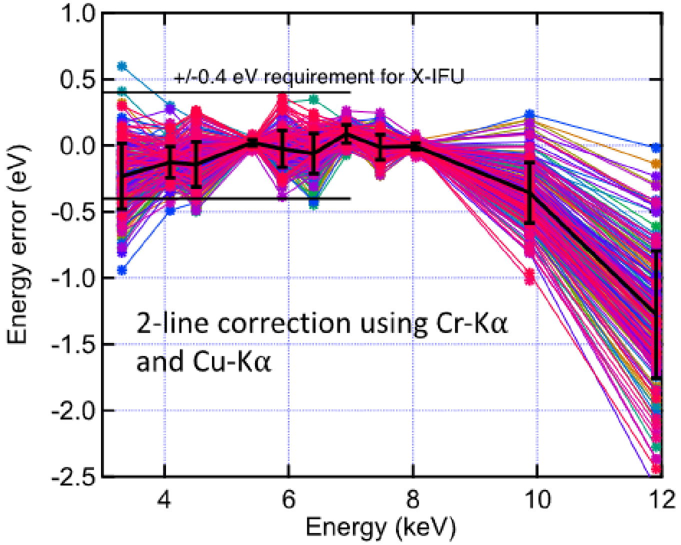

Smith+23

WHAT IS NEXT FOR X-IFU?

cnes

Long term X-IFU timeline

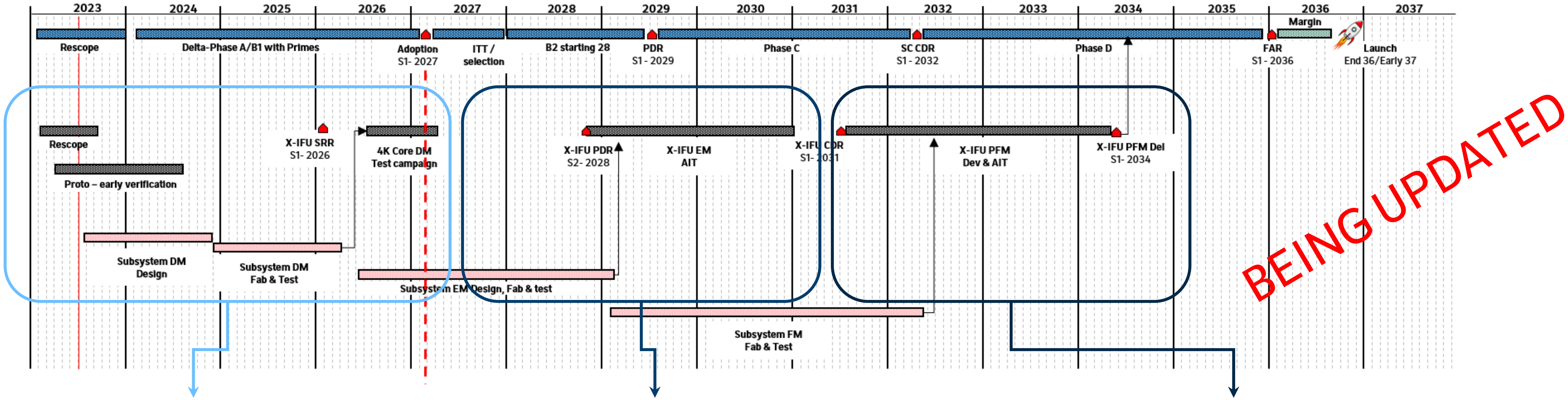

Demonstration activities

Objective = TRL5 at adoption (2027)

EM instrument

Test in dedicated Thermal GSE at CNES

Delivery to ESA for coupled tests at PLC level (2031)

PFM instrument

Test in dedicated Thermal GSE at CNES

Delivery to ESA 2034

Short term detection-related demonstration activities

- **Detection chain « early verification » (ongoing, up to 2025)**
  - Validation of differential detection chain design at warm and then coupled to a cold differential focal plane
- **Cold harness breadboarding (ongoing)**
  - Crosstalk characterization
  - Thermalization performance
  - Connectorization
  - …
- **FPA DM1.1 (build 2024, test up to ~ mid 2026)**
  - At scale FPA demonstration model with differential TDM cold electronics
  - Re-use of FPA DM1.0 structure
  - High fidelity prototypes of cold electronics
- **4K Core DM (AIT and test mid 2026 to mid 2027)**
  - Demonstration model of 4K core, with ADR DM and FPADM1.1
  - Objectives
    - Validation of ability to integrate full 4K core
    - Compatibility between ADR and FPA
    - 4K core thermal regulation optimization and thermal model correlation
    - Assessment of sensitivity to external perturbations (microvibrations, thermal stability, mag field – TBC)

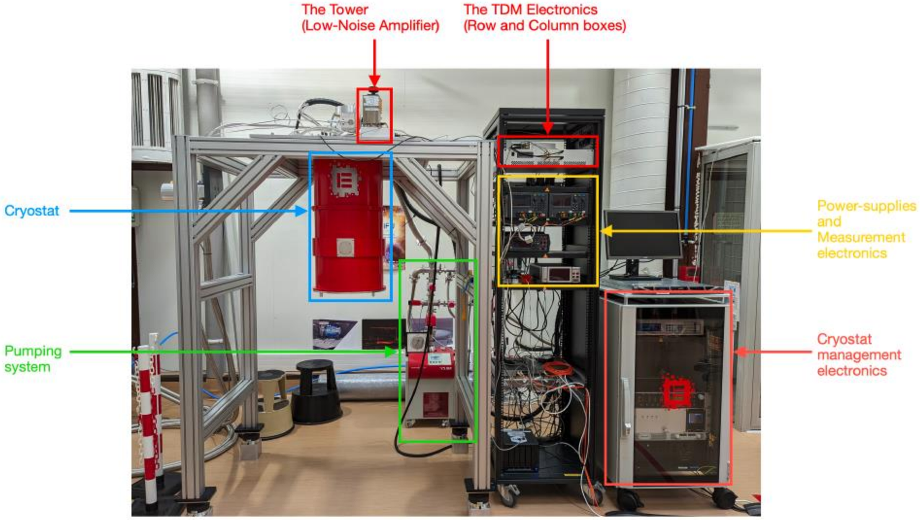

Short term detection-related demonstration activities

- **Detection chain « early verification » (ongoing, up to 2025)**
  - Validation of differential detection chain design at warm and then coupled to a cold differential focal plane
- **Cold harness breadboarding (ongoing)**
  - Crosstalk characterization
  - Thermalization performance
  - Connectorization
  - …
- **FPA DM1.1 (build 2024, test up to ~ mid 2026)**
  - At scale FPA demonstration model with differential TDM cold electronics
  - Re-use of FPA DM1.0 structure
  - High fidelity prototypes of cold electronics
- **4K Core DM (AIT and test mid 2026 to mid 2027)**
  - Demonstration model of 4K core, with ADR DM and FPADM1.1
  - Objectives
    - Validation of ability to integrate full 4K core
    - Compatibility between ADR and FPA
    - 4K core thermal regulation optimization and thermal model correlation
    - Assessment of sensitivity to external perturbations (microvibrations, thermal stability, mag field – TBC)

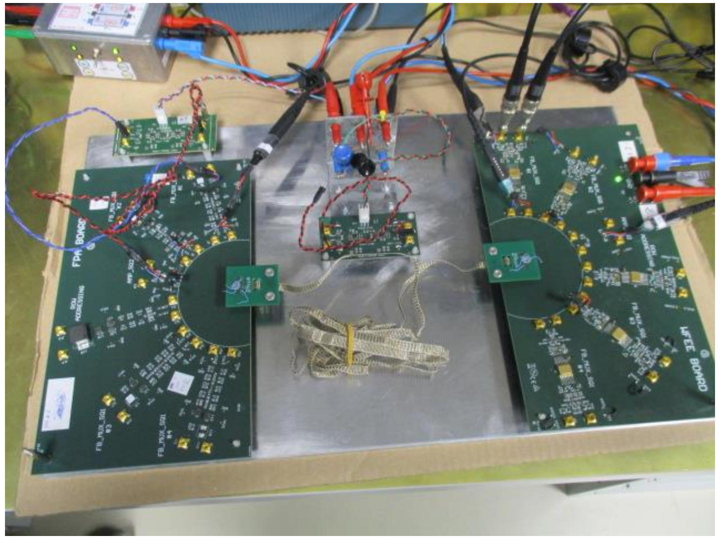

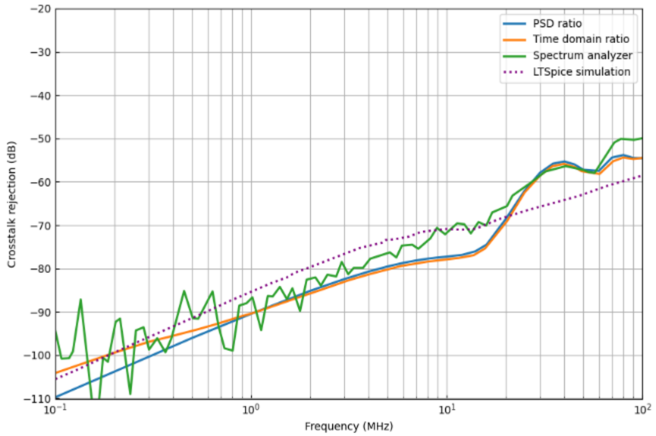

Geoffray+24

Short term detection-related demonstration activities

- **Detection chain « early verification » (ongoing, up to 2025)**
  - **Validation of differential detection chain design at warm and then coupled to a cold differential focal plane**
- **Cold harness breadboarding (ongoing)**
  - **Crosstalk characterization**
  - **Thermalization performance**
  - **Connectorization**
  - **…**
- **FPA DM1.1 (build 2024, test up to ~ mid 2026)**
  - **At scale FPA demonstration model with differential TDM cold electronics**
  - **Re-use of FPA DM1.0 structure**
  - **High fidelity prototypes of cold electronics**
- **4K Core DM (AIT and test mid 2026 to mid 2027)**
  - **Demonstration model of 4K core, with ADR DM and FPADM1.1**
  - **Objectives**
    - Validation of ability to integrate full 4K core
    - Compatibility between ADR and FPA
    - 4K core thermal regulation optimization and thermal model correlation
    - Assessment of sensitivity to external perturbations (microvibrations, thermal stability, mag field – TBC)

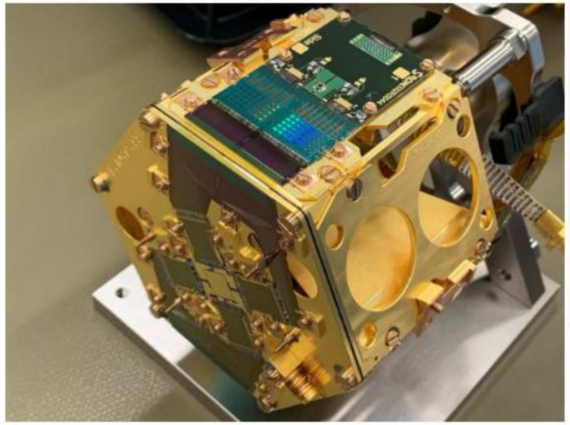

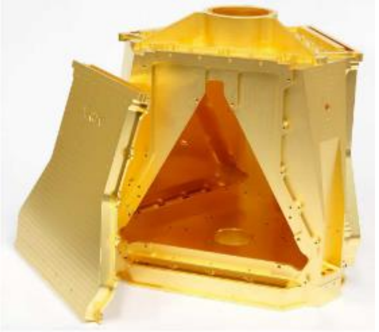

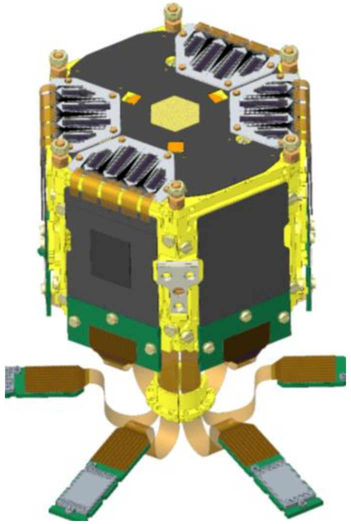

Credit: SRON

Short term detection-related demonstration activities

- **Detection chain « early verification » (ongoing, up to 2025)**
  - **Validation of differential detection chain design at warm and then coupled to a cold differential focal plane**
- **Cold harness breadboarding (ongoing)**
  - **Crosstalk characterization**
  - **Thermalization performance**
  - **Connectorization**
  - **…**
- **FPA DM1.1 (build 2024, test up to ~ mid 2026)**
  - **At scale FPA demonstration model with differential TDM cold electronics**
  - **Re-use of FPA DM1.0 structure**
  - **High fidelity prototypes of cold electronics**
- **4K Core DM (AIT and test mid 2026 to mid 2027)**
  - **Demonstration model of 4K core, with ADR DM and FPADM1.1**
  - **Objectives**
    - Validation of ability to integrate full 4K core
    - Compatibility between ADR and FPA
    - 4K core thermal regulation optimization and thermal model correlation
    - Assessment of sensitivity to external perturbations (microvibrations, thermal stability, mag field – TBC)

Credit: Absolut System

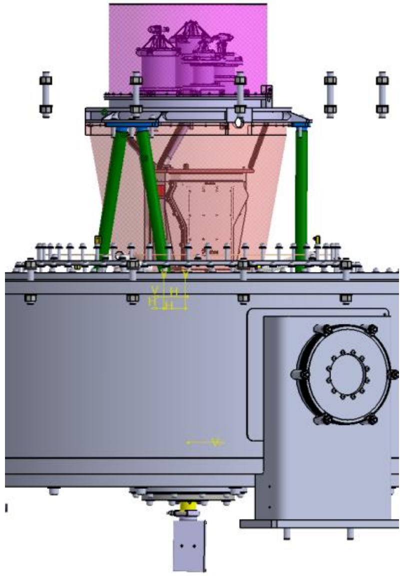

Conclusion

- **Athena and X-IFU restarting at full speed following mission rescope**
- **Several similarities with other low temperature detection experiment**
  - **Happy to discuss this with you further**
  - **Good ideas welcome!**
- **Numerous demonstration activities on-going/planned in the coming years**
  - **Major step forward for the instrument**
  - **Excited to share these results soon with the community**

BIBLIOGRAPHY

Bibliography

- **Reviews for TES detectors and associated readout chains particularly relevant for X-ray astronomy**
  - McCammon D., 2005, cpd..book, 1. doi:10.1007/10933596_1
  - Irwin K. D., Hilton G. C., 2005, cpd..book, 63. doi:10.1007/10933596_3
  - Gottardi, L., Nagayashi, K., 2021, Appl. Sci., *11*, 3793. doi:10.3390/app11093793
  - Gottardi L., Smith S., 2022, hxga.book, 103. doi:10.1007/978-981-16-4544-0_22-1
- **Latest full X-IFU instrument description paper (pre-rescope configuration, new architecture to be published this year)**
  - Barret D., Albouys V., Herder J.-W. den ., Piro L., Cappi M., Huovelin J., Kelley R., et al., 2023, ExA, 55, 373. doi:10.1007/s10686-022-09880-7

Bibliography

- **Other articles cited in this presentation (in order of citation)**

- Wakeham+23: Wakeham N. A., Adams J. S., Bandler S. R., Beaumont S., Chervenak J. A., Cumbee R. S., Finkbeiner F. M., et al., 2023, ITAS, 33, 3253067. doi:10.1109/TASC.2023.3253067
- Lindeman+00: Lindeman, M. A., "Microcalorimetry and the transition-edge sensor", PhDT, 2000
- Gottardi+21: Gottardi L., de Wit M., Taralli E., Nagayashi K., Kozorezov A., 2021, PhRvL, 126, 217001. doi:10.1103/PhysRevLett.126.217001
- Doriese+09: Doriese, W. B., "Optimal filtering, record length, and count rate in transition-edge-sensor microcalorimeters", in *The Thirteenth International Workshop on Low Temperature Detectors - LTD13*, 2009, vol. 1185, no. 1, pp. 450–453. doi:10.1063/1.3292375
- Smith+16: Smith S. J., Adams J. S., Bandler S. R., Betancourt-Martinez G. L., Chervenak J. A., Chiao M. P., Eckart M. E., et al., 2016, SPIE, 9905, 99052H. doi:10.1117/12.2231749
- Nagayoshi+20: Nagayoshi K., Ridder M. L., Bruijn M. P., Gottardi L., Taralli E., Khosropanah P., Akamatsu H., et al., 2020, JLTP, 199, 943. doi:10.1007/s10909-019-02282-8
- Smith+21: Smith S. J., Adams J. S., Bandler S. R., Beaumont S., Chervenak J. A., Denison E. V., Doriese W. B., et al., 2021, ITAS, 31, 3061918. doi:10.1109/TASC.2021.3061918
- Gottardi+17: Gottardi L., Akamatsu H., van der Kuur J., Smith S. J., Kozorezov A., Chervenak J., 2017, ITAS, 27, 2655500. doi:10.1109/TASC.2017.2655500
- de Wit+20: de Wit M., Gottardi L., Taralli E., Nagayoshi K., Ridder M. L., Akamatsu H., Bruijn M. P., et al., 2020, JAP, 128, 224501. doi:10.1063/5.0029669
- Gonzalez+24: Gonzalez M., Parot Y., Kirsch C., Cucchetti E., Peille P., Murat D., et al. 2024, JLTP, in press
- Durkin+23: Durkin M., Backhaus S., Bandler S. R., Chervenak J. A., Denison E. V., Doriese W. B., Gard J. D., et al., 2023, ITAS, 33, 3264175. doi:10.1109/TASC.2023.3264175

Bibliography

- **Other articles cited in this presentation (in order of citation)**

- Doriese+12: Doriese W. B., Alpert B. K., Fowler J. W., Hilton G. C., Hojem A. S., Irwin K. D., Reintsema C. D., et al., 2012, JLTP, 167, 595. doi:10.1007/s10909-012-0509-7
- Durkin+21: Durkin M., Adams J. S., Bandler S. R., Chervenak J. A., Denison E. V., Doriese W. B., Duff S. M., et al., 2021, ITAS, 31, 3065279. doi:10.1109/TASC.2021.3065279
- Kirsch+22: Kirsch C., Lorenz M., Peille P., Dauser T., Ceballos M. T., Cobo B., Merino-Alonso P. E., et al., 2022, JLTP, 209, 988. doi:10.1007/s10909-022-02700-4
- Peille+18: Peille P., Dauser T., Kirsch C., den Hartog R., Cucchetti E., Wilms J., Barret D., et al., 2018, JLTP, 193, 940. doi:10.1007/s10909-018-1964-6
- Smith+23: Smith S. J., Witthoeft M. C., Adams J. S., Bandler S. R., Beaumont S., Chervenak J. A., Cumbee R. S., et al., 2023, ITAS, 33, 3258908. doi:10.1109/TASC.2023.3258908
- Geoffray+24: Geoffray H., Adams J., Fossecave H., Cucchetti E., Bellouard E., Peille P., Daniel C., et al. 2024, JLTP, in press